UNITED NATIONS UNIVERSITY
GEOTHERMAL TRAINING PROGRAMME
Orkustofnun, Grensásvegur 9,
IS-108 Reykjavík, Iceland

Reports 2008
Number 2

PRODUCTION CAPACITY ASSESSMENT OF THE BACON-MANITO GEOTHERMAL RESERVOIR, PHILIPPINES

MSc thesis
Department of Mechanical and Industrial Engineering
University of Iceland

by

Jaime Jemuel C. Austria, Jr.
PNOC Energy Development Corporation
Merritt Road, Fort Bonifacio, Taguig,
P.O. Box 2102, MCPO
PHILIPPINES
austria.jjc@energy.com.ph

United Nations University
Geothermal Training Programme
Reykjavík, Iceland
Published in December 2008

ISBN 978-9979-68-248-6
ISSN 1670-7427

This MSc thesis has also been published in June 2008 by the
Faculty of Engineering – Department of Mechanical and Industrial Engineering,
University of Iceland

INTRODUCTION

The Geothermal Training Programme of the United Nations University (UNU) has operated in Iceland since 1979 with six month annual courses for professionals from developing countries. The aim is to assist developing countries with significant geothermal potential to build up groups of specialists that cover most aspects of geothermal exploration and development. During 1979-2008, 402 scientists and engineers from 43 countries have completed the six month courses. They have come from Asia (44%), Africa (26%), Central America (15%), and Central and Eastern Europe (15%). There is a steady flow of requests from all over the world for the six month training and we can only meet a portion of the requests. Most of the trainees are awarded UNU Fellowships financed by the UNU and the Government of Iceland.

Candidates for the six month specialized training must have at least a BSc degree and a minimum of one year practical experience in geothermal work in their home countries prior to the training. Many of our trainees have already completed their MSc or PhD degrees when they come to Iceland, but several excellent students have made requests to come again to Iceland for a higher academic degree. In 1999, it was decided to start admitting UNU Fellows to continue their studies and study for MSc degrees in geothermal science or engineering in co-operation with the University of Iceland. An agreement to this effect was signed with the University of Iceland. The six month studies at the UNU Geothermal Training Programme form a part of the graduate programme. Six UNU-GTP MSc Fellows completed their MSc degree in 2008, the biggest group to date.

It is a pleasure to introduce the twelfth UNU Fellow to complete the MSc studies at the University of Iceland under the co-operation agreement. Mr. Jaime Jemuel C. Austria, Jr., BSc in Mechanical Engineering from the University of the Philippines in Diliman, of PNOC-EDC, completed the six month specialized training in Reservoir Engineering at the UNU Geothermal Training Programme in October 2003. His research report was entitled “Database system and applications developed for reservoir modelling and monitoring of geothermal fields in the Philippines”. Three years later, in September 2006, he came back to Iceland for MSc studies in Reservoir Engineering at the Department of Mechanical and Industrial Engineering within the Faculty of Engineering of the University of Iceland. In May 2008, he defended his MSc thesis presented here, entitled “Production capacity assessment of the Bacon-Manito geothermal reservoir, Philippines”. His studies in Iceland were financed by a fellowship from the Government of Iceland through the UNU Geothermal Training Programme. We congratulate Mr. Jaime Austria Jr. on his achievements and wish him all the best for the future. We thank the Department of Mechanical and Industrial Engineering of the University of Iceland for the co-operation, and his supervisors for the dedication.

Finally, I would like to mention that Jamie’s MSc thesis with the figures in colour is available for downloading on our website at page *www.unugtp.is/yearbook/2008.*

With warmest wishes from Iceland,

Ingvar B. Fridleifsson, director
United Nations University
Geothermal Training Programme

ACKNOWLEDGEMENTS

My sincerest gratitude to The Government of Iceland, through the United Nations University Geothermal Training Programme, for granting a Fellowship grant for this MSc study; and to PNOC Energy Development Corporation (PNOC EDC) for officially supporting this MSc study.

My sincerest thanks to the following people from PNOC EDC: Mr. Paul Aquino, Mr. Manuel Ogena, and Dr. Cedric Malate for giving support for this MSc study; Mr. Francis Sta. Ana for ensuring reservoir data is available and accurate and for giving valuable technical advice and comments regarding my thesis; and Ms. Juvy Pagador-Belangel for providing field data and reports punctually.
My sincerest thanks to the following people from Iceland: Mr. Kjartan Reynir Hauksson, for providing timely network, hardware, and software support; Mr. Andri Arnaldsson for his technical support regarding the use of UNIX pre-processor; Dr. Gudni Axelsson, who is also the head of my thesis review panel, for providing comprehensive materials on reservoir simulation; Mr. Jónas Ketilsson for the very informative lectures, for painstakingly reviewing my work, and for setting the direction for my work when it mattered most; Dr. Páll Valdimarsson, for providing administrative support and liberal direction for the thesis, for the practical advice about graduate study in general, and for some encouraging tips regarding the 'mildew' phase during thesis preparation; and Mr. Grímur Björnsson, my main thesis supervisor, for the long consultation hours, which included weekends and holidays, spent on the UNIX scripts, TOUGH2 and iTOUGH2, for constantly advising me to work on the scripts with a fresh mind, and for instilling in me the patience and stubbornness of a reservoir engineer. My friendship with the staff of Iceland GeoSurvey, Orkustofnun, professors and classmates from Háskóli Islands will forever be remembered.

And most importantly, my heartfelt gratitude to Dr. Ingvar Birgir Fridleifsson and Mr. Lúdvík S. Georgsson, for giving me the opportunity to specialize further in geothermal reservoir engineering which is not easily affordable for people coming from developing countries like the Philippines.

DEDICATION

I dedicate this work to my dear wife Cynthia and my two lovely children – Joshua and Carylle, and to my parents. Nothing can replace the time spent away from my family; but seeing the fruits of my labour, time did no go for naught.

ABSTRACT

A sustainable production capacity of the Bacon-Manito geothermal system (BacMan) is assessed in this study by three numerical models of different complexity. A base case of 150 MW electrical generation is considered and production is constant up to end of Geothermal Service Contract for BacMan (year 2031). The numerical models considered are based on volumetric, lumped-parameter and a full scale, 3D well-by-well methods. A conceptual reservoir model is first proposed based on previous geoscientific research and downhole data. The geothermal reservoir has an estimated area of 23 km^2, its thickness exceeds 1500 m and temperatures range from 240 to 320°C. A volumetric model, using Monte Carlo style simulation, indicates that a production capacity of 200 MWe can be maintained for another 25 years with 90% probability. The lumped model predicts an annual pressure drawdown of 0.67 bars, resulting in a manageable total drawdown of 25 bars in year 2031. For the well-by-well method, a distributed parameter numerical model was developed using the simulator iTOUGH2. The simulator reduces poor matching between observed and simulated response by optimizing a set of 15 model parameters. These include mass and enthalpy of hot and deep recharge and 12 permeability values. Optimization resulted in far-field permeability of 0.5-5 milli-Darcies while the productive wellfield ranges from 25 to 100 milli-Darcies. The deep recharge was calibrated as 98 kg/s of 1830 kJ/kg enthalpy. Sensitivity analyses show that the model is most sensitive to pressure drawdown data followed by enthalpy of flowing wells. The model predicts that at least five more production and three reinjection wells are needed for future high-pressure steam requirement of the 150 MW powerplant. Stable enthalpies of production wells are predicted for the 23 years studied, indicating that reservoir temperature drawdown will be moderate. Reservoir boiling will, however, be intensive and change pressure gradients from hydrostatic to vapour static in the centre field. Instead of predicting reservoir performance for tens or hundreds of year, it was decided to stop production in year 2031 and monitor recovery of heat and mass reserves. Lumped model predicts a year of recovery for every year of production (optimistic scenario) while distributed parameter model predicts two years of recovery for every year of production (pessimistic scenario).

TABLE OF CONTENTS

Page

Page

LIST OF FIGURES

Page

LIST OF TABLES

1. INTRODUCTION

Interest in renewable energy sources has been increasing due to rising oil prices. In the Philippines, the government is aiming to lessen the utilization of high-price oil-based plants. Pursuing the Renewable Energy Policy Framework of 2003, the Philippine government aims to increase the share of renewable energy-based capacity from 4449 MWe in 2002 to 9147 MWe by 2013. 1200 MWe, or 25% of this capacity, will come from geothermal (DOE website).

Geothermal energy is a result of limitless heat emanating from the interior of the Earth and therefore considered as a renewable energy source. The Philippines have a considerable number of high-temperature, liquid-dominated geothermal resources and is considered as the world's second largest geothermal producer next to the United States. The Philippines has an installed capacity of 1959 MWe which generated 10.2 TWh accounting for 18.4% of the power generation mix. The rest of power generation comes from natural gas (29%), coal (27%), hydro (18%), and oil-based (8%) plants (Ocampo, 2007).

Geothermal energy, although renewable and abundant as in the Philippines, can be utilized sustainably or excessively depending on rate of exploitation. The former World Commission on Environment and Development defined sustainable development as:

> *"Sustainable development is development that meets the needs of the present without compromising the ability of future generations to meet their own needs."*
>
> Brundtland Commission (1987)

Sustainability can be assessed by analyzing reservoir response to production load by numerical modelling. Lumped parameter models may be used at constant temperature, single-phase conditions while detailed numerical models is more appropriate when boundary recharge and two-phase conditions has to be considered.

The aim of this thesis is to assess the sustainability of Bacon-Manito geothermal resource operating at its present operating capacity of 150 MWe until year 2031 using a lumped parameter and a well-by-well numerical model. Availability of fourteen years of production data is sufficient to warrant a well-by-well numerical modelling approach. The sustainability assessment is timely since the power plants in BacMan will be rehabilitated by 2010 and operated at full-load capacity of 150 MWe until end of Geothermal Service Contract for BacMan (year 2031). Results from well-by-well and lumped parameter models will be compared to the estimate obtained from volumetric model.

BacMan is located along the boundaries of Bacon in Sorsogon and Manito in Albay, 300 km southeast of Manila in the Philippines. BacMan lies within Pocdol Mountains, a swarm of volcanic zones of late Tertiary to Quaternary age, which form part of the Bicol arc (Figure 1). This volcanic complex is part of a NW-SE trending volcanic chain that runs through south-eastern Luzon, which includes active volcanoes such as Mt. Mayon located 35 km northwest of BacMan, and Mt. Bulusan situated 50 km southeast of BacMan. Presently, 50 wells having vertical depths from 372 m to 2973 m have been drilled in BacMan of which 37 wells are deviated (PNOC, 1985).

To accomplish the thesis objective, the present conceptual reservoir model will be revised firstly through careful analysis of all available downhole pressure and temperature data. Secondly, generating capacity will be robustly estimated using a volumetric model. Then a lumped model will be used to predict pressure response to production using pressure data from a monitoring borehole and net generation rate. Finally, a numerical model will be formulated and calibrated against 14 years of production data. A program for parameter estimation, sensitivity analysis, and uncertainty propagation analysis, iTOUGH2 (Finsterle, 2007), will be used to estimate model parameters.

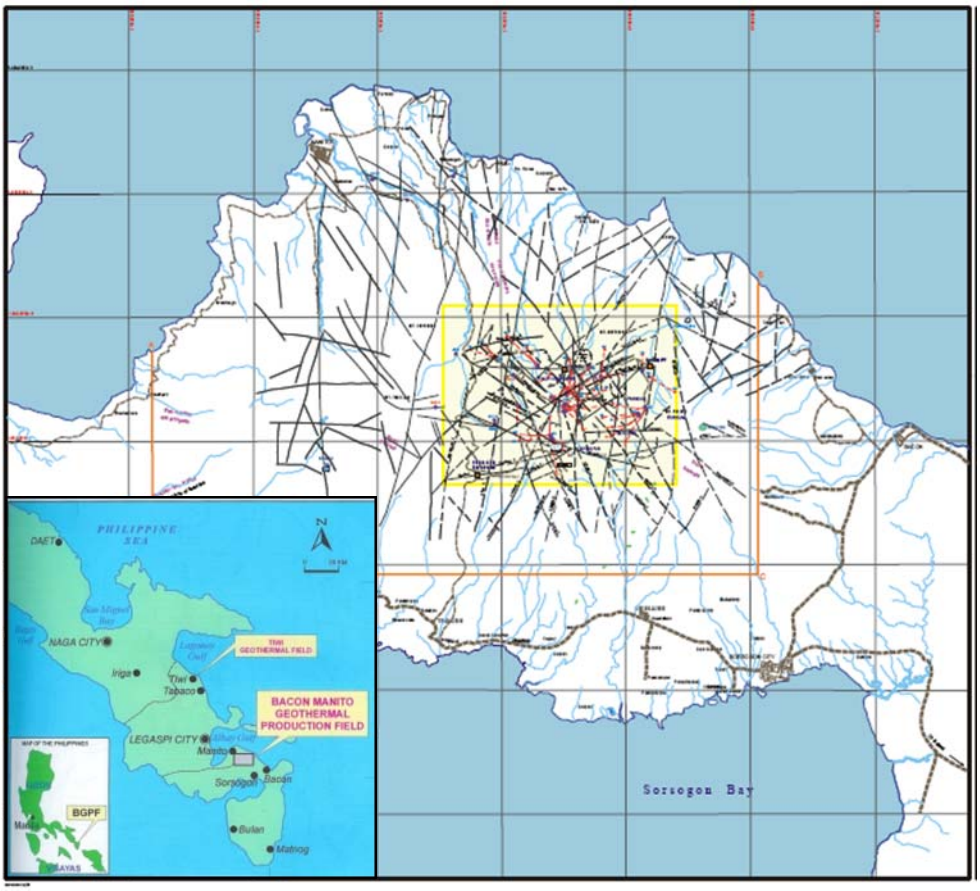

FIGURE 1: Location of Bacon-Manito geothermal field

Chapter two*: Specifications* discusses modelling of geothermal systems, idealization of geothermal reservoirs as numerical models, and sustainable production capacity. Development of BacMan field, data sources and how data is managed for this modelling study, physical reservoir characteristics derived from various scientific studies and integration of these physical characteristics into a coherent conceptual model are discussed in Chapter three: *Bacon-Manito Geothermal System*. Chapter four: *Volumetric Model* discusses estimation of generating capacity using volumetric model improved by assigning probability distribution on model parameters. Chapter five: *Lumped Parameter Model* discusses the theory behind lumped parameter modelling, validation of lumped parameter models, and application of lumped models in assessing sustainability. Chapter 6: *Distributed Parameter Model* discusses mathematical and numerical theory, parameter optimization, pre- and post-processors used to set-up computational mesh and process simulation results, numerical model parameters, validation of model reliability and application of well-by-well numerical model in assessing sustainability. The model does not include matching chemical parameters such as CO_2 which will be considered in future improvement of the model. Results from volumetric, lumped parameter, and detailed numerical models are compared in Chapter seven: *Comparison of Different Models*. In *Chapter eight*: *Conclusions and Recommendations,* the author summarizes what he has learned from this study and his recommended further work.

2. SPECIFICATIONS

The physical characteristics of geothermal reservoirs, general approaches in modelling of geothermal systems, idealization of a geothermal reservoir into a conceptual model, translation of a conceptual into a numerical model, and concept of sustainable capacity are discussed.

2.1 Physical characteristics

A typical high-temperature geothermal system involves large-scale convection of heat and mass driven by deep input of heat from a magmatic body or hot intrusion. Energy is transferred in the form of a continuous flow of mass and energy passing from a heat source to top layers; water flows from pores into a fracture. Cold water from above sinks and hot water from below rises due to density difference of hot and cold water and a convection cell is formed. Cooling by fluid convection at deeper end of fracture causes contraction of rock and extends fracture downward with time (Flovenz, 2007).

Convection occurs if conductive heat flux q (W/m^2) and permeability within reservoir are high enough. Onset of convection in a homogenous isotropic medium is described by dimensionless critical Rayleigh number.

$$\mathbf{Ra_c} = \frac{\mathbf{g \propto \Delta T d^3}}{\mathbf{vk}} \tag{1}$$

where α is thermal expansion coefficient, ν is kinematic viscosity, and k is thermal diffusivity. If Rayleigh number is below critical value, heat transfer is by means of conduction; if Rayleigh number is above critical value then convection occurs.

Convection mines heat and dissolves minerals near bottom of open fracture and deposits minerals on surface or at shallow depth by chemical precipitation from cooling brine. Mineral precipitate also forms a low permeability "cap rock" which seals path to surface (Flovenz, 2007).

Geothermal reservoirs are characterized by physical conditions and properties of the rock and fluid. Most significant of these physical properties controlling response and production potential of a reservoir are: (1) intrinsic permeability of the formation $\boldsymbol{k}$, or the ability to transmit fluids (typically 10-300 milliDarcy where 1 milliDarcy $\approx 1x10^{-15}$ m^2); (2) porosity $\boldsymbol{\phi}$, or fraction of void spaces in material; and (3) storage capacity or storativity (kg/m^3Pa) representing the ability of reservoir to store and release fluid in response to changes in pressure (Axelsson, 2007).

Other properties of importance are: heat capacity C which determines amount of stored energy and varies between 850 to 1050 J/kg°C (Bodvarsson and Witherspoon, 1989); thermal conductivity $\boldsymbol{\lambda}$ which controls heat transfer by conduction and typically ranges from 1.5 to 4.0 W/m°C; density or mass content; enthalpy or energy content; and viscosity or mobility. In some cases, fluids in geothermal reservoirs are not pure water but brine containing dissolved solids and non-condensible gases typically sodium chloride (NaCl) and carbon dioxide (CO_2) respectively; in such cases, correlations for effect of temperature and pressure must be used (Michaelides, 1981).

Physical properties and conditions of a reservoir are estimated using: (1) geological information describing type of formation, rock type or permeability distribution, formation temperatures based on alteration, structural control, and boundary conditions; (2) geophysical measurements estimating possible reservoir depths and reservoir boundaries based on resistivity measurements, and reservoir mass balance based on gravity measurements; (3) geochemical information describing distribution of thermal features, formation temperature from geothermometers, and possible heat source configurations; and (4) collection of downhole data and well test analyses, e.g. pressure transients, temperature logs, and production test data.

2.2 Modelling of geothermal systems

The aim of modelling of geothermal systems is to obtain information on reservoir conditions and on natural properties of the system as well as to predict reservoir response to future production and estimate sustainable production potential of a system. Different modelling approaches include simple analytical models, lumped parameter models, and detailed numerical models.

Simple analytical models have greatly simplified geometry and structure. Analytical expressions can be derived to describe model response. Lumped parameter models ignore geometry, integrates properties into lumped values, and response is given by analytical functions. Detailed numerical models can accurately simulate complex geometry and structures and variable properties. Response in detailed numerical models must be calculated numerically. Detailed numerical models can accurately simulate pressure, temperature, and chemistry simultaneously (Axelsson, 2007).

The most significant physical properties of a geothermal reservoir are synthesized from conflicting opinions, interpretations, and extrapolations of data into a coherent and sensible integrated conceptual model. A conceptual model is a descriptive or qualitative model of a geothermal system that combines essential physical features of a system that have been revealed through analysis of all available exploration, drilling and testing data. A conceptual model can be shown as a graphical representation of the plan view and vertical sections of a geothermal system. An adequate conceptual model should at least demonstrate flow pattern in reservoir, size and shape of reservoir, location of up-flow zones, boiling zones, recharge zones, barriers and/or main flow paths, and heat source for reservoir. An adequate conceptual model is the basis for a successful numerical modelling. Subsequent process of developing a conceptual model into a numerical model derives profoundly from works of experienced modellers as summarized by O'Sullivan et al. (2001).

Size and boundary conditions are two important matters to be decided on in setting up a model of a geothermal system. Due to the enormity in scale of convective systems, its entirety is usually not covered in the model but is rather represented by boundary conditions. For side or lateral boundaries, side boundaries are set sufficiently distant from production and injection areas so that model performance over simulated lifetime is not affected by choice of boundary. Modellers apply various boundary conditions: no-flow boundary conditions (heat or mass); background linear temperature and hydrostatic pressure; constant temperature and pressure "open" boundary conditions which allows mass flow into or out of boundary blocks at a rate proportional to pressure drop; or "active" lateral boundary conditions having specified mass injection or production. In the early days when computing power was limited, latter approach was used thus limiting the number of model elements that may be used. O'Sullivan et al. (2001) states that this approach makes lateral flows or constant pressure and temperature boundary conditions a dominant part of model calibration instead of a permeability structure thus limiting usefulness of model for prediction. In this study, computing power is not limited hence the boundaries are made large enough so that model structure will determine model behaviour and not boundary conditions.

A deep magmatic heat source is usually represented by a suitable combination of heat and mass sources. For vapour-dominated systems, constant pressure and vapour saturation boundary conditions are applied. For liquid-dominated, two-phase systems, constant pressure and temperature boundary conditions are used instead of no-flow boundary conditions. This approach, however, must be used with caution as this may cause a false quasi-steady state where unlimited recharge from constant pressure boundary matches the production rate (O'Sullivan et al., 2001). Extended history of pressure drawdown should minimize the risk of specifying a constant pressure boundary in a numerical model (Björnsson, 2008).

For surface boundary conditions and for models that are truncated below ground surface, the following boundary conditions are implemented: a closed top with no mass flow representing a low permeability cap rock commonly with constant pressure and temperature; no mass flow but having conductive heat loss; or constant atmospheric pressure and temperature at top of model (most common). In most cases, atmospheric conditions are implemented at the position of water table and not at the ground surface.

Some modellers use flat water table at constant elevation while others adjust the thickness of the top model elements using actual elevations to match variable elevation of water table (O'Sullivan et al., 2001). In this study, the surface is truncated below ground surface and is set inactive allowing only conductive heat loss.

Furthermore, to represent surface features such as fumaroles, modellers use artificial sinks located in near surface layers and operating on deliverability. To improve representation of shallow zones, some modellers included unsaturated zone between ground surface and water table which then appears as blocks with high mass fraction of air under situations where the shallow-reservoir may flash into steam layer due to pressure drawdown. Accuracy is improved by using a number of thin layers at top layers (O'Sullivan et al., 2001). Artificial sinks operating on deliverability are used this study to represent hot springs.

Before a good match between field data and transient physical conditions was obtained, a lot of manual trial-and-error changes have to be done in the past to adjust permeability and porosity distribution, amount of heat and mass injected into reservoir base, and productivity indices of production wells. This study has been spared from this very time consuming and tedious calibration procedure and has greatly benefitted from automatic history-matching using iterative parameter estimation implemented in iTOUGH2 (Finsterle, 2007). iTOUGH2 is a program for parameter estimation, sensitivity analysis, and uncertainty propagation analysis. iTOUGH2 is based on the TOUGH2 simulator for non-isothermal multiphase flow in porous and fractured media (Pruess, 1999). Using iTOUGH2, parameters can be estimated by automatically calibrating multiphase flow model against measured data of system response. Inferring model-related parameters from observations by means of a process model is termed inverse modelling.

The general model calibration procedure developed over the last decade involves a model with boundary conditions as earlier discussed and initial conditions like a temperature gradient (°C/km) and a corresponding hydrostatic pressure gradient. Model is run at a geologic time scale, e.g. 100000 years, until a steady-state condition is reached. When steady-state conditions match the natural-state of conceptual model, then production history is simulated. When a good match of production history is obtained, then model may be used for prediction of future field behaviour at different production conditions. This model uses a temperature gradient of 83°C/km and initial pressure of 2 bar at top layer to match the linear gradient and hydrostatic profiles of most observation wells. The model uses the automatic steady-state save feature of iTOUGH2 allowing it to attain steady-steady after 10000 years and shift to history matching afterwards.

2.3 Sustainability assessment

Axelsson et al. (2001) proposed this definition for the term "sustainable production of geothermal energy from an individual geothermal system." This definition does neither consider economic aspects, environmental issues, nor do technological advances, all of which may be expected to fluctuate with times:

> *For each geothermal system, and for each mode of production, there exists a certain level of maximum energy production, $\mathbf{E_o}$, below which it will be possible to maintain constant energy production from the system for a very long time (100-300 years). If the production rate is greater than $\mathbf{E_o}$, it cannot be maintained for this length of time. Geothermal energy production below, or equal to $\mathbf{E_o}$, is termed sustainable production while production greater than $\mathbf{E_o}$ is termed excessive production.*

In Figure 2, the difference between sustainable and extensive production is shown.

A maximum sustainable energy production level can both be estimated and approached through stepwise development and even excessive production (Figure 3). In this case, the field developer decides to gradually build-up power plant capacity by adding new moderate size units (20 to 40 MWe) say every five years. Meanwhile the reservoir response to generation is observed and modeled. A recovery period should then follow a period of excessive production (Stefansson and Axelsson, 2005). The installation of a higher level of plant capacity and addressing steam supply decline with make-up drilling, however, is more economical.

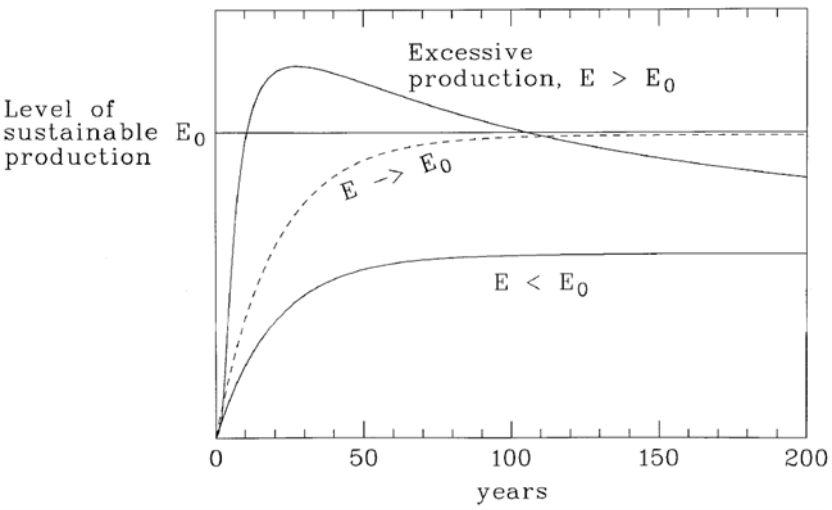

FIGURE 2: Difference between sustainable and excessive production (Axelsson et al., 2004)

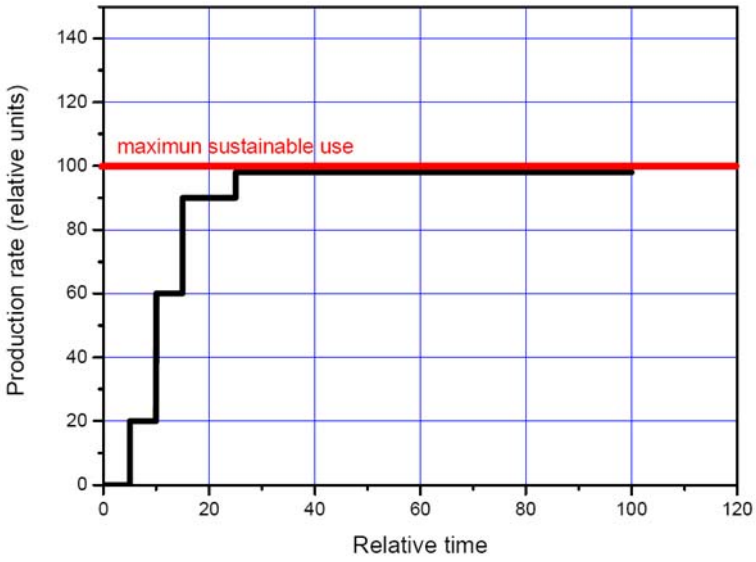

FIGURE 3: Stepwise development of a geothermal resource (Stefansson and Axelsson, 2005)

Sarmiento and Björnsson (2007) pointed out that, based on Icelandic experience, detailed numerical model conservatively estimate maximum generating capacity while simple volumetric heat reserve models may lead to aggressive production strategies. Based on Philippine experience, and in light of extensive field management programs like make-up drilling, deeper drilling, relocation of injection sites and less acidity of steam caps, Sarmiento and Björnsson concluded that $\boldsymbol{E_o}$ is a highly transient number. In the case of the Philippines, it has risen considerably from what was technically feasible in 1978 when the first large-scale testing took place in Tiwi. Availability of new techniques may therefore push production levels from being initially excessive to sustainable.

3. BACON-MANITO GEOTHERMAL SYSTEM

The following topics are discussed in this chapter: field development; review of related work in geology, geochemistry, geophysical; analysis of rock temperature and pressure from logs; and synthesis of various interpretations into an integrated conceptual model.

3.1 Field development

Map of different sectors and location of wells of BacMan is shown in Figure4. Based on logistical and technical criteria, development of BacMan field can be separated into BacMan 1 or Palayan-Bayan and BacMan 2 which is defined as all areas outside BacMan 1 capable of supporting 20 MWe (PNOC EDC, 1989). The definition of BacMan 2 is in-line with the concept of modular development of geothermal resources, or the use of smaller capacity power plants, proposed by the National Power Corporation (NPC). NPC operates all of PNOC EDC's power plants before PNOC EDC undertook build-operate-and transfer contracts discussed in Vasquez et al. (1999). Two 55-MWe turbine-generator units are installed in BacMan 1 and another two 20-MWe modular power plants are installed in BacMan 2 for a total installed capacity of 150 MWe. The succeeding discussion on field development history is based from the review report of PNOC EDC (1985) regarding the development strategy for the initial 110 MWe development in BacMan 1.

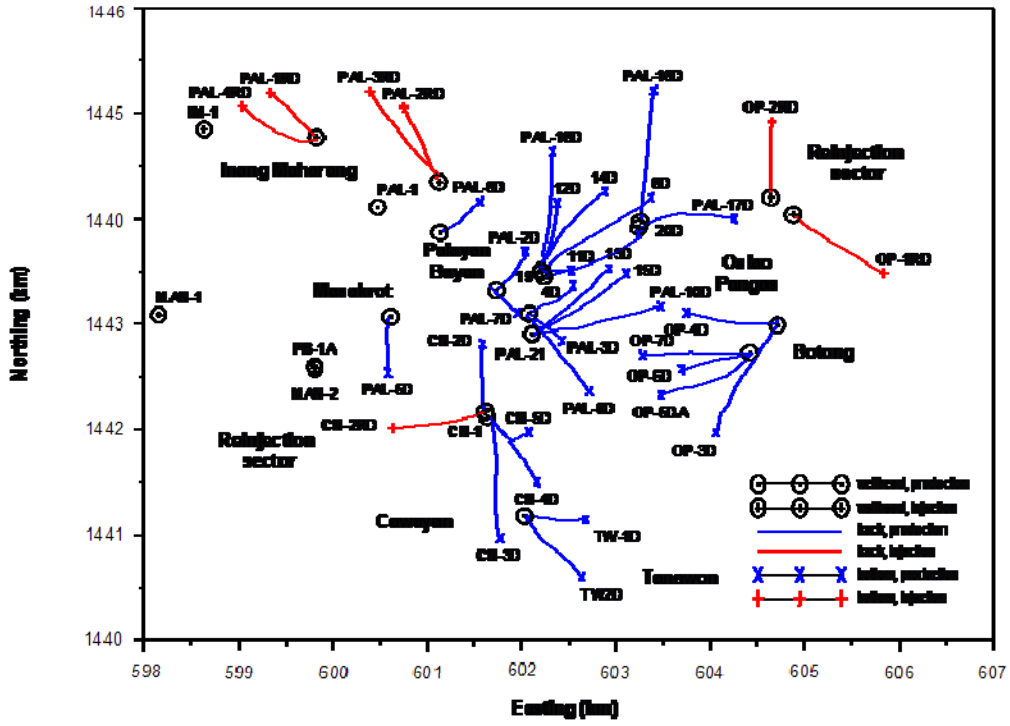

FIGURE 4: Wellhead locations, well tracks, and different sectors

The exploration approach for BacMan has been developed throughout years borrowing extensive experience from other geothermal developments in the Philippines, such as Tongonan and Palinpinon. Exploration began with a survey of all surface thermal manifestations in the region. Geothermal Energy New Zealand Ltd. (GENZL) conducted a reconnaissance survey in Paron, Naghaso, and Inang Maharang followed by geoscientific surveys covering 188 km^2 in 1977. Geochemical results from reconnaissance were combined with preliminary geologic mapping to prioritize additional exploration targets. Detailed geologic mapping, geophysical surveys and geochemical sampling followed. Interpretation of aerial photographs, mapping and regional resistivity surveys such as Schlumberger profiling and vertical electrical soundings (VES) are some of the activities included.

Notwithstanding the extensive experience derived from other geothermal developments, the road to BacMan development is not without challenges. The first two exploratory wells drilled in 1979, 1368 m deep Manito 1 (MAN-1) and 1637 m deep Manito 2 (MAN-2), both failed to sustain flow despite having temperatures of 214ºC and 248ºC respectively. Drilling proceeded in the southern portion of BacMan in the 1980's, in Cawayan, Manito, and Inang Maharang, after obtaining promising results from resistivity, gravity and passive seismic surveys and obtaining funding from the New Zealand government.

The first successful well is the 2546 m deep CN-1 which was spudded on 26 April 1981. CN-1 was drilled 2 km east-southeast of MAN-2 to test the temperature and permeability near a 2-ohm meter resistivity anomaly delineated by shallow resistivity surveys. CN-1 measured a maximum temperature of 272ºC and discharged successfully with a power output of 11.3 MWe. The first directional well, CN-2D, spudded on 13 January 1982 was drilled to 1716 mVD (1881 mMD) and measured temperature of 240ºC. CN-2D sustained flow but its output is non-commercial. Exploratory drilling was moved to Manito lowlands. Drilling of 1573 m deep Malanto 1 (MO-1) began on 17 March 1982; 1092 m deep MO-2 on 23 April 1982; and 1200 m deep MO-3 on 8 April 1984. The maximum temperature recorded is 223ºC for MO-1, 216ºC for MO-2, and 218ºC for MO-3. The wells produced liquid water with enthalpy ranging from 930 to 1010 kJ/kg which is suitable for binary and direct-use. In October 1998, a 1.5 MWe power plant using backpressure turbine-generator and a multi-crop drying facility were installed to provide a livelihood project for the local marginalized community.

Development of northern sector of Palayan-Bayan kicked-off with the drilling of PAL-1 and PAL-2D in 1981. After testing these two wells, production areas were identified followed by the drilling of more wells to delineate the resource: PAL-3D in 1982; PAL-4D, PAL-5D, PAL-6D, PAL-7D and PAL-8D in 1983; PAL-9D, PAL-10D, PAL-11D and PAL-12D in 1984; PAL-13D in 1985; PAL-14D in 1986; PAL-15D in 1989; PAL-16D , PAL-17D and PAL-18D in 1991; PAL-19 in 1993; and PAL-20D and PAL-21 in 1994. The first reinjection well, PAL-1RD was drilled in 1983, followed by PAL-2RD and PAL-3RD in 1984, and PAL-4RD in 1985.

Two wells, OP-1D and OP-2D in Osiao–Pangas were drilled for BacMan 2 in 1987. Both wells have poor discharge output and were later utilized for reinjection and renamed OP-1RD and OP-2RD respectively. Drilling shifted to Botong area with OP-3D in August 1988; OP-3D was successfully discharged with a mass flow of 12 kg/s and an enthalpy of 1800 kJ/kg making it the first commercial well in Botong. Drilling of OP-4D in 1989, OP-5DA in 1992, OP-6D in 1990, and OP-7D in 1995 followed; all the wells have commercial output.

Cawayan is another area that was tapped for BacMan 2. The third well drilled in Cawayan, CN-1RD, was intended as a reinjection well but was later converted into a production well and coded CN-3D when it gave a commercial output during discharge testing. Drilling of reinjection wells CN-2RD and CN-3RD followed in November 1990 and March 1991 respectively and production wells CN-4D and CN-5D in June 1994 and February 1995 respectively.

A 110 MWe power plant was commissioned in BacMan 1 in 1993 followed by a 20 MWe modular power plant in BacMan 2 (Cawayan) in 1994 and another 20 MWe modular power plant in BacMan 2 (Botong) in May 1998.

3.2 Data sources

Data that is systematically collected is important in understanding a geothermal resource in its natural state and in monitoring changes in the resource during exploitation.

Main data sources for this study include:

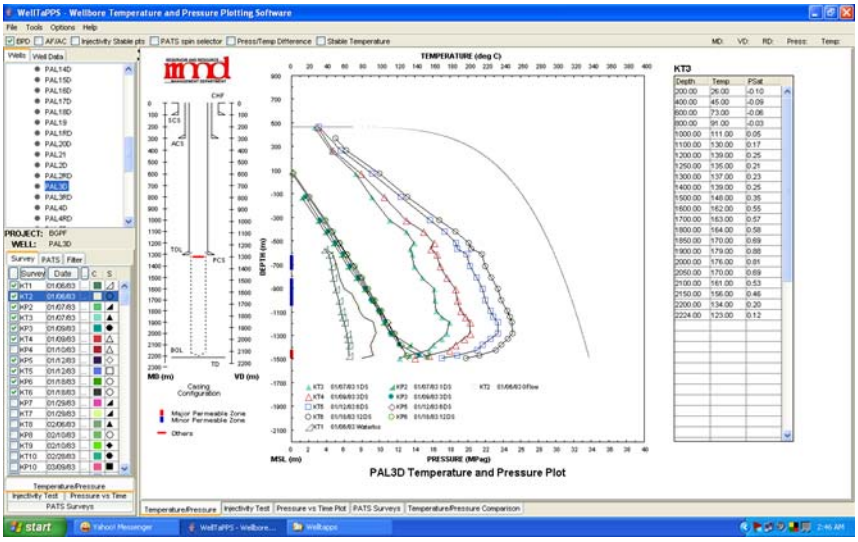

FIGURE 5: Screenshot from database application WellTaPPs

- Conceptual model from many researches including resource assessment of BacMan 1 (PNOC EDC, 1985) and BacMan 2 (PNOC EDC, 1989) done by scientists and engineers of PNOC EDC and field review by consultants (Mesquite Group et al., 1990);
- Reservoir parameters from work of Gerona (PNOC EDC, 1989), Castillo (Castillo, 1990), and Fajardo et al. (Fajardo et al., 2004);
- Evaluation of BacMan reservoir including description of pre-exploitation and field status, estimate of generating capacity, and a lumped-parameter model by Fajardo et al. (2004);
- Field monitoring data consisting of temperature and pressure logs, well production histories and pressure drawdown curves; and
- Geothermal database containing a collection of well tracks, temperatures, pressures, casing configurations, permeable zones, and blockages.

WellTaPPS, a web-based database application developed by reservoir engineers of PNOC EDC using Java, was used in this study to process BacMan data and facilitate revision of reservoir conceptual model. A screenshot of WellTaPPS is illustrated in Figure 5 showing multiple data sets of temperature, pressure, and casing data from many Oracle database tables as discussed by Esberto et al. (2005).

3.3 Physical characteristics

3.3.1 Geological overview

Reyes et, al. (1995) divides Bacon-Manito geothermal system into West and East BacMan. East BacMan is further subdivided into northern Manito lowlands and Pocdol highlands, about 10 km to the south. Within Pocdol highlands, eight geographical sectors are distinguished, namely: Inang Maharang (IM), Puting Bato (PB), Palayan-Bayan (PAL), Cawayan (CN), Tanawon (TW), Osiao, Pangas and Botong (OP) (Reyes et al., 1995).

Thermal manifestations such as warm to boiling springs, solfataras, areas of gas vents and cold altered ground, cover an area of 225 km^2. Neutral chloride hot springs with temperatures of 89°C to 96°C are found in Manito lowlands. Solfataras are found in Cawayan and Pangas, with areas of gas vents in Tanawon, south of Cawayan. In west BacMan, only cold to warm SO_4 springs and cold-altered grounds are found. The most recent volcanic events in Pocdol highlands occurred more than 40 thousand years ago. They are related to the formation of Tanawon and Cawayan craters, and extrusion

of Botong and Pangas domes. The youngest volcanics generally occur in regions of high subsurface temperatures, permeable formations, and active thermal manifestations (Reyes et al., 1995).

The wells in Palayan-Bayan intersected andesitic to basaltic lava flows and hyaloclastites, Late Miocene to early Pliocene limestones and calcareous breccias and an intrusive complex. The intrusive complex is a sequence of cross-cutting dikes intruding the volcanic and sedimentary formations. There are about six distinct dike compositions: monzogabbro, pyroxene gabbro/diabase, hornblende and/or pyroxene microdiorite, hornblende quartz microdiorite, monzodiorite and rare aplite. Cross-cutting relationships among dikes indicate multiple intrusive events (Reyes et al., 1995).

The major and oldest structure that has remarkable influence in the tectonic field setting of the field is NW-SE strike-slip fault which is believed to be an extension of the Philippine rift. Other geological structures defined in the area include volcanic centres and a collapse structure.

3.3.2 Geophysical overview

A recent review of the geophysical data of BacMan came up with an updated but arbitrary geophysical boundaries following renewed interest in expansion in Tanawon and Kayabon areas, south and north of Inang Maharang respectively. The interpreted geophysical boundaries are based on the 1999 and 2001 magneto-telluric (MT) data (Layugan, 2008). The boundaries were drawn using contours of resistivity anomalies and elevations of the base of conductive zones.

The geophysical boundaries enclose an anomaly covering BacMan and another in Kayabon located northwest of BacMan. The boundary in BacMan covers an area of approximately 26 to 36 km^2. The provisional boundary in Kayabon covers a geophysical anomaly from 12 to 18 km^2. In Figure 6, an area proximal to the interpreted geophysical boundary in BacMan based on MT survey is considered in this study.

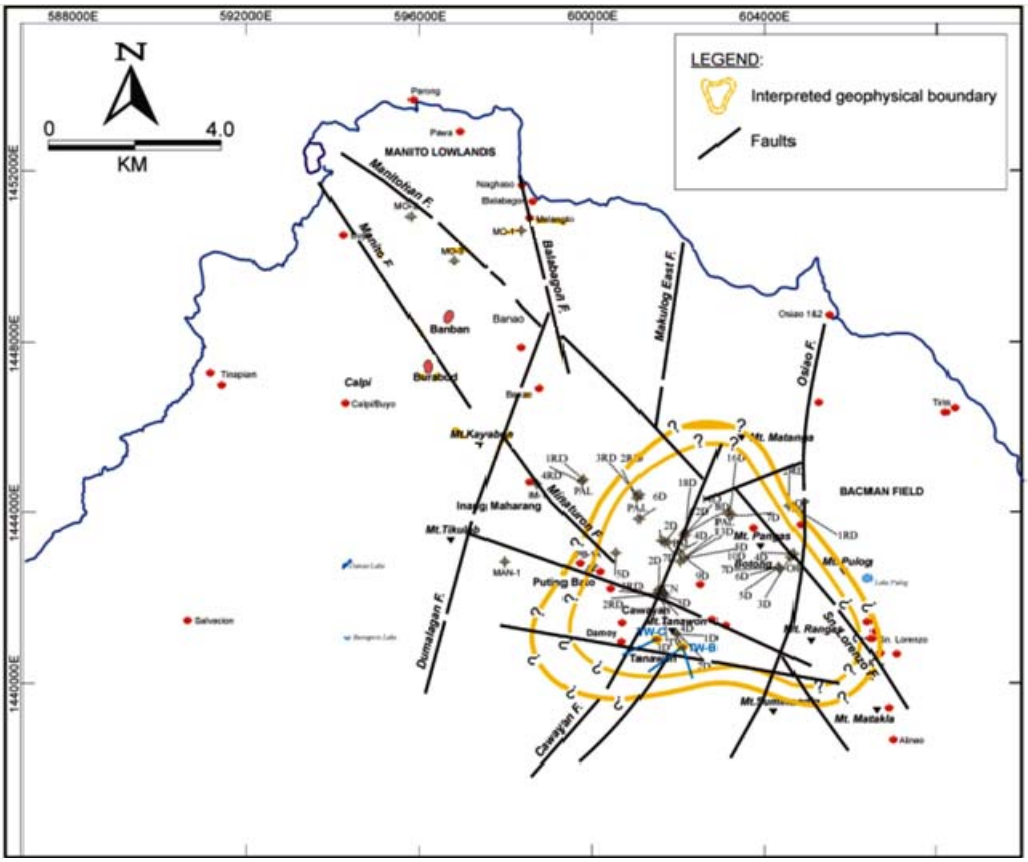

FIGURE 6: Geophysical boundaries based on MT (Layugan, 2008)

3.3.3 Geochemical overview

Highest chloride concentration is observed in eastern sector of Palayan-Bayan where upflow zone is postulated. Isoquartz temperature contours give highest value of 290°C in eastern Palayan-Bayan sector which is lower than the highest measured temperature of 326°C. Nevertheless, geochemical field trends are in generally in good agreement with measured temperature trends as shown in Figure 7.

Deep reservoir boiling is caused by a shift from less permeable sedimentary Gayong sedimentary formation to more permeable volcanics in Palayan-Bayan sector. By the time fluid reaches Cawayan area at well CN-1, Inang Maharang and PAL-1RD, fluid has already degassed (Solis et al., 1994).

Meanwhile, highest gas concentrations, in the form of CO_2, H_2S, and residual gases are measured in Botong suggesting proximity to heat source. Consistent with isotope data, Botong waters, especially from wells OP-3D and OP-6D, are most O^{18} shifted from meteoric water line (Solis et al., 1994).

The preferential major outflow direction is towards the north-northwest where fluids emerge as springs in the Manito lowlands. The southeasterly fluid flow direction towards Rangas is facilitated by structural permeabilities related to Makabug, Botong, and Dome faults. These fluid flow directions are consistent with magnetotelluric and geochemical data which define major outflows to the northwest and southeast towards Manito lowlands and Sorsogon, respectively (Ramos, 2002).

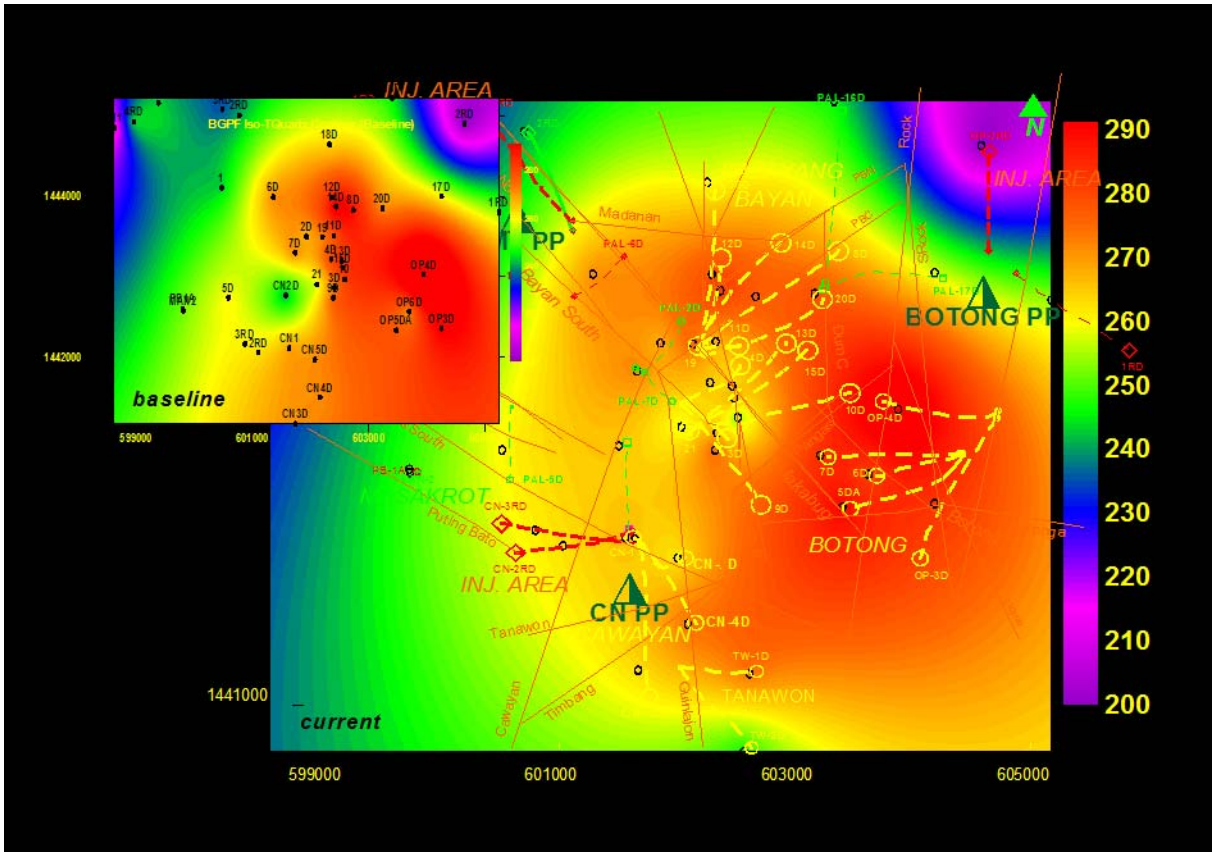

FIGURE 7: T_{quartz} contour (PNOC EDC, Geoservices, 2003)

Uniform chloride concentration is observed from north to south in Palayan-Bayan sector. In Figure 8, it is seen that chloride concentration decreases going westward, faster going southwest compared to northwest suggesting that deep reservoir fluid is barred from mixing with dilute meteoric water by a "caprock" or a layer of impermeable formation or mineral deposition.

Majority of BacMan wells discharge near neutral sodium chloride water containing 0.9 to 1.04% by weight NaCl before flash. Chemical characteristics of discharge fluids, however, vary laterally and vertically fieldwide as shown by downhole samples and chemistry changes during output tests. At shallower depths, different types of fluids are encountered such as dilute neutral sodium chloride fluids, neutral bicarbonate-rich low chloride fluids; and acidic sulfate-rich fluids (PNOC EDC, 1985).

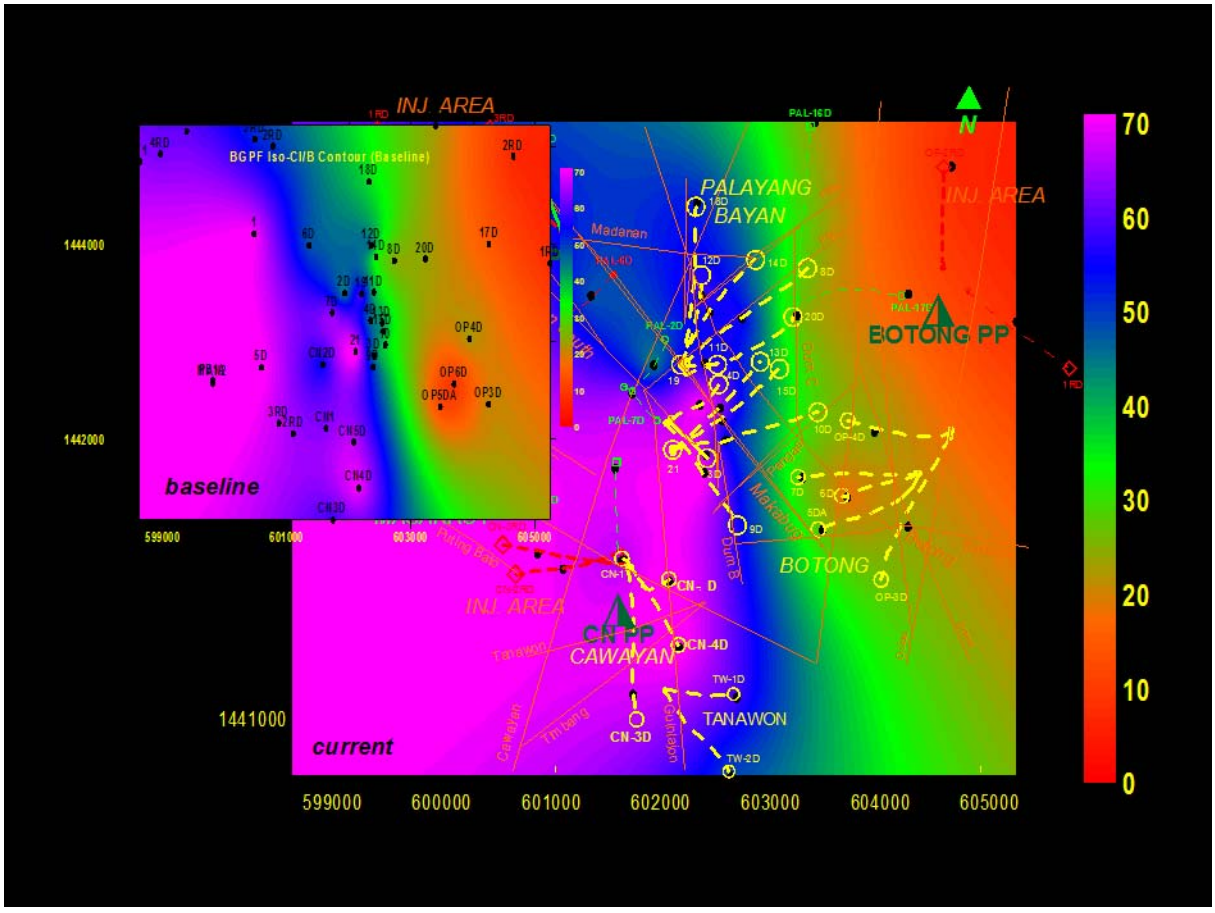

FIGURE 8: Chloride/boron contour (PNOC EDC, Geoservices, 2003)

After producing BacMan field for several years, reservoir response based on chemical and physical changes are described by: (1) boiling and mixing with low boron fluids from PAL-6D area; (2) boiling and vapour formation; (3) mixing with Masakrot fluid from west; and (4) dilution with cooler acid-SO_4 fluids from shallow feed zones in Cawayan area (See, 2001). Except for dilution with cooler acid-SO_4 fluids, all processes are beneficial to BacMan reservoir as indicated by stable chemical and physical trends. Recharge fluids provide pressure support. No injection return has been detected in production wells (See, 2001& 2004).

3.3.4 Analysis of temperature and pressure logs

After drilling, geothermal wells in the Philippines undergo a completion test consisting of the following set of standard procedures: (1) sinker bar survey to measure maximum clear depth; (2) waterloss (temperature) survey to identify permeable zone/s; (3) injectivity test to measure downhole pressure at different injection rates and estimate an injectivity index ($\Delta_{\text{injection rate}}/\Delta_{\text{downhole pressure}}$); (4) fall-off test which measures pressure decline subsequent to closure of injection. Analysis of fall-off tests determines reservoir permeability-thickness product (kh) and shows whether well productivity is affected by wellbore effects (skin) or by the reservoir at large.

Physical logs of temperature and pressure generated by WellTaPPs are analyzed to determine stable formation temperature and pressure for each well as a function of depth. Some downhole temperature

logs are affected by internal wellbore flows requiring thorough interpretation before they can be used. For some cases, a Horner method contained in computer program Berghiti is used to estimate formation temperature from recovery data. Berghiti uses temperature recovery data and extrapolates heat recovery curve to infinite time. Berghiti is part of a reservoir engineering software package Icebox developed by Orkustofnun partly for the UNU Geothermal Training Programme (Arason et al., 2004).

For some wells suspected of having two-phase conditions, the boiling point with pressure and temperature curves are used to establish formation temperature and pressure (Björnsson, 2004). FORTRAN code BOILCURV from Icebox (Arason et al., 2004) is used to generate boiling point with depth curves generally at a few hundred meter depth interval, that correspond to top-layers of geothermal reservoir, next to its caprock.

Downhole pressure logs collected during thermal recovery offers a firm estimate of the so-called pivot point. For wells with high gas content, the pivot point may be the only point where correct formation temperature and pressure is observed since true formation temperature and pressure above and below pivot point may be masked by the presence of gas or cold circulating fluid. In such cases, it is helpful to use the pivot point as a match point for boiling point with depth curves provided of course that measured temperature at the pivot point depth corresponds to saturation temperature at the pivot point pressure.

Stable temperature and pressure are synthesized using UNIX scripts with embedded FORTRAN interpolation codes from Björnsson (2004) and Generic Mapping Tool (GMT) software by Wessel and Smith (2007). Various planes and vertical sections of reservoir pressure and temperature distribution are generated using UNIX scripts planesP and planesT, and vsection**.** These images indicate direction of mass and heat flow and boundary conditions in the reservoir (see Section 3.4).

More than 300 Kuster temperature and pressure logs from 40 wells were considered in this study for determining rock temperature and pressure. Typical rock temperature and pressure profiles found in BacMan wells are discussed in this part of the study.

BacMan wells characteristically have a linear temperature gradient along cased-off zone due to conductive heating in the low permeable caprock and a convective flow which is marked by sharp drop in temperature gradient along open borehole section. Bottom of linear gradient profile is defined at approximately –500 mRSL where most production casing shoes are set. Temperature gradient estimated from open wellbore section is 83°C/km.

Rock temperatures and pressures in some wells, e.g. in wells PAL-8D and PAL-10D, follow boiling with depth profiles for long depth intervals (Figure 9,10). These wells are gassy and can continuously discharge pure steam or steam and non-condensible gas mixture when kept open. Rising steam in the well condenses at upper portion of casing while gas in stream remains and continues to rise up the well. Gas

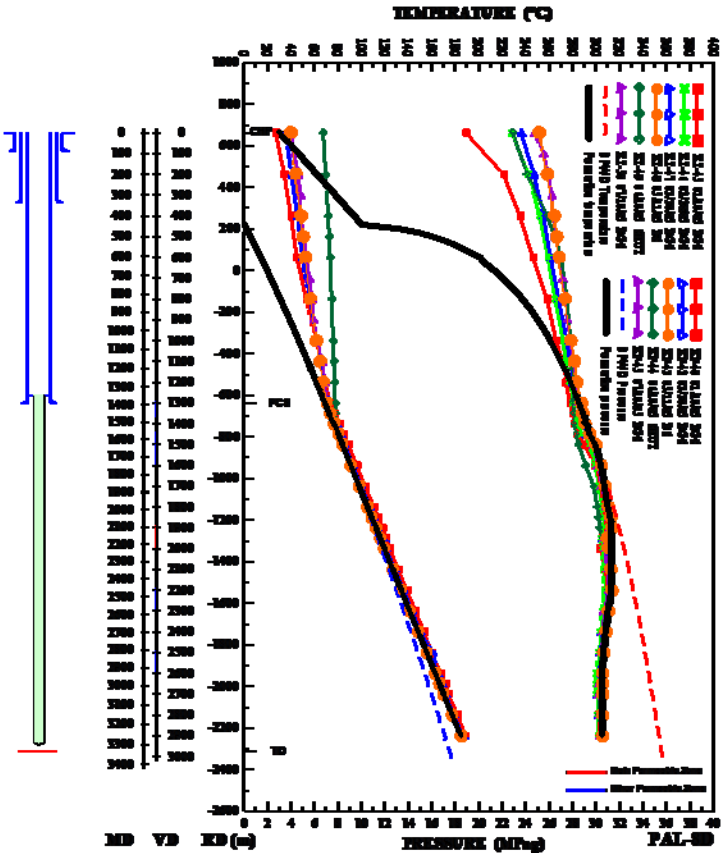

FIGURE 9: PAL-8D rock temperature and pressure

accumulation results in high pressure at wellhead as observed in pressure profiles. PAL-8D, as shown in Fig 9, has a total depth of 2973 mVD (3333.1 mMD).

Waterloss surveys during the completion test detected a major zone at 1900-2000 mVD and several minor zones at 1300-1370 mVD, 1450-1600 mVD, 2200-2300 mVD, and 2500-2600 mVD. Compared to other BacMan wells, PAL-8D has a very high injectivity index of 147 L/(s MPa) and permeability-thickness product (20 Darcy-meters). Boiling water enters well at its major feed at 1900-2000 mVD and rises, boiling further as pressure drops. Highest temperature of 313°C is observed at 1900 mVD. Temperature and pressure profiles follow boiling point with depth profile from 2000 mVD upwards.

PAL-10D, as shown in Figure 10, has a total depth of 2485.1 mVD (2930 mMD). It has an injectivity index of 31 L/(s MPa) at vacuum wellhead pressure. A major loss zone was detected at 1700-1800 mVD and several minor zones at 1150-1250 mVD, 1400-1500 mVD, 2100-2200 mVD, and 2400 mVD. Analysis of well test data gave a permeability-thickness product of 5.3 Darcy-meters and a negative (-4.7) skin. Drilled towards upflow zone, hottest temperature of 326°C is measured in this well. PAL-10D follows the boiling-point with depth profile.

A nearly isothermal profile associated with downflowing fluids is observed in BacMan, like in wells PAL-3D, PAL-6D, PAL-9D and PAL-13D to name a few. When these wells are shut or throttled, fluid in well enters permeable zone at upper part and cross flows to bottom well section masking true temperatures in the process. In this case, downflow occurs only in wellbore and does not truly represent natural-state of reservoir. In this study, many of the wells only have formation temperature defined to depth of shallow feed zone.

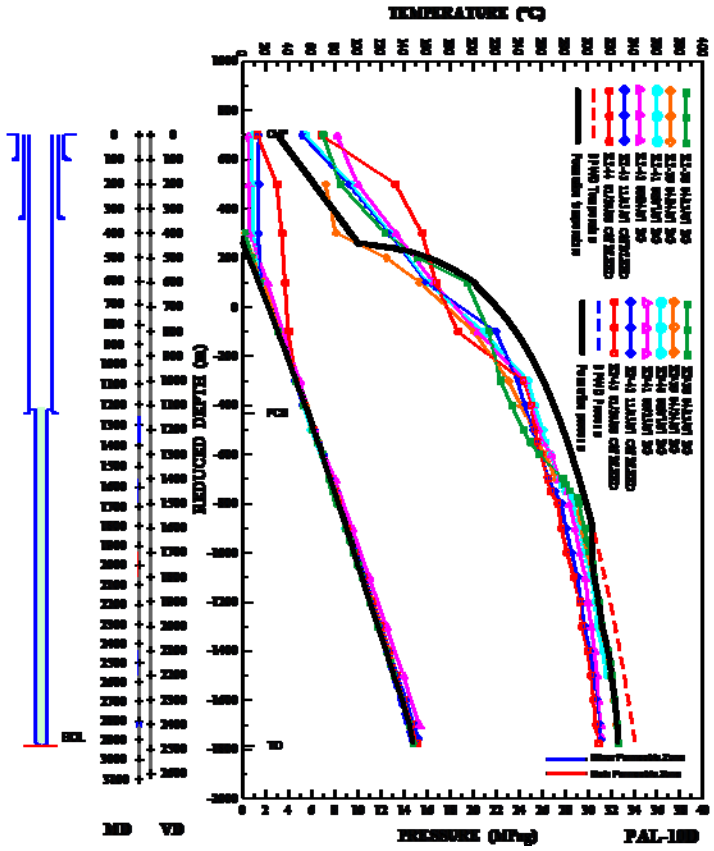

FIGURE 10: PAL-10D rock temperature and pressure

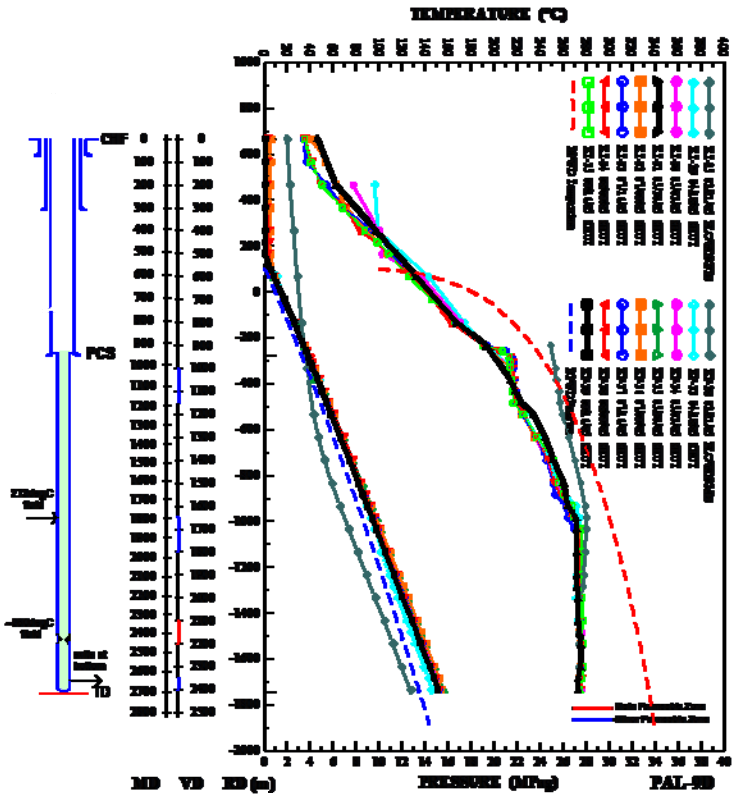

FIGURE 11: PAL-9D rock temperature and pressure

PAL-9D, as shown in Figure 11, has a total depth of 2409.3 mVD (2697.8 mMD). It has an injectivity index of 17 L/(s MPa) at vacuum wellhead pressure. A major loss zone is detected at 2100-2200 mVD and several minor zones at 1000-1150 mVD, 1650-1800 mVD and 2350-2400 mVD. Analysis of well test data gave a permeability-thickness product of 2.5 Darcy-meters and a negative (-1) skin. Hottest temperature measured in the well is 280°C at 1650 mVD. Temperature profiles are nearly isothermal (272°C) from 1650 mVD to bottom due to downflowing fluid from 1650-1800 mVD. Temperature log at flowing condition (KT-25) suggests a temperature of 280°C near its major feed zone.

Downflowing profile of temperature is typical along resource boundary, e.g. as observed in injection wells IM-1, PAL-1, PAL-1RD, PAL-2RD and PAL-3RD which are delineating northwest boundary leading to outflow area and also observed in well PAL-16D which is delineating northern resource boundary. Downflowing profile is displayed by wells intersecting edges of reservoir with a classic mushroom-shaped temperature distribution. In the outflow zone, deeper reservoir has lower pressure potential than shallow one due to cooler water entering convective cells beneath these outflow areas where it is heated to high temperatures. The heated water rises through other faults and its place taken by incoming meteoric water.

An example is IM-1, as shown in Figure 12, drilled to a total depth of 2553.3 and is located at outflow region of BacMan. Completion test detected a major permeable zone at 850-1000 m and minor permeable zones at 1300-1400 m and 2400-2550 m. Well test analysis gave an injectivity index of 32 L/(s MPa), permeability-thickness product of 2 Darcy-meters, and a negative (-4) skin.

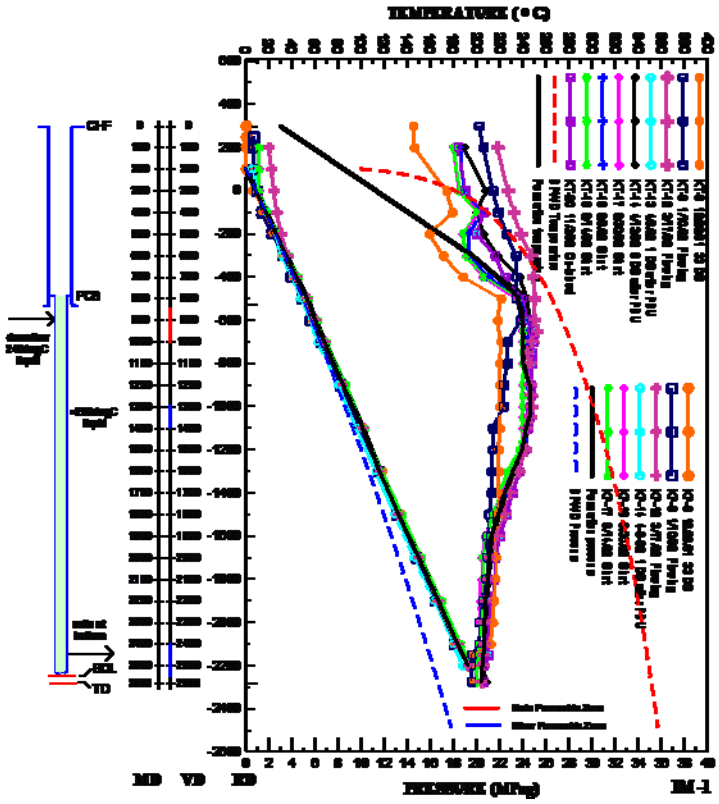

FIGURE 12: IM-1 rock temperature and pressure

A conductive gradient is observed up to production casing shoe. At shut-in condition, 240°C liquid flows from 850 m down to 2400 m resulting in a proximal isothermal profile as observed from shut survey KT-19. Downflowing liquid loses some heat conductively to wellbore vicinity hence cools slightly as it flows down. Hotter fluid at 1300 mVD, which can be greater than 252°C as observed from flowing survey KT-12, is also being suppressed by downflow. At flowing condition, 205°C fluid at bottom flows and is joined by hotter fluid at 1300 m resulting to a higher temperature of 252°C.

PAL-16D, as shown in Figure 13, has a total depth of 2789.5 mMD (2314.2 mVD) and has it tract directed towards north of Palayan-Bayan. A major permeable zone is detected at 2100-2200 mVD and minor zones at 1700-1800 mVD and at bottom. PAL-16D has an injectivity index of 14.6 L/(s MPa), permeability-thickness product of 7 Darcy-meters, and a negative skin (-3.8). Stable formation temperature profiles show a downflow from 1750 mVD to bottom indicating this well may have delineated northern boundary of resource. PAL-16D is currently being used as a pressure monitoring well.

Complete information regarding rock temperature and pressure profiles and basic well data are included in Appendices 1 and 2 respectively.

3.4 Conceptual model

Synthesizing physical properties from geology, geochemistry, geophysics and including analyses of temperature and pressure logs, a conceptual model is proposed and used in this study.

In this conceptual model, a plume is clearly observed from the temperature planes and vertical temperature sections (Figure 14, 15, 18, 20). The source of upwelling fluid is identified by presence of fumaroles in Mt. Pangas and steam-heated waters at high elevation. Deep drilling has confirmed that reservoir fluid flows up centrally between wells OP-4D and PAL-10D. This upflowing fluid has a maximum logged temperature of 326°C.

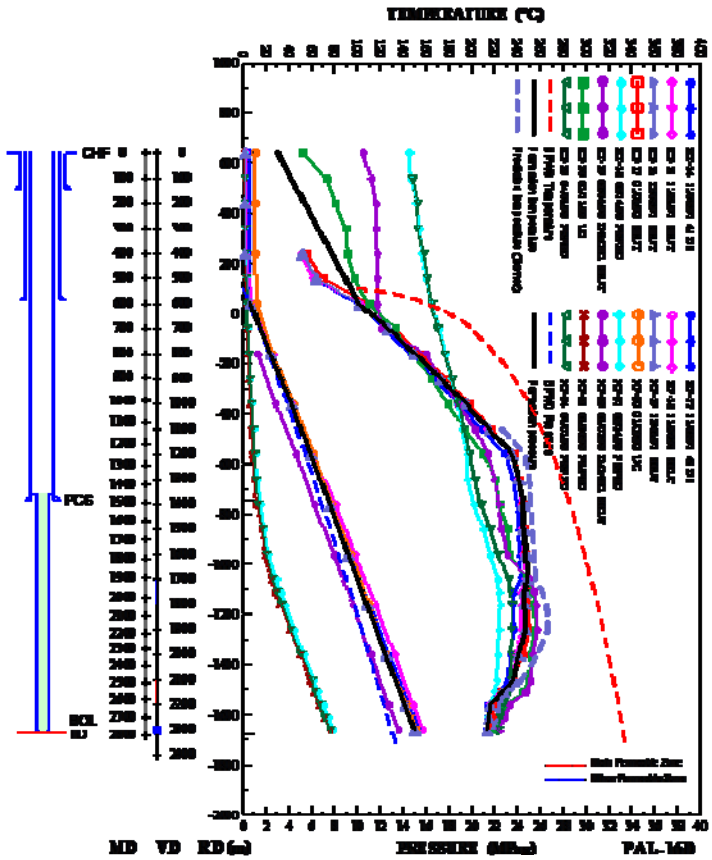

FIGURE 13: PAL-16D rock temperature and pressure

Caprock seals upper part of Palayan-Bayan and creates a cap trapping non-condensible gases and steam from beneath (Castillo, 1990). A conductive temperature gradient is observed from temperature profiles within the upper part of BacMan wells inferring this low permeability caprock (Appendix 1).

According to Castillo (1990), the presence of youthful volcanic rocks from Tanawon and Cawayan and mineral geothermometers done on well OP-3D also indicate a minor upflow in Cawayan.

Ramos (2002) claims that the west-northwest (W-NW) and northwest-southeast (NW-SE) trending faults have great influence on flow pattern. The preferential major outflow direction is towards the north-northwest where alkali-chloride fluids emerge as hot chloride springs at Naghaso, Pawa, and in Manito lowlands as observed by Solis et al. (1994). Inang Maharang and reinjection area of Palayan-Bayan lies along outflow path. The outflow towards Inang Maharang is observed from Figure 18 as an elongated plume towards the northwest and is supported by the downflow observed in wells drilled in this area like PAL-1, PAL-1RD, PAL-3RD, PAL-4RD, and IM-1 (*Appendix 1*). According to Ramos, the southeasterly fluid flow direction towards Rangas is facilitated by structural permeabilities related to Makabug, Botong, and Dome faults. These fluid flow directions are consistent with magnetotelluric and geochemical data which define major outflows to the northwest and southeast towards Manito lowlands and Sorsogon, respectively.

Northern boundary of resource has been delineated by PAL-16D and is marked by a downflow as observed in the temperature profiles *(Appendix 1)*. As seen in Figure 14 and 15, the northern boundary delineation is marked by a 220°C isotherm in the temperature planes. From Figure 14 and 15, it can be seen that the southeast, an open boundary remains as field temperature and pressure contours have not changed with addition of data from newly-drilled wells TW-1D and TW-2D. Unusually high pressures in Osiao-Pangas wells OP-1RD and OP-2RD manifest presence of a geologic barrier between Palayan-Bayan and Osiao-Pangas/Botong (Figure 16).

A gas-rich vapour zone exist from -400 to -850 mRSL of Palayan-Bayan and Botong as seen from the temperature and pressure profiles of Palayan-Bayan (PAL-8D, PAL-10D, PAL-11, and PAL-20D) and Botong wells (OP-4D and OP-6D) (Figures 17-20). Two-phase expansion in Palayan-Bayan is

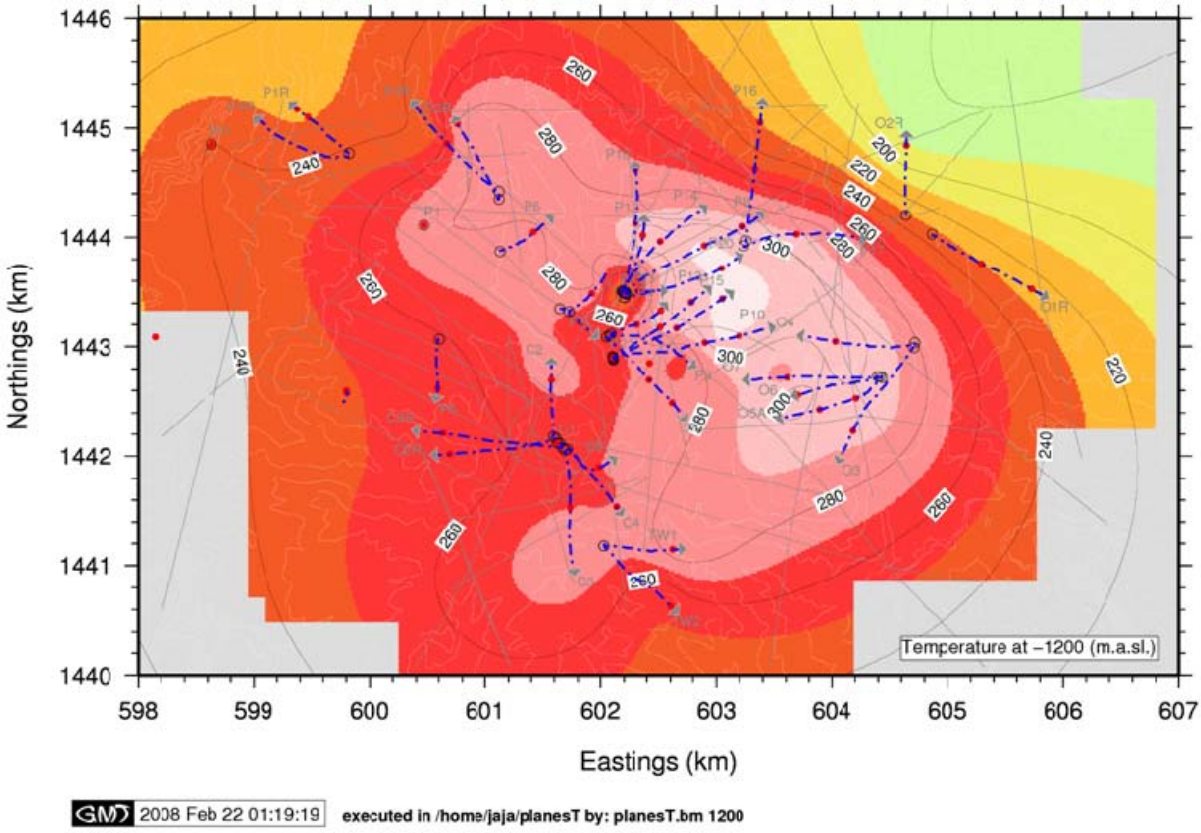

FIGURE 14: Temperature distribution at -1200 mRSL

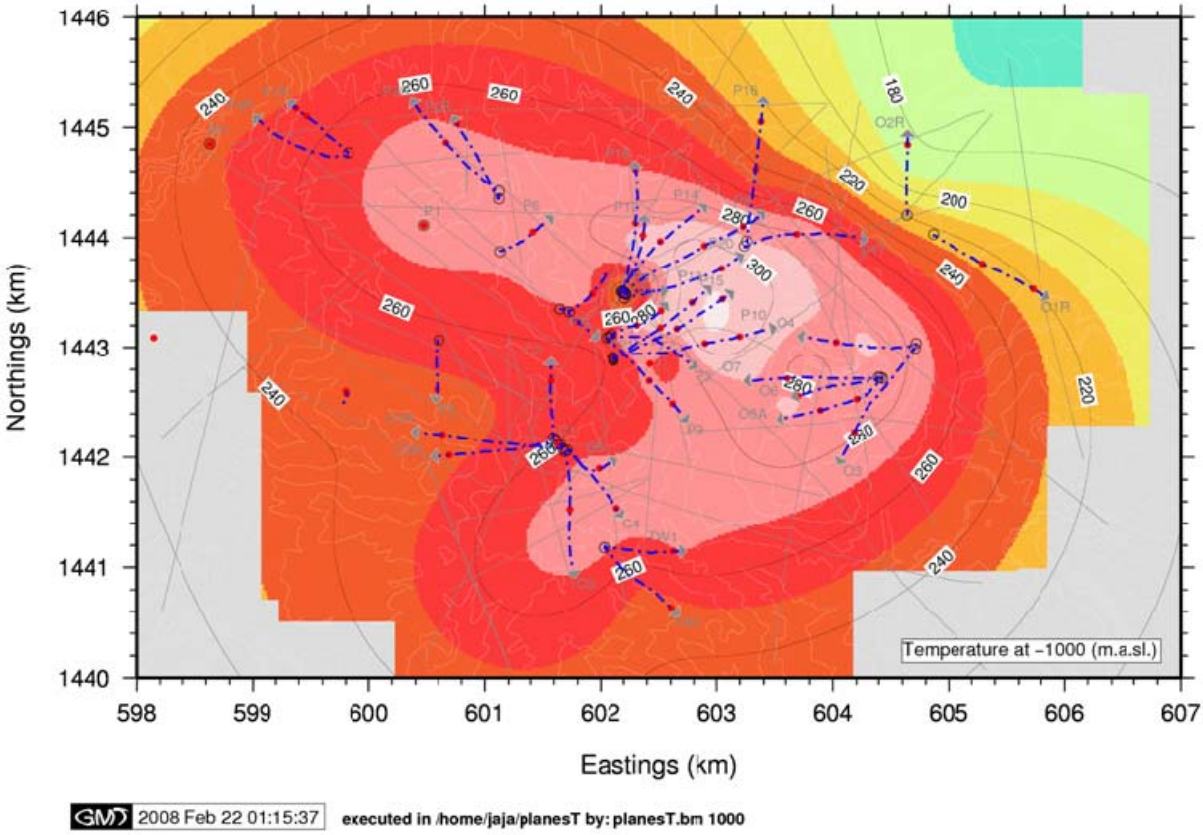

FIGURE 15: Temperature distribution at -1000 mRSL

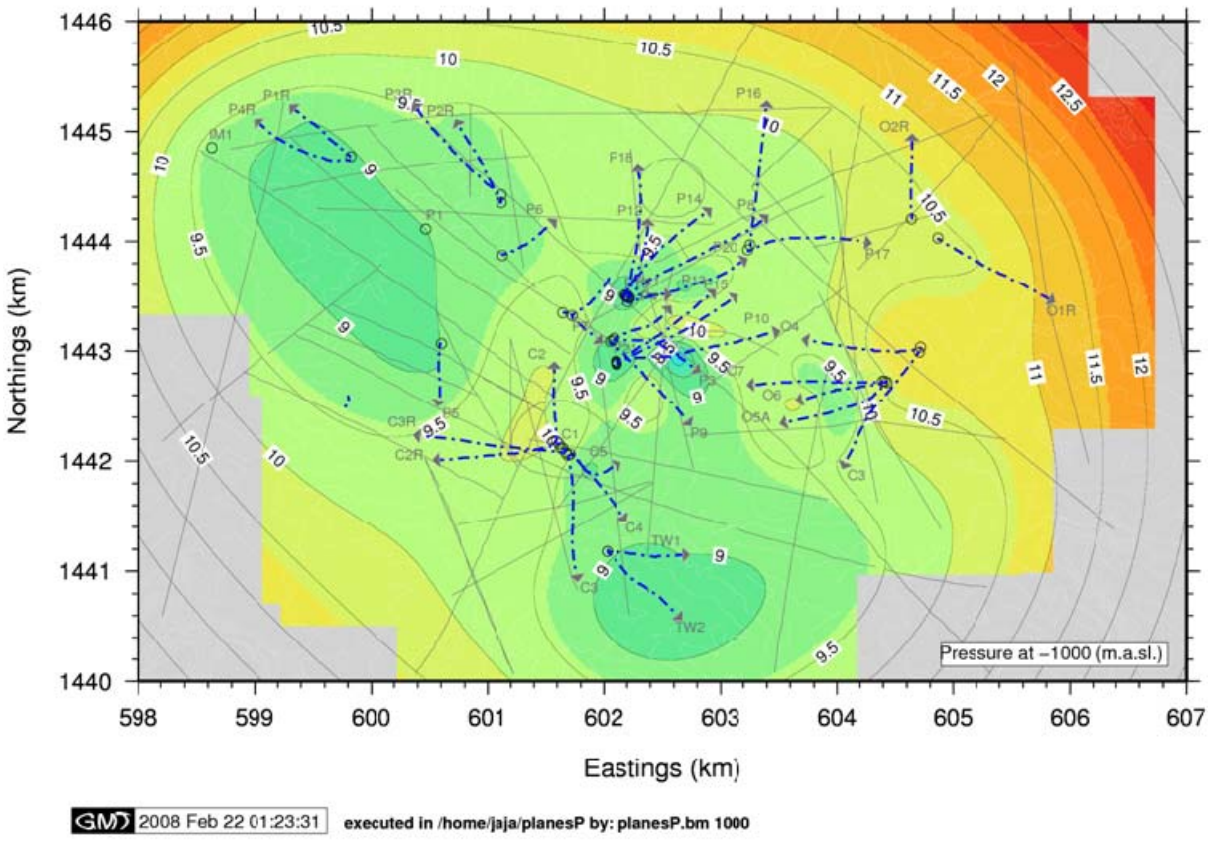

FIGURE 16: Pressure distribution at -1000 mRSL

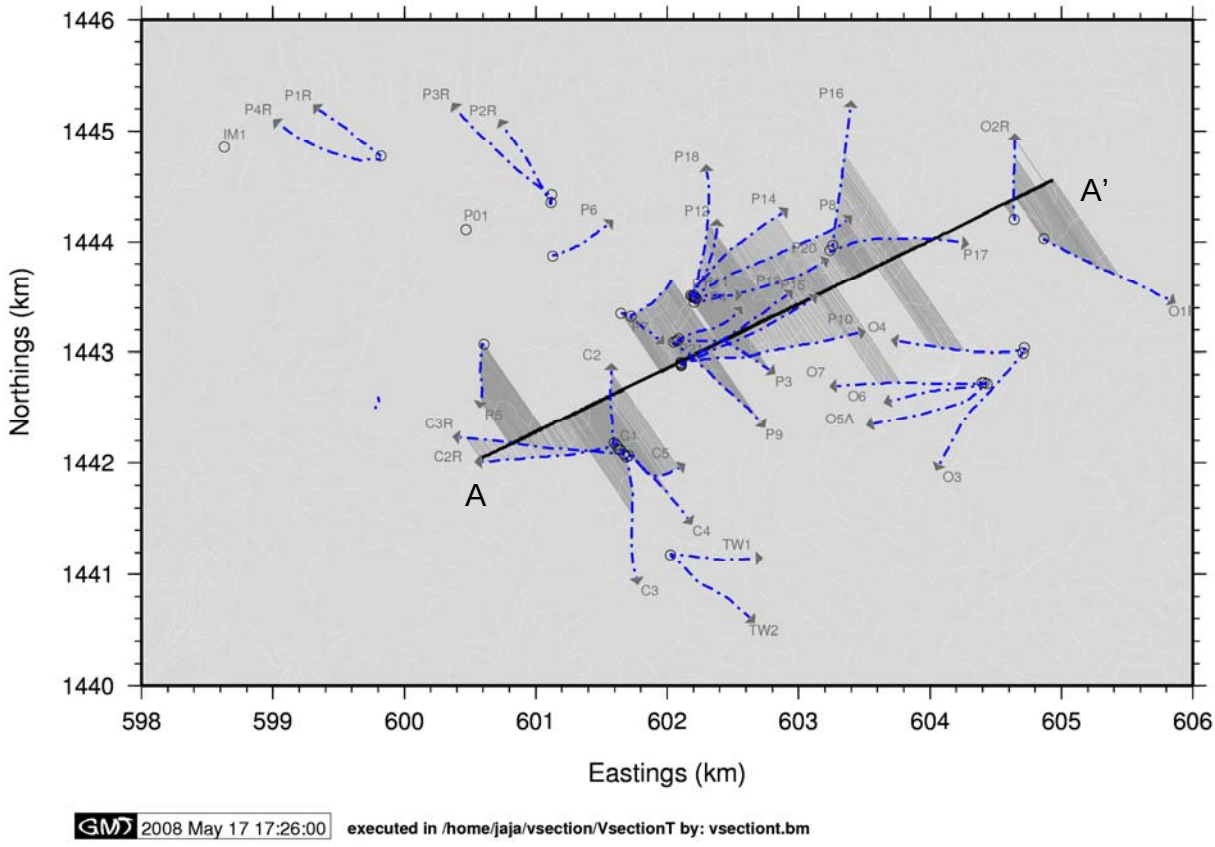

FIGURE 17: Projection plane A-A'

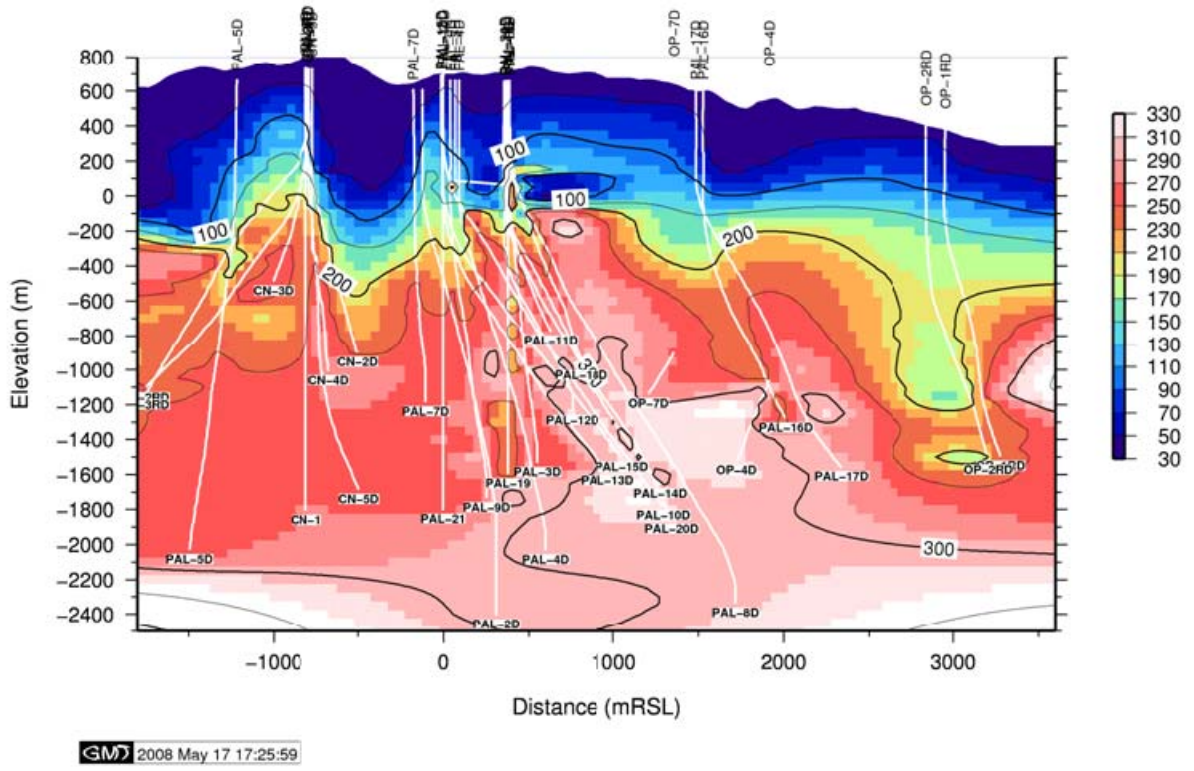

FIGURE 18: Temperature contour along A-A

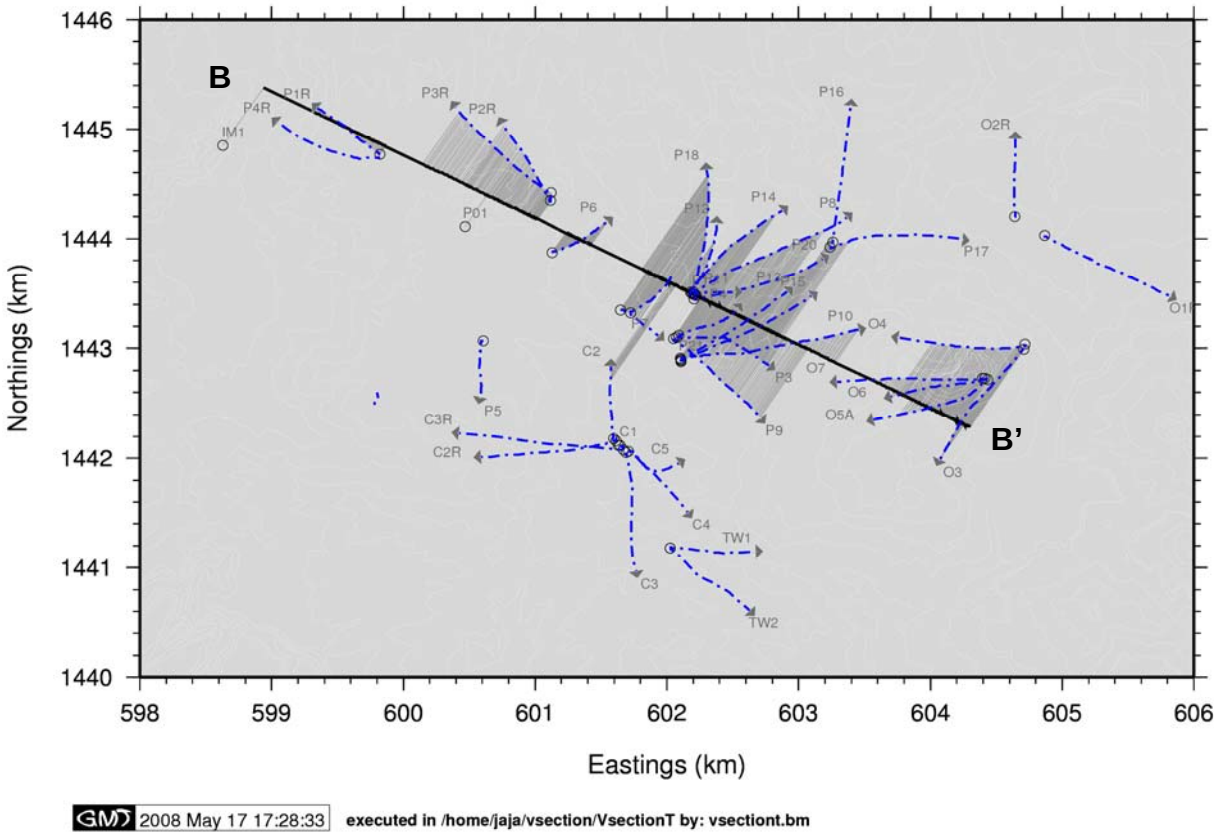

FIGURE 19: Projection plane B-B'

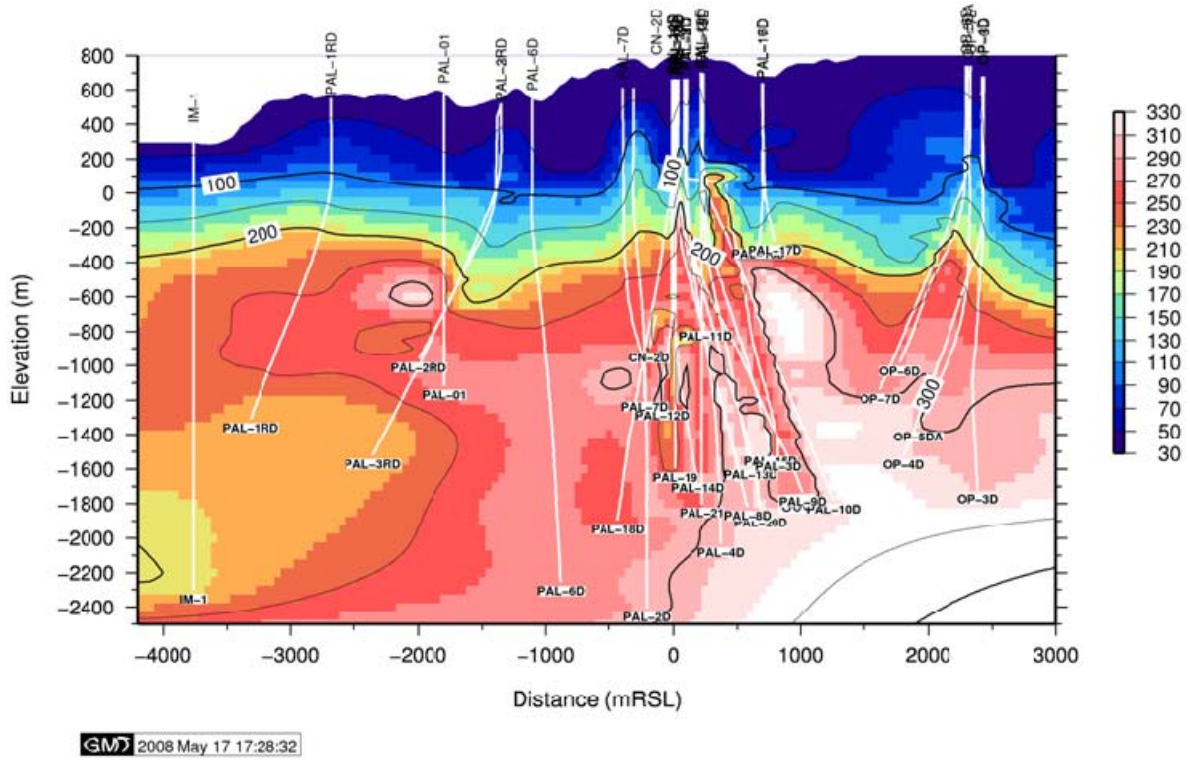

FIGURE 20: Temperature contour along B-B'

delineated based on temperature and pressure data from 1998. The original two-phase in Palayan-Bayan and in Botong has progressed with field exploitation. Expansion of two-phase region in the areas of PAL-8D in Palayan-Bayan and in Botong, as seen in Figure 21, is in agreement with observed pressure drawdown. The two-phase expansion may have slowed down with the entry of relatively lower temperature fluids from Masakrot (Fajardo et al., 2004).

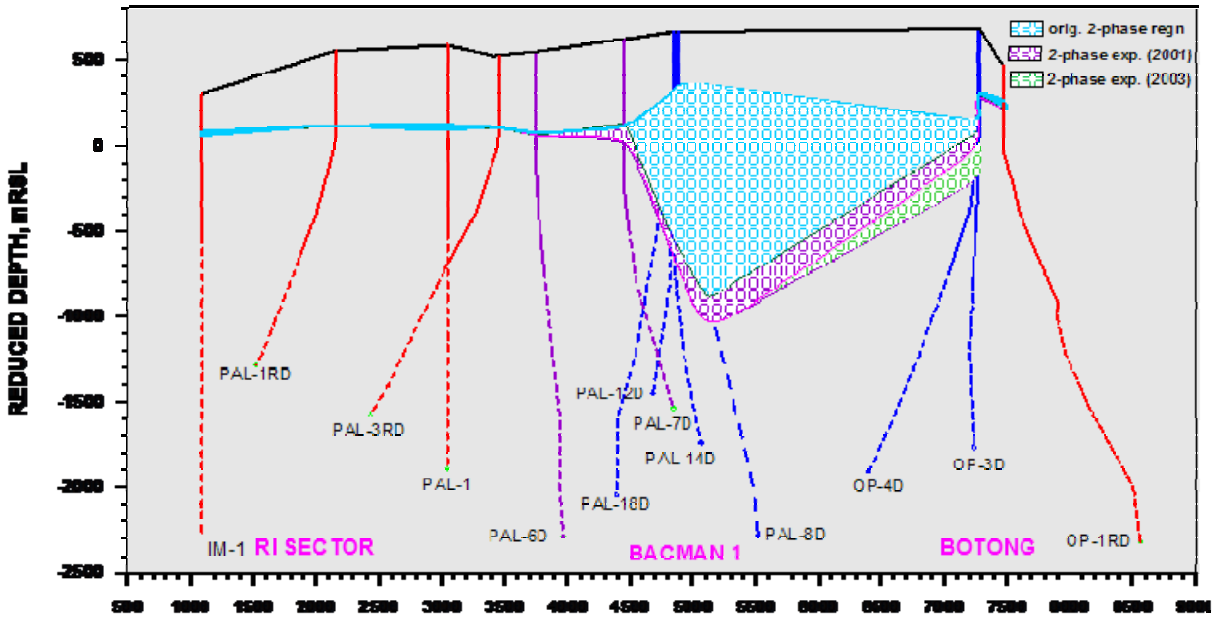

FIGURE 21: Cross-section showing two-phase zone (Fajardo, 2004)

4. VOLUMETRIC MODEL

Volumetric method using simple stored heat models, adapted from mineral exploration and oil industry, can provide a simple and robust approach for estimating generating capacity of a geothermal reservoir and can give useful estimates even few wells are drilled. Volumetric method is accepted worldwide in determining a geothermal resource's initial generating potential; often used as a first stage assessment when data is limited. Generating potential of BacMan prior to start of production was estimated using volumetric method as discussed in PNOC EDC (1985).

4.1 Theory

Volumetric method uses conservation of mass and heat principles but does not account for boundary recharge as reservoir pressure declines with mass withdrawal. Volumetric method is about calculation of total heat energy stored in a volume of rock as compared to some reference temperature. For power generation purposes, reference temperature is also referred to a rejection temperature or the minimum temperature at which geothermal fluid is suitable for power generation; a temperature of ≥180°C is used by PNOC EDC (1985). Total heat energy is the sum of energy stored in rock matrix and thermal energy of fluid in rock pores and is given by:

$$E = E_{rock} + E_{fluid} \tag{2}$$

$$E_{rock} = V(1 - \emptyset)\rho_{rock}K_{rock}(T_{res} - T_{ref}) \tag{3}$$

$$E_{fluid} = V\emptyset\rho_{fluid}K_{fluid}(T_{res} - T_{ref}) \tag{4}$$

Where ρ is density (kg/m^3); $\emptyset$ is porosity, K is heat capacity (J/kg°C), V is reservoir volume (m^3), T_{res} is reservoir temperature, reservoir (°C); T_{ref} is rejection temperature (°C).

The geothermal resource base is all heat below the earth's crust which is delineated by a geothermal resource area defined by structures, resistivity model, isotherms, and the conceptual reservoir model. The accessible resources base is the energy at shallow depths that can be tapped by drilling; presently around 3 km deep but this limit may be deepened to 4 to 5 km depending on the results from pending studies such as the Iceland Deep Drilling Project (IDDP website, 2008).

In Figure 22, it is shown that geothermal resource is a fraction of accessible resource base, represented by a recovery factor, which can be extracted economically and legally at some reasonable future time. Geothermal reserve is the part of a geothermal resource that can be extracted at present at a cost competitive with other energy sources (Axelsson, 2007). Correction factors are applied to arrive at a generating potential of a field. A recovery factor of 15% is used assuming that 15% of total energy in-place can be extracted economically. Percentage is based upon theoretical recovery factor as a function of reservoir porosity as discussed in Muffler (1977).

Overall efficiency factor is used in converting energy of hot fluids into useful energy (MWe or MWt) over a given time period. This conversion efficiency is basically a function of reservoir temperature while time period is generally a specified plant life. The intrinsic weakness of volumetric method lies in the assumption of a fixed recovery factor, while energy recovery strongly depends on the physical conditions and properties of the reservoir (Ketilsson, 2007). Permeability of the productive zone is the main factor that controls recovery factor and this is not taken into account in volumetric approach (Bodvarsson and Witherspoon, 1989).

Uncertainties inherent in parameters used in volumetric method are dealt with by using a Monte Carlo style of simulation (Sarmiento and Björnsson, 2007). Monte Carlo determines the probability distribution of capacities based on inferred range of input parameters. This statistical approach accounts for uncertainties in resource properties built-in the volumetric calculation by replacing them

with probability distribution functions. Excel spreadsheet was initially used for computations but later adopted statistical software @RISK due to availability of built-in probability distributions for assigning to computational values.

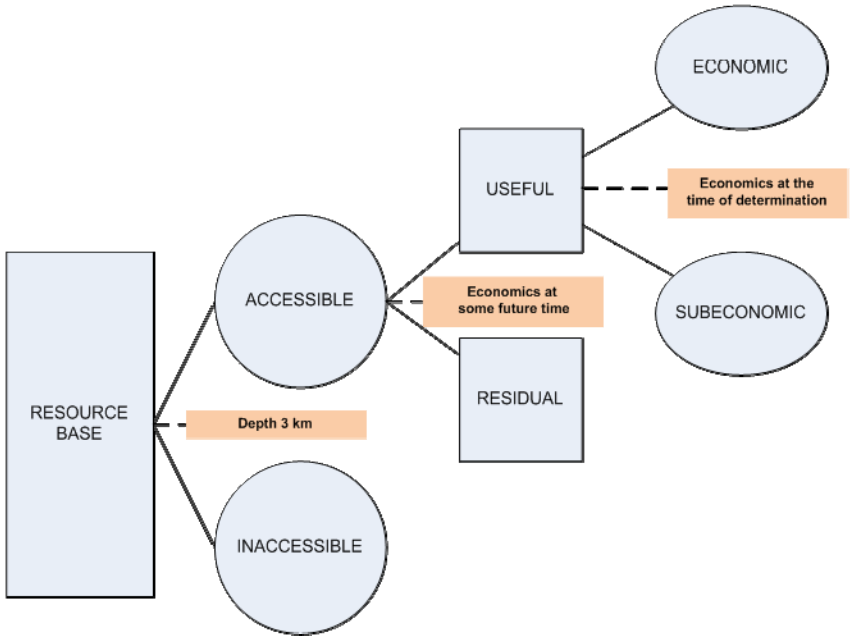

FIGURE 22: Subdivision of geothermal resources base adopted from Axelsson (2007)

4.2 Results

BacMan resource has been assessed from 1985 to1992 to estimate production capacity. Resource estimate is based on a single-phase reservoir model. Isotherms, resistivity contours, and structures identified in conceptual model are used to define resource boundaries. Resource assessment of 1985 estimated a production capacity of 118.8 MWe for 25 years while resource assessment of 1992 estimated a production capacity of 54 MWe for Cawayan and 62 MWe for Botong for 25 years respectively (Fajardo et al., 2004). In Figure 23, the resource blocks of estimates from 1985 and 1992 are shown.

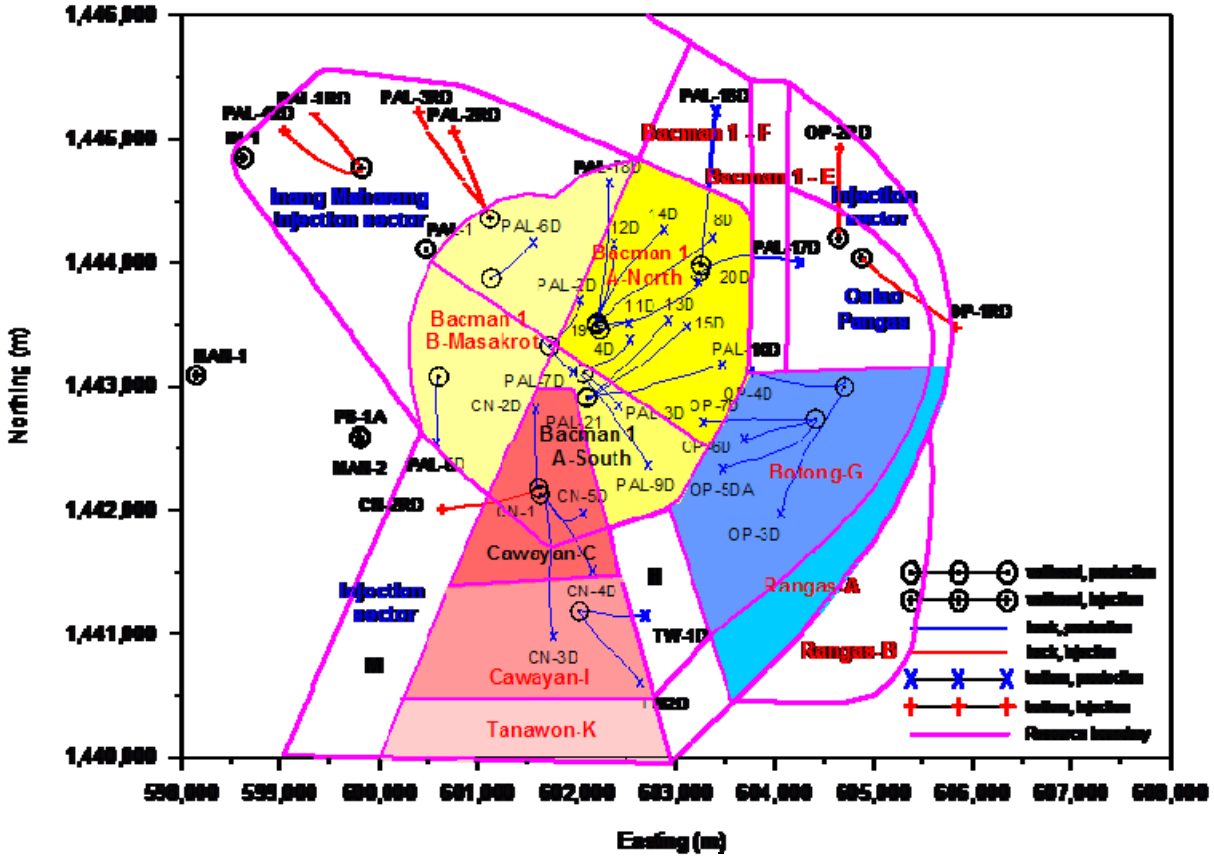

FIGURE 23: Resource blocks in early estimates (PNOC EDC 1985, 1992)

Potential of BacMan field was reassessed in this study using Monte Carlo method considering changes brought about by continuous field exploitation which include pressure and temperature changes and formation of a two-phase zone overlying the liquid reservoir. Two-phase layers are in Palayan-Bayan and Botong and are found where pressure decline is pronounced and a steam cap has initially existed. Parameters used in the reassessment are derived from work of Fajardo et al. (2004).

Probable area of two-phase zone, approximated from temperature and pressure measurements taken from wells, is estimated to be from 2.1 to 6.6 km^2 for Palayan-Bayan and 1.7 to 2.6 km^2 for Botong. Thickness of two-phase zone is estimated from the baseline water level down to about –800 mRSL where liquid zone starts. For Palayan-Bayan and Botong, two-phase layer is estimated to be from 600 m to 1000 m thick. For liquid region, minimum thickness is taken as depth of deepest well drilled less maximum thickness of two-phase zone. A 250- and 500-m drainage radius is added to get most likely and maximum thickness respectively.

For BacMan 1, resource area, as shown in Figure 24, ranges from 4.8 to 9.2 km^2. Some Cawayan wells are excluded from BacMan 1 since these wells are targeted towards and are extracting from Cawayan reservoir despite being collared in BacMan 1. BacMan 2 resource blocking includes Cawayan, Botong, and Rangas (Figure 24). Liquid reservoir is 1200 to 2100 m thick with a most likely thickness of 1650 m. Temperatures are based on current field contours. For BacMan 2, increase in temperature from earlier 270°C to present 280°C is based on temperatures observed from well OP-5D. For porosity, a mean value of 6% is assumed with standard deviation of 2%, from which a recovery factor of 15% was obtained from the chart of theoretical geothermal recovery factor as a function of porosity (Muffler, 1981). This chart may be found in *Appendix 3*.

The volumetric model is tapped for 25 years, from baseline of 2006 up to 2031. A load factor of 92.5%, based on a 30-day preventive maintenance period/year, is considered in the calculation. Reservoir properties are summarised for BacMan 1 and 2 (Tables 1, 2).

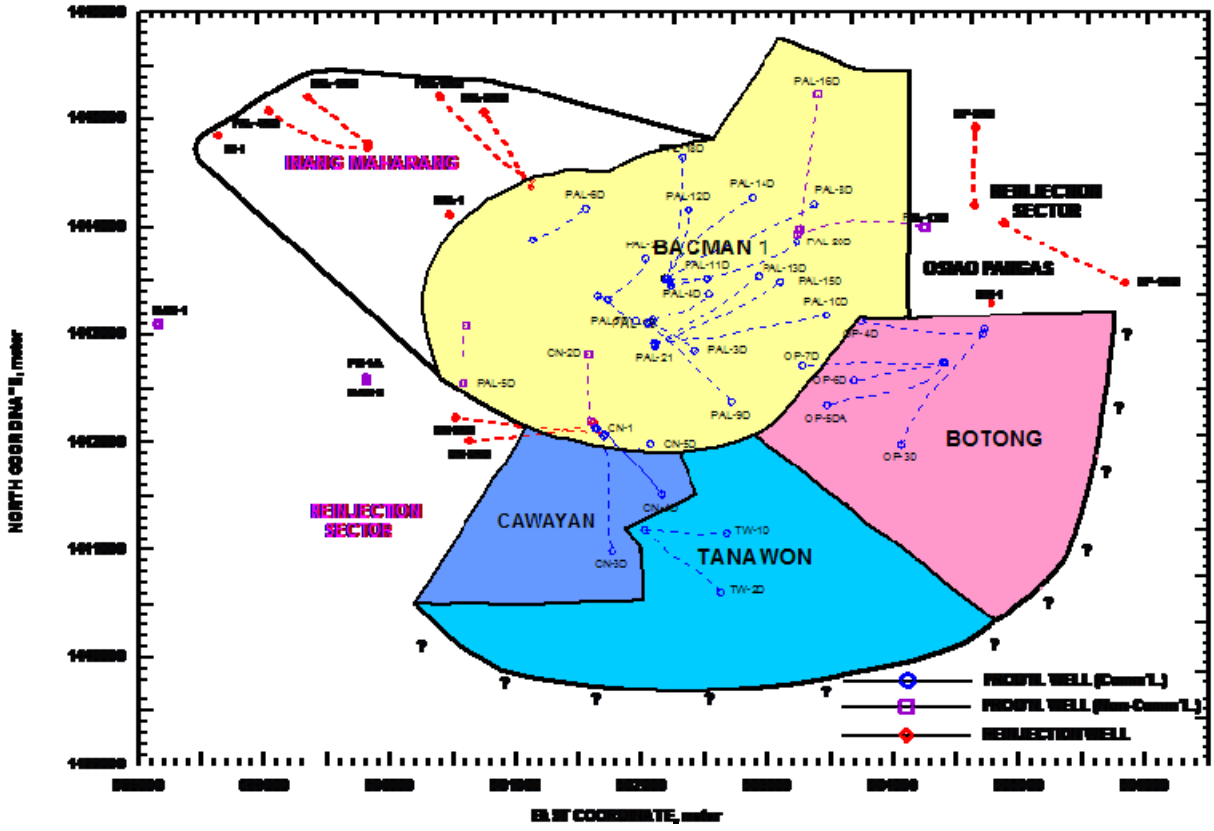

FIGURE 24: Resource blocks this study (Fajardo et al., 2004)

TABLE 1: Volumetric parameters for BacMan 1, two-phase condition

INPUT VARIABLES (USER DEFINED/DERIVED)	UNITS	MOST LIKELY	MIN	MAX	MEAN	SD	PROBABILITY DISTRIBUTION	
Two-phase volume								
Area	km^2	4.33	2.08	6.58			**4.33**	triangular
Thickness (2-phase zone)	m	800	600	1000			**800**	triangular
Rock density	kg/m^3	2700	2600	2800			**2700**	triangular
Porosity					0.06	0.02	**0.06**	lognormal
Recovery factor		0.15					**0.15**	=f(por)
Rock specific heat	kj/kg°C	0.9	0.8	1.0			**0.9**	triangular
Temperature	°C	240	220	260			**240**	triangular
Fluid density	kg/m^3	16.7	11.6	23.7			**17.3**	triangular
Conversion efficiency		0.11	0.105	0.118			**0.112**	=f(temp),triangular
Fluid specific heat	kj/kg°C	3.67					**3.67**	=f(temp)
Plant life	years	25					**25**	single value
Load factor			0.92	0.8	1.0		**0.91**	triangular
Rejection temperature	°C	180					**180**	single value
Liquid-phase volume								
Area	km^2	7	4.78	9.23			**7**	triangular
Thickness (liquid phase)	m	1950	1500	2400			**1950**	triangular
Rock density	kg/m^3	2700	2600	2800			**2700**	triangular
Porosity					0.06	0.02	**0.06**	lognormal
Recovery factor		0.15					**0.15**	=f(por)
Rock specific heat	kj/kg°C	0.9	0.8	1.0			**0.9**	triangular
Temperature	°C	270	260	280			**270**	triangular
Fluid density	kg/m^3	769.6					**769.6**	=f(temp)
Conversion efficiency		0.13	0.12	0.134			**0.127**	=f(temp),triangular
Fluid specific heat	kj/kg°C	5.13					**5.13**	=f(temp)
Plant life	years	25					**25**	single value
Load factor			0.92	0.8	1.0		**0.91**	triangular
Rejection temperature	°C	180					**180**	single value
Output variable								
Power capacity								
Two-phase	MWe	**11.1**						
liquid	MWe	**83.0**						
TOTAL	MWe	**94.1**						

Simulation results, as seen in Figure 25, show that there is 90% probability that the mean reserve of BacMan 1 is 94.1 MWe for an operating period of 25 years from 2006 to 2031; 11.1 MWe coming from steam-cap and 83 MWe from liquid reservoir. This is equivalent to 2352 MWe-years and a power density of 12.2 MWe/km^2. The probability of getting less than 46 MWe and more than 167 MWe from BacMan 1 is only 5%.

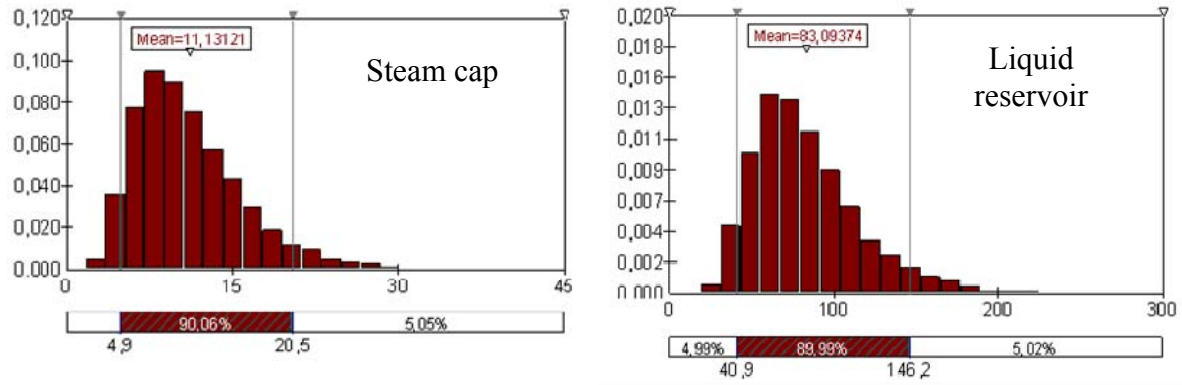

FIGURE 25: Histogram for power output (MWe) for BacMan 1

TABLE 2: Volumetric parameters for BacMan 2, two-phase condition

INPUT VARIABLES (USER DEFINED/DERIVED)	UNITS	MOST LIKELY	MIN	MAX	MEAN	SD	PROBABILITY DISTRIBUTION	
Two-phase volume								
Area	km^2	2.15	1.65	2.65			**2.15**	triangular
Thickness (2-phase zone)	m	800	600	1000			**800**	triangular
Rock density	kg/m^3	2700	2600	2800			**2700**	triangular
Porosity					0.06	0.02	**0.06**	lognormal
Recovery factor		0.15					**0.15**	=f(por)
Rock specific heat	kj/kg°C	0.9	0.8	1.0			**0.9**	triangular
Temperature	°C	240	220	260			**240**	triangular
Fluid density	kg/m^3	16.7	11.6	23.7			**17.3**	triangular
Conversion efficiency		0.11	0.105	0.118			**0.112**	=f(temp),triangular
Fluid specific heat	kj/kg°C	3.67					**3.67**	=f(temp)
Plant life	years	25					**25**	single value
Load factor			0.92	0.8	1.0		**0.91**	triangular
Rejection temperature	°C	180					**180**	single value
Liquid-phase volume								
Area	km^2	10.04	6.62	13.47			**10.04**	triangular
Thickness (2-phase zone)	m	1650	1200	2100			**1650**	triangular
Rock density	kg/m^3	2700	2600	2800			**2700**	triangular
Porosity					0.06	0.02	**0.06**	lognormal
Recovery factor		0.15					**0.15**	=f(por)
Rock specific heat	kj/kg°C	0.9	0.8	1.0			**0.9**	triangular
Temperature	°C	270	260	280			**270**	triangular
Fluid density	kg/m^3	769.6					**769.6**	=f(temp)
Conversion efficiency		0.13	0.12	0.134			**0.127**	=f(temp),triangular
Fluid specific heat	kj/kg°C	5.13					**5.13**	=f(temp)
Plant life	years	25					**25**	single value
Load factor			0.92	0.8	1.0		**0.91**	triangular
Rejection temperature	°C	180					**180**	single value
Output variable								
Power capacity								
Two-phase	MWe	**5.5**						
liquid	MWe	**100.8**						
TOTAL	MWe	**106.3**						

On the other hand, it is seen from Figure 26 that there is 90% probability that the mean reserve for BacMan 2 is 106.3 MWe for same period of operation; 5.5 MWe from two-phase and 100.8 MWe from liquid-phase. This is equivalent to 2657 MWe-years and a power density of 7.9 MWe/km^2. The probability of getting less than 52 MWe and more than 187 MWe from BacMan 2 is only 5%.

The regression sensitivity for power output indicates that power output is most sensitive to recovery factor, which in this case is a function of porosity, and then to resource area.

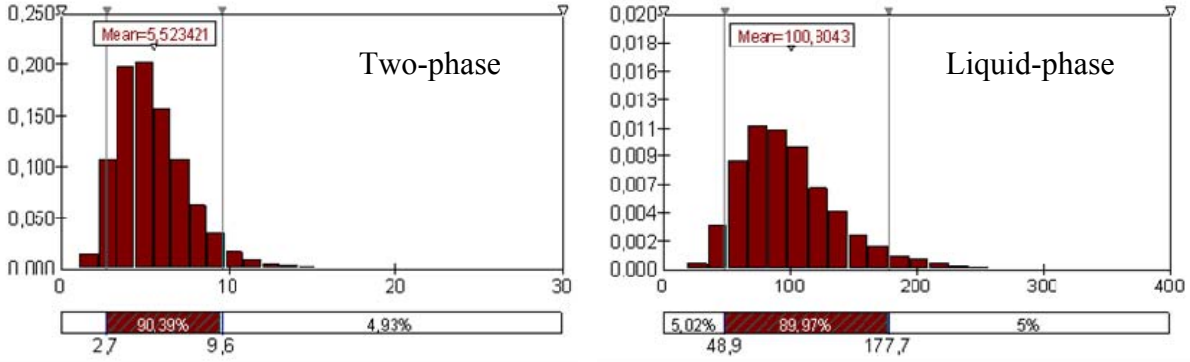

FIGURE 26: Histogram for power output (MWe) for BacMan 2

Combined, BacMan 1 and 2 can support 200 MWe until 2031. Estimated generating capacity for BacMan 1 is lower than installed capacity of 110 MWe if the volumetric method applies. Production capacity for BacMan 1 may improve if recharge to system from outer boundaries is considered. Excess capacity from BacMan 2 can be used to support full-load operation of BacMan 1. Another alternative is to optimize plant loading to allow incremental load reduction until 2031.

Result of volumetric estimates show that there is no need to distinguish contributions of liquid and two-phase zones since bulk of stored heat in two-phase zone is in the liquid component. To simplify the estimate, it would be better to take the whole volume and compute the stored heat assuming only liquid condition.

5. LUMPED PARAMETER MODEL

Lumped parameter modelling is a simple method for estimating generating capacity where reservoir is modeled in different sectors, each of them having some determined hydrological properties. Those properties are lumped together, simplifying the reservoir characteristics into a few dependent variables (Axelsson, 1989).

The software LUMPFIT developed by Axelsson and Arason (1992) is used here for lumped parameter modelling of BacMan. LUMPFIT simulates pressure change with lumped parameter models as an inverse problem and simulates pressure histories very accurately provided data quality is sufficient. LUMPFIT enables automatic fitting of analytical response functions of lumped models to the observed data using a non-linear iterative least-squares technique, from which reservoir parameters are estimated. Nonlinear least squares regression can fit a broad range of functions and can produce good estimates of unknown parameters even in models with minimal production history.

5.1 Theory

A general lumped parameter model consists of a few tanks and flow resistors. The tanks simulate storage capacity of different parts of the geothermal system. Hot water is generated out of the innermost tank, which causes the model pressure to decline.

Models can vary from a simple one-tank model to a network of tanks. The outermost tank can be specified either closed or open to a constant pressure boundary. In an open model, a resistor connects the tank to an infinitely large imaginary reservoir, maintaining a constant pressure. In contrast, a closed model is isolated from any external reservoirs.

The solution used by Axelsson (1989) for lumped parameter modelling is described. Consider a three-tank open lumped model presented consisting of a total of N = 3 capacitors or boxes with capacitances or storage coefficients κ (Figure 27)**.** A capacitor has a mass capacitance $\boldsymbol{\kappa}$ when it responds to a load of mass m with a pressure $p = m/\kappa$. The capacitors are serially connected by up to N(N-1)/2 conductors (resistors) of conductance σ_{ik} $(\sigma_{ii} = 0)$. The mass conductance of a conductor is σ when it transfers $q = \sigma\Delta p$ units of liquid mass per unit time at the impressed pressure differential Δp. The particular element $\boldsymbol{\sigma_{ik}}$ connects the *ith* and *kth* capacitor and because of linearity $\sigma_{ik} = \sigma_{ki}$. The network is open in the sense that the ith capacitor is connected by a conductor of conductance σ_i to an external capacitor that maintains equilibrium pressure of magnitude zero. The network is closed when $\sigma_i = 0$ for i = 1, 2 …N.

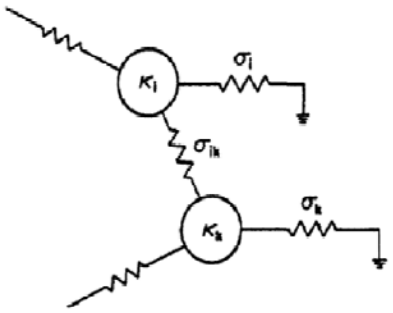

FIGURE 27: General lumped capacitor/conductor network based from Axelsson (1989)

Let $p_i(t)$ be the pressure in *ith* capacitor and $q_{ik}(t)$ be the mass flow from *kth* to *ith* element. Then the basic equations are the mass flow equation and the conservation of mass *Equation 5 and 6.*

$$q_{ik} = \sigma_{ik}(p_k - p_i) \tag{5}$$

$$\kappa_i \frac{dp_i}{dt} = \sum_{\kappa=1}^{N} q_{ik} - \sigma_i p_i + f_i \tag{6}$$

where f_i represents an external source mass flow into the *ith* capacitor. Combining *Equations 5* and *6*, the basic system equations are obtained in matrix form:

$$\kappa \frac{d\vec{p}}{dt} + A\vec{p} = \vec{f} \tag{7}$$

where the vectors and matrices are defined as follows:

$$\kappa = [k_i b_{ik}]$$

$$A = \left[\left(\sum \sigma_{ij} + \sigma_i\right)\delta_{ik} - \sigma_{ik}\right] \tag{8}$$

$$\vec{p} = (p_i), \vec{f} = (f_i)$$

To obtain general solutions of the systems of equations, *Equation 7*, the response of the network to an impulsive drive of the k_{th} capacitor at time $t = 0$ is derived and given by:

$$f_i = 0 \; for \; i \neq k, f_k = \delta_+(t) \tag{9}$$

The $\delta_+(t)$ is the delta function in time, centred at $t = 0^+$. The response to this particular drive is $\vec{h}_k(t)$ the *kth* impulse response vector of the network that is the solution of *Equation 7* with $\vec{f}$ given by *Equation 9*. If the network is driven by a general causal drive $\vec{f}$, and can be taken to be in equilibrium at t = 0, the response is obtained by convolution:

$$\vec{p}(t) = \sum_{\kappa=1}^{N} \left[\int_0^t \vec{h}_\kappa(t-\tau) f_k(\tau) d\tau\right], t > 0 \tag{10}$$

Equation 7 can be solved by considering associated eigenvector problem:

$$A = \lambda\kappa\vec{\tau} \tag{11}$$

where $\vec{\tau}$ and λ are eigenvectors and eigenvalues respectively. *Equation 11* has up to N non-negative eigenvalues. The matrix *A* can be diagonalised as:

$$T'AT = \Lambda \text{ or } A = KT\Lambda T'K \tag{12}$$

Where Λ is a diagonal eigenvalue matrix, *T* the eigenvector matrix formed out of the column vectors $\overrightarrow{\tau_j}$ and T' is the transpose of matrix T. The solution of *Equation 7* with a drive given by *Equation 9* is given by:

$$\overrightarrow{h_k}(t) = \mathrm{T}e^{-t\Lambda}\mathrm{T}'\Delta_k, \quad t > 0 \tag{13}$$

Where $\overrightarrow{\Delta_k}$ is a vector having only one non-vanishing component equal to unity at *kth* entry. The response of the *ith* capacitor to an impulsive drive of the *kth* capacitor is given by:

$$h_{ik}(t) = \sum_{j=1}^{N} \tau_{ij}\tau_{kj}e^{-\lambda_j t}, t > 0 \tag{14}$$

The more practical step response is used to get response of ith capacitor to a mass flow input q_k, for t>0 into kth capacitor by using *Equation 10:*

$$p_{ik}(t) = q_\kappa \sum_{j=1}^{N} \frac{\tau_{ij}\tau_{jk}}{\lambda_j}\left[1 - e^{-\lambda_j t}\right], t > 0 \tag{15}$$

The corresponding eigenvector has components $\tau_{i1} = V^{-\frac{1}{2}}$ where $V = \sum K_i$. The solution in *(14)* remains valid for a closed system, but in the case of the step response *(15)* the first term of the sum becomes t/V.

An appropriate lumped model is selected to simulate pressure response data from a liquid-dominated geothermal reservoir. Water is produced from one of the capacitors at a variable rate *q(t),* the rate of production from geothermal reservoir. Resulting pressure *p(t)* is observed in any given capacitor of lumped model. Resulting pressure can be written:

$$p(t) = \int_0^t h(\tau - r)\, q(\tau) d\tau \tag{16}$$

Where *h* is the impulse of lumped model for specific production and observation capacitors. The impulse response is given by *Equation10* which can be rewritten as:

$$h(t) = \sum_{j=1}^{N} m_j e^{-m_j + N^t} \tag{17}$$

Where *N* is the number of capacitors in the lumped model chosen. An iterative least squares technique described by Menke (1984) is used to fit *Equations 16* and *17* to observed data *p(t)* and estimate parameters *mi*, which in turn depend on properties of the model. The observed pressure data is discretised as:

$$p_i = p(t_i); t_i = i\Delta t, i=1,2 \ldots M \tag{18}$$

Where *Δt* is a fixed time interval, and flow rate data is approximated by:

$$q(t) = q_i \text{ for } (i\text{-}1)\, \Delta t \leq t < i\Delta t \tag{19}$$

Equation 16 can be written as:

$$\vec{g}(\vec{m}) = \vec{p} \tag{20}$$

Where $\vec{g}$ is a vector valued function and:

$$\vec{m} = (m_i), i = 1,2 \ldots 2N \tag{21}$$

$$\vec{p} = (p_i), i = 1,2 \ldots M$$

$$\vec{g} = (g_i);\ g_i(\vec{m}) = p(t_i)$$

Expanding *Equation 20* into a Taylor series, the following iterative scheme can be setup to estimate best fit parameters $\vec{m}$ for a given model:

$$G_n \Delta \vec{m}_{n+1} = \vec{p} - \vec{g}(\vec{m}_n^{est}) \tag{22}$$

$$\vec{m}_{n+1}^{est} = \vec{m}_n^{est} + \vec{m}_{n+1}$$

Where an $\vec{m}_0^{est}$ initial guess for the parameters and matrix *G* is is defined as:

$$(G_n)_{ij} = \frac{\partial g_i}{\partial m_j}\Big|_{\vec{m}=\vec{m}_n^{est}}, j = 1,2 \ldots 2N \tag{23}$$

The least squares solution of *Equation 18* is given by Menke (1984):

$$\Delta \vec{m}_{n+1} = (G_n^T G_n)^{-1} G_n^T [\vec{p} - \vec{g}(\vec{m}_n^{est})], n = 0,1,2 \ldots \tag{24}$$

Where G_n^T is the transpose of G_n.

5.2 Results

Lumped parameter model is used to assess sustainability of BacMan reservoir through predictions of pressure responses to changes in production load. Pressure data is also added to validate model reliability.

5.2.1 Validation of model reliability

A simple lumped parameter model for BacMan field is formulated using pressure data from a centrally-located well PAL-7D and the total generation minus reinjection. PAL-7D, located in western part of Bacman, is a non-productive well and has therefore been used as a monitoring well since 1993. Well profile of PAL-7D is available in *Appendix 1*. Pressure observations from PAL-7D taken at 650 m depth are translated by a factor of 78.1 bar to approximate pressures at deeper reservoir (1650mVD, -1000 mRSL). Readings are regularly checked by downhole pressure surveys. In Figure 28, it is seen that pressure changes in PAL-7D correspond very well to changes in field production. Pressure decline is mass extraction-dependent and computed to be 42×10^{-12} bars/kg of mass extracted (Fajardo, 2000).

A closed two tank capacitor model is used to simulate pressure observations from 1993 to 2001. Water is produced from first capacitor (K_1) and pressure is monitored in same capacitor. First capacitor is analogous to representing innermost part of geothermal reservoir; second capacitor as outer and deeper parts of reservoir.

In order to demonstrate reproducibility of predictions, coefficients of lumped model are provided. Satisfactory match is obtained between observed and calculated pressure using a closed two-tank model giving a coefficient of determination (R^2) of 97.4% *(Table 3)*. R^2 is the proportion of variability in a data set that is accounted for by a statistical model. An open two-tank model is also tested but L_2 model coefficient gave a physically unfeasible negative result.

TABLE 3: Simulation results from 1993 to 2001 with variable sized models

Model	**1**	**2**	**3**
Number of tanks	**1**	**1**	**2**
Model type	**Closed**	**Open**	**Closed**
A_1		0.185924E-3	0.433478E-3
L_1		0.058216	0.230359
A_2			
L_2			
B	0.477604E-4		0.181822E-4
K_1 (Kappa, ms^2)	55175.4	14173.5	5834.5
K_2			139099
σ_1 (Sigma, 10^{-6} ms)		0.313117-3	0.489496E-3
σ_2			
R^2	40%	93.2%	97.4%

Using the best lumped model, calculated predictions regarding reservoir response to production loads may be forecasted. These predictions serve as a useful tool for managing geothermal resources and minimizing financial risks.

Reservoir response at full load capacity with BacMan 1 operating at 110 MWe, Cawayan at 20 MWe and Botong at 20 MWe is predicted from year 2002 to 2005 using two tank closed model defined *(Table 3)*. Production from months 108 to 116, designated as T_{y9}, is erratic due to abnormal plant loading. There is no adjustment in utilization of wells in the field despite nonstandard plant loading therefore pressure monitoring in PAL-7D is unaffected. Simulated pressure follows observed pressure from 1993 to 2001. Following the trend, further reduction in pressure is observed at 1.15 bar/year (Figure28).

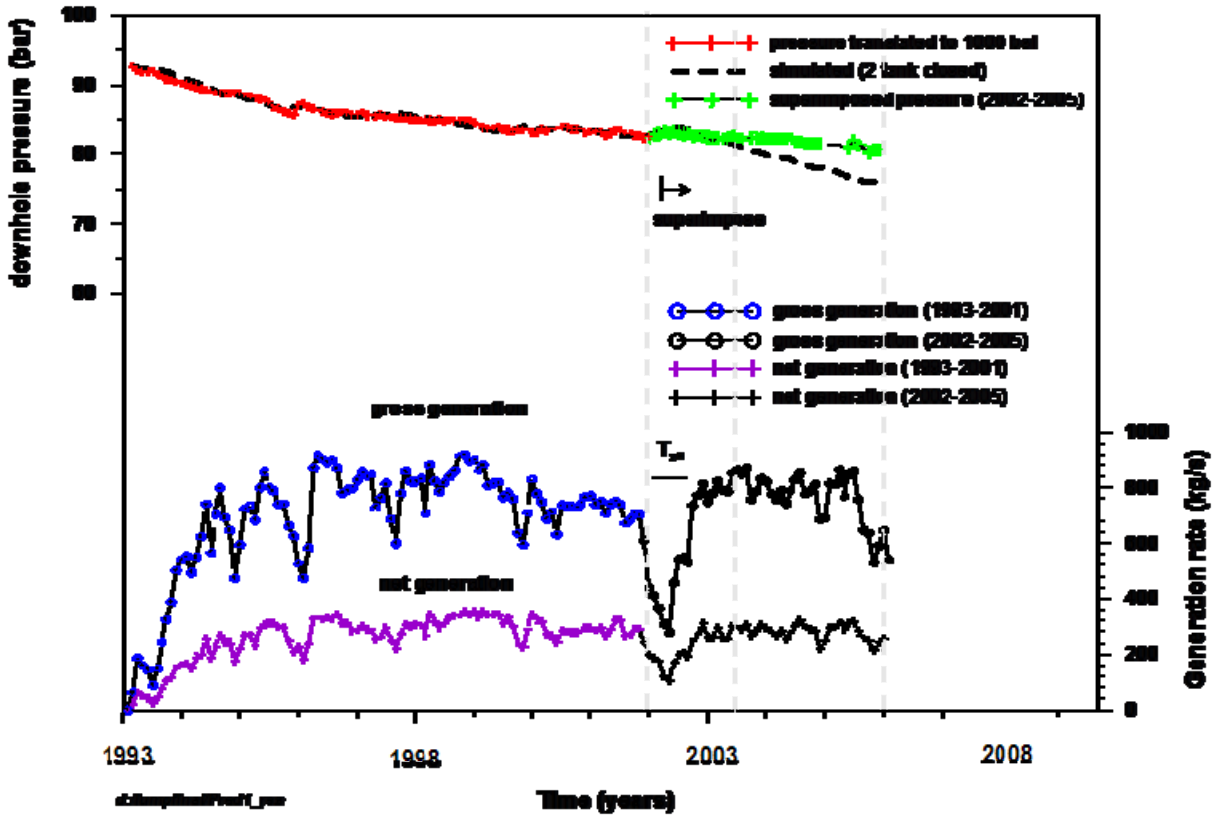

FIGURE 28: Observed and simulated pressure changes from 1993 to 2001

In Figure 28 shown above, pressure data from January 2002 to December 2005 is excluded on purpose from data set used during model building and parameter estimation in order to validate reliability of lumped model. Subsequent superimposition of excluded data (green cross symbol) from 2002 to 2005 on plot of predicted values showed very good agreement especially for the first 18 months with a slight deviation of 5 bar afterwards. Good agreement between simulated and superimposed data reflects the efficiency and reliability of prediction.

Data set for calibrating lumped model is lengthened by including pressure observations from January 2002 to April 2005 as can be seen in Figure 29. Pressure response at full load operation is predicted using this longer data series. The best lumped model is model 4, or a two-tank open model, which gave an R^2 value of 97% *(Table 4)*. This best model corresponds well to changes in generation rate and was able to match an observed "hump" in pressure from 2006 to 2007 due to a decrease in generation in period designated by T_{y14}. Superimposed data set from 2006 to 2007, which was not available initially for the study, was found to be in good agreement with predicted pressure trend.

TABLE 4: Simulation results, 1993 to 2005, with variable sized models

Model	**1**	**2**	**3**	**4**
Number of tanks	**1**	**1**	**2**	**2**
Model type	**Closed**	**Open**	**Closed**	**Open**
A_1		0.113853E-3	0.337341E-3	0.368583E-3
L_1		0.0282333	0.181016	0.211081
A_2				0.226206E-4
L_2				0.223279E-2
B	0.389156E-4		0.189862E-4	
K_1 (Kappa, ms^2)	67715.9	23145.7	7395.4	6736.1
K_2			131400	112264
σ_1 (Sigma, 10^{-6} *ms*)		0.247981-3	0.480938E-2	0.508699E-3
σ_2				0.100893E-3
R^2	38.2%	88.3%	97%	97%

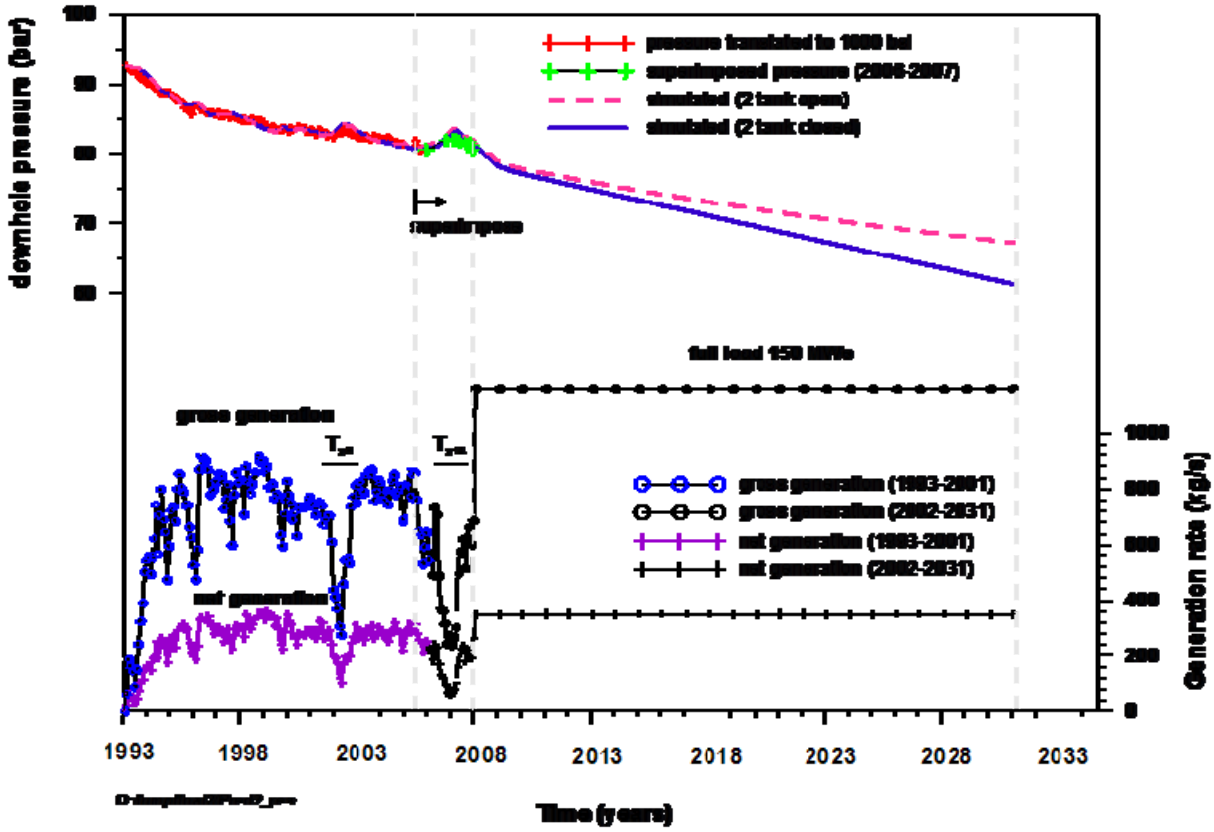

FIGURE 29: Observed and simulated pressure changes from 1993 to 2005

Results of predictions using different data sets and models are summarized *(Table 5)*.Pressure drawdown is predicted to be 0.81 bar/year (model 3, closed 2 tank) and 0.67 bar/year (model 4, open 2 tank) using longer data series (1993-2005) compared to 1.15 bar/year (closed 2 tank) using shorter data series (1993-2001). R^2 values are also comparable for these models: 97.4% (model 3, 2-tank closed, 1993-2001); 97% (model 3, 2-tank closed, 1993-2005); and 97% (model 4, 2-tank open, 1993-2005).

TABLE 5: Prediction results using different data sets and models

Data series	**1991-2001**	**1993-2005**	**1993-2005**
Model/number of tanks	model 3/ 2	model 3/ 2	model 4/ 2
Model type	Closed	Closed	Open
R^2	97.4%	97%	97%
Predicted decline (bar/year)	1.15	0.81	0.67

5.2.2 Sustainability assessment

Sustainability of BacMan reservoir or the ability of the reservoir to deliver required separated steam to power plant is evaluated anticipating present power plants will be renewed and operated at full-load capacity of 150 MWe until 2031. The best model (model 4, two-tank open, *Table 5*) is used to predict pressure response and recovery after operating at full-load until 2031. Two-tank open model predicts that after year 2010, a total pressure drop of 15 bar will be encountered after extracting 360 kg/s until 2031 (Figure 29). At a drawdown rate of 0.67 bar/year, BacMan reservoir can support full-load operation for the study period of 23 more years. In Figure 30, an imaginary no-load production scenario is simulated to evaluate reversibility after producing the field at full-load until 2031.

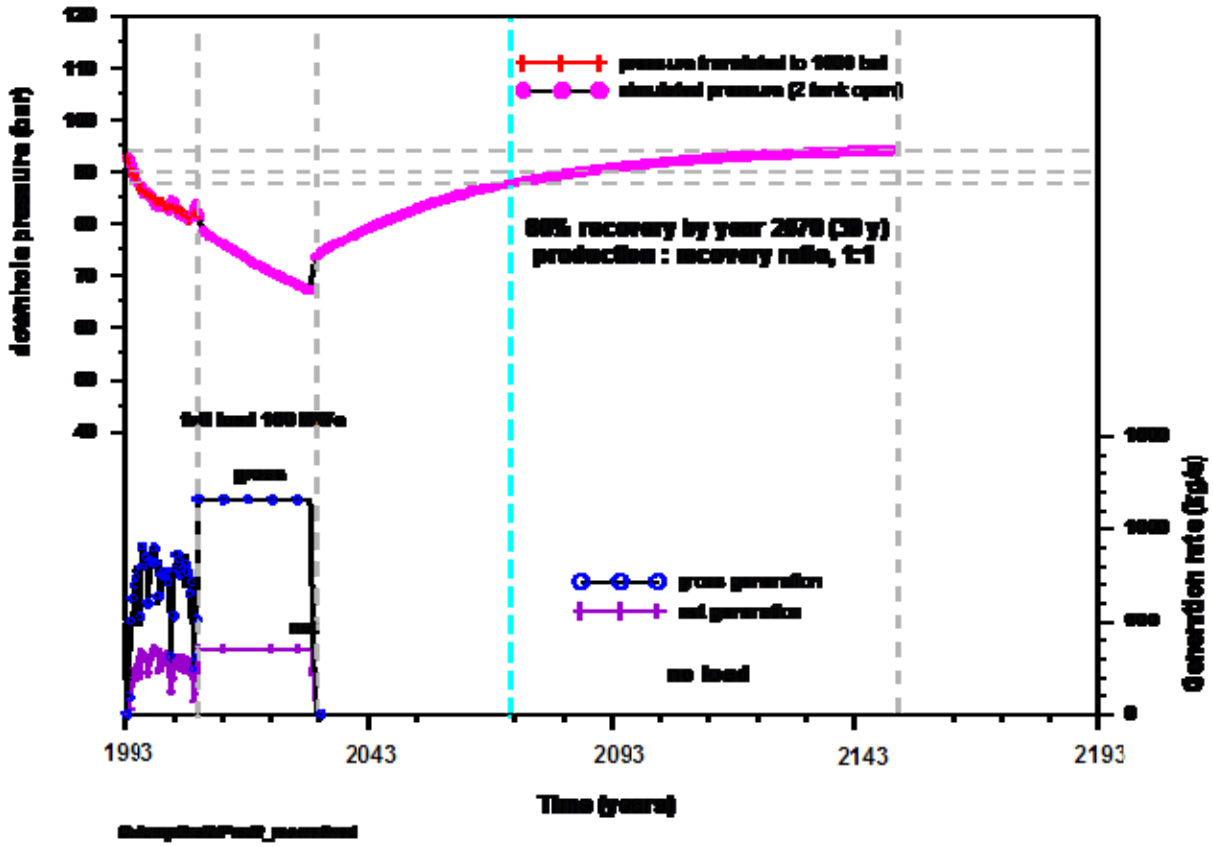

FIGURE 30: Simulated drawdown and recovery from lumped model

Recovery of pressure is estimated only up to 80% since the remaining 20% of pressure takes a long time to recover. 80% recovery is attained after 39 years indicating that full-load operation is sustainable.

Two-tank closed (model 3, *Table 5*) and two-tank open model (model 4, *Table 5*) predicted pressure drawdown at 0.81 bar/year and 0.67 bar/year respectively. Two-tank open model gives more optimistic predictions since equilibrium between production and recharge is eventually reached during long-term production. The system is in quasi-steady state where the inflow of energy into the system matches outflows from production and surface discharges. On the other hand, two-tank closed model gives conservative predictions since no recharge is allowed for such model. Differences in results of predictions using closed and open models show the inherent uncertainty in all such predictions (Axelsson, 2005).

Although lumped parameter models have been developed for isothermal, single phase conditions, lumped parameter models are able to match measured responses very accurately. Care, however, should be put in using lumped models for boiling reservoirs as the governing equations are based on mass conservation only excluding conservation of heat.

6. DISTRIBUTED PARAMETER MODEL

In distributed parameter modelling, the reservoir system is divided into numerous sub-volumes or grid-elements numbering from a few hundred to a several thousand. Hydrological and thermal properties are assigned to each element. Sinks and sources are assigned to selected elements to simulate inflow, outflow, production wells and injection wells.

Finite-difference or finite-element methods are used to solve relevant equations for conservation and flow of mass and heat. Such model simulates pressure conditions, energy content, flow patterns, and chemical changes. The simulators used to implement these complex models are TOUGH2, MULKOM, TETRAD, and STAR. TETRAD and STAR can handle rectangular mesh structure while MULKOM and TOUGH2 can handle irregular mesh (O'Sullivan et al., 2001).

TOUGH2 originated from code MULKOM meaning "MULTI-KOMPONENT." MULKOM recognizes that governing equations for non-isothermal, multi-phase, multi-component flow are the same, regardless of the nature and number of fluids present. The MULKOM code was never finalized but progressed into a collection of program modules for specialized applications. Nuclear-waste oriented applications prompted an effort to finalize and document a version of MULKOM for non-isothermal two-phase flows of water and air, which became TOUGH (Transport Of Unsaturated Groundwater and Heat) (Pruess et al., 1996). TOUGH2 became the successor of TOUGH. TOUGH2 provides the full multi-component, multi-phase flexibility previously available only in the MULKOM collection of modules. The name MULKOM is now used to refer to the particular architecture of the codes, while actual coding implementations are referred to as TOUGH and TOUGH2 (Pruess et al., 1996). In this thesis, iTOUGH2, a program for parameter estimation, sensitivity analysis, and uncertainty propagation analysis based on TOUGH2 simulator is used to implement the model.
Assessment of sustainability of BacMan resource is taken a step further by doing a detailed well-by-well numerical model. After more than 14 year of operation, reservoir data is sufficient to allow well-by-well history-matching to produce a simulation model capable of indicating future response. In this detailed numerical model, both heat and mass conservation are considered, thus effect of relatively lower temperature recharge and injection returns are accounted for.

6.1 Theory

6.1.1 Mathematical theory

In Pruess et al. (1999), the mass and energy balance equation in TOUGH2 is derived as a multiphase volume balance equation for a subdomain and its general form is given as:

$$\frac{d}{dt}\int_{V_n} M^\kappa \, dV_n = \int_{\Gamma_n} \vec{F}^\kappa \cdot \vec{n} \, d\Gamma_n + \int_{V_n} q^\kappa \, dV_n \tag{25}$$

The integration is over an arbitrary subdomain V_n of the flow system under study bounded by closed surface Γ_n. The left hand side of the equation is the accumulation term. Quantity M represents mass or energy per volume, with $\kappa = 1 \ldots NK$ for mass components (like water, air, H_2, solutes) and $\kappa = NK+1$ for heat component. $\vec{F}$ denotes mass heat flux. q denotes sinks and sources. $\vec{n}$ is a normal vector on surface element $d\Gamma_n$ pointing inward into V_n. In the first term on the right, $\vec{F}$ is integrated over the entire subvolume surface area with normal vector $\vec{n}$ on surface element $d\Gamma_n$ pointing inward into V_n. In the second term on the right hand side, flow of mass and energy inwards, or outwards, subvolume V_n is integrated through sources or sinks connected to the subvolume.

The fluid mass per unit volume, or mass accumulation term, for multi-phase multi-component condition in its general form is given as:

$$M^\kappa = \emptyset \sum_\beta S_\beta \rho_\beta X_\beta^\kappa \tag{26}$$

Where ϕ is porosity; S_β is saturation of phase β, i.e., the fraction of pore volume occupied by that phase; ρ_β is the density of phase ß; and X_β^κ is the mass fraction of component κ present in phase β.

Similarly, fluid heat per unit volume, or heat accumulation term, for a multi-phase multi-component condition in its general form is given as:

$$M^{NK+1} = (1 - \emptyset)\rho_R C_R T + \emptyset \sum_\beta S_B \rho_\beta u_\beta \tag{27}$$

Grain density is symbolized by ρ_R; C_R is rock specific heat; T is temperature; and μ_β is internal energy in phase β.

The advective mass flux $\overline{F}$ in (*Equation 25*) is expressed using Darcy velocity as:

$$F_{adv}^\kappa = \sum_\beta X_\beta^\kappa F_\beta = \sum_\beta X_\beta^\kappa \rho_\beta \vec{u}_\beta = \sum_\beta X_\beta^\kappa \rho_\beta (-k \frac{k_{r\beta}}{\mu_\beta} (\nabla \vec{P}_\beta - \rho_\beta \vec{g}) \tag{28}$$

Where $\vec{u}_\beta$ is the Darcy velocity according to the multiphase version of Darcy's law incorporating absolute k and relative $k_{r\beta}$ permeability, viscosity μ_β, fluid pressure in phase β, and acceleration due to gravity $\vec{g}$.

In addition to Darcy flow, mass transport can also occur by diffusion and hydrodynamic dispersion as follows:

$$F_{dis}^\kappa = -\sum_\beta \rho_\beta \vec{D}_\beta^\kappa \nabla X_\beta^\kappa \tag{29}$$

$\vec{D}_\beta^\kappa$ represents the hydrodynamic dispersion tensor.

The heat flux includes conductive and convective components:

$$F^{NK+1} = -\lambda \nabla T + \sum_\beta h_\beta F_\beta \tag{30}$$

Where λ thermal conductivity and $h_ß$ is specific enthalpy in phase ß.

By applying Gauss' divergence theorem, *(Equation 25)* can be converted into the following partial differential equation:

$$\frac{\partial M^\kappa}{\partial t} = -div F^\kappa + q^\kappa \tag{31}$$

Equation 31 is commonly used as the starting point for deriving finite difference or finite element discretisation approaches.

6.1.2 Numerical theory

In TOUGH2, the continuous space and time variables presented in *Section 6.1.1* are discretized for numerical simulation using the integral finite difference method (IFDM) as discussed in (Pruess et al., 1999).

The accumulation term in *Equation 25* is discretized, using IFDM, as:

$$\int_{V_n} M dV = V_n M_n \tag{32}$$

Where *Vn* is a volume normalised extensive quantity and M_n is the average value of *M* over V_n. The energy and mass flux surface integrals are approximated as discrete sum of averages over surface segments A_{nm} between volume elements V_n and V_m:

$$\int_{\Gamma_n} F^{\kappa} \cdot n d\Gamma = \sum_m A_{nm} F_{nm} \tag{33}$$

Where F_{nm} is the average value of energy or mass flux normal to the surface segment A_{nm}. The subscripts (nm) denote a suitable averaging at the interface between grid blocks n and m (interpolation, harmonic weighting, upstream weighting) as shown in Figure 31.

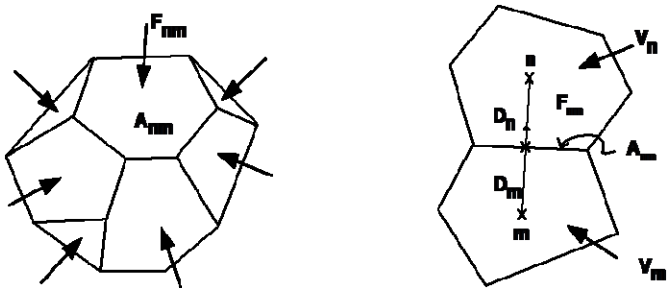

FIGURE 31: Space discretisation and geometry data in IFDM (Pruess, 1999)

6.1.3 Optimization

In forward modelling, site-specific parameter values describing hydrogeological and thermophysical properties are entered into a numerical model together with proper initial and boundary conditions. The model then predicts the future state of the system.

In inverse modelling, system observations in discrete points in time and space are used in estimating site-specific model parameters. Estimates are obtained by automatic matching of observed and computed values. Computed and observed values are compared and provide a measure of goodness-of-fit via the so-called objective function. A précis of the concept of inverse modelling, as explained in Finsterle et al. (1999), follows.

The objective function $\boldsymbol{S_{obj}}$ is a hypersurface in the n-dimensional parameter space. The global minimum represents the best parameter set. A linear model yields a parabolic objective function where the minimum is easy to identify. For non-linear models, the topography away from minimum becomes intricate and may exhibit a global minimum, multiple local minima, inflection points, etc. making difficulties for optimization algorithm to iteratively proceed towards minimum. The standard objective function, however, is a sum of squares and is close to parabolic with elliptical contour lines near the global minimum. Visualization of objective function in two-dimensional space is provided in Figure 32.

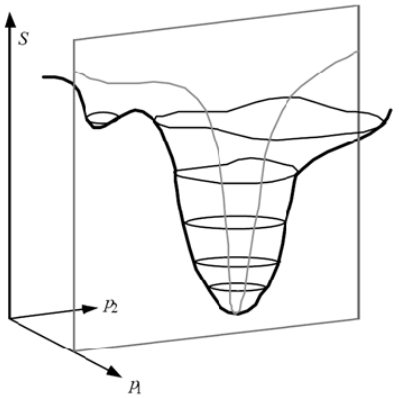

FIGURE 32: Objective function S_{obj} in two-dimensional space (Finsterle, 2007)

An objective function $\boldsymbol{S_{obj}}$ has to be chosen to obtain a total measure of deviation between observed and calculated response. The choice of $\boldsymbol{S_{obj}}$ can be based on maximum likelihood method which consists of finding a parameter set that is most likely to have produced the data. Measurement errors that are normally-distributed lead to least squares criterion *Equation 34*:

$$S_{obj} = r^T C_{zz}^{-1} r \tag{34}$$

The term *r* is the residual vector with elements $r = z_i^* - z_i(p)$, where z_i is an observation at a given point in space and time, and z_i is the prediction from simulation which depends on vector $\boldsymbol{p}$ of unknown parameter to be estimated. The i_{th} diagonal element of covariance matrix C_{zz}^{-1} is the variance representing the measurement error of observation z_i. The objective function $\boldsymbol{S_{obj}}$ has to be minimized in order to maximize the likelihood of reproducing the observed system state. An iterative procedure is

required to minimize S_{obj} because of nonlinearities in the functions z_i. A number of minimization algorithms are available in iTOUGH2. The minimization algorithm reduces S_{obj} by iteratively updating parameter vector $\boldsymbol{p}$ based on sensitivity z_i with respect to p_j. The Levenberg-Marquardt method is found to perform well for most iTOUGH2 applications (Finsterle, 2007) and thereby used here. Levenberg parameter λ_{Lev} is relatively large during first few iterations leading to small steps along gradient of S_{obj} This rough approach is to ensure that $S_{obj}(p_k+1) < S_{obj}(p)$. The factor $1/\nu_{Marq}$ is used to reduce λ_{Lev} to increase the step lengths and increase efficiency. Steps proposed by Levenberg-Marquardt are shown in Figure 33.

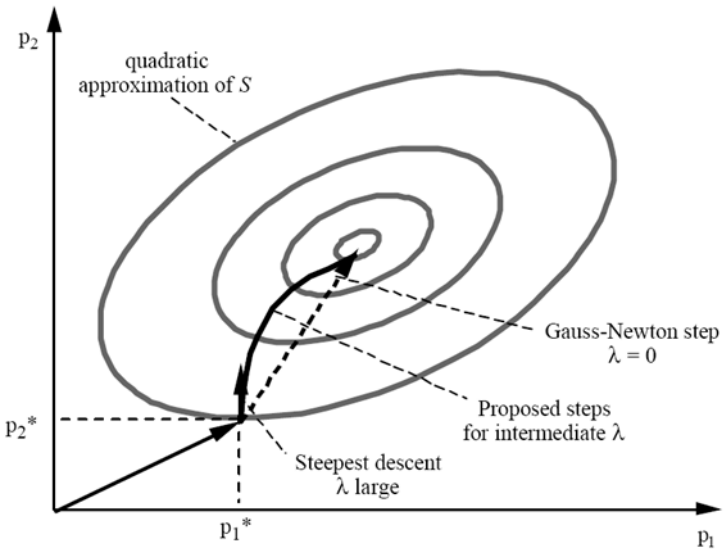

FIGURE 33: Steps proposed by Levenberg-Marquardt method (Finsterle, 2007)

If minimization algorithm reaches the stopping criteria after some iterations using updated parameter, error analysis is performed using best estimated parameters. Error analysis provides insight into the uncertainty of estimated parameters, adequacy of model structure, relative importance of individual data points and parameters, and parameter correlations. The formalized sensitivity, residual, and error analyses make inverse modelling more preferable over the trial-and-error model calibration. The steps of inverse modelling are shown (Figure 34).

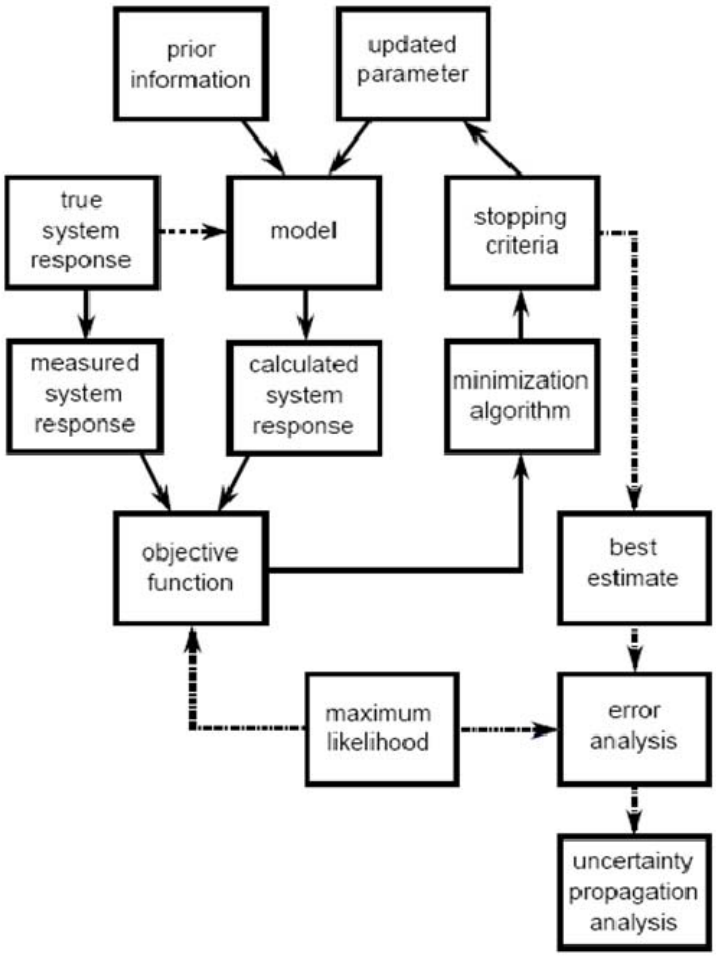

FIGURE 34: Inverse modelling flowchart (Finsterle, 2007)

6.2 Model pre-processor and post-processor

Inverse simulation using iTOUGH2 requires two input files: a file for forward simulation and another for inversion. The input file for forward simulation, which has same format as TOUGH2 input deck, must be capable of simulating general features of system under measurement conditions. The 'forward file' described relevant physical processes mathematically and numerically, defines boundary geometry, assigns initial boundary conditions, provides discretisation in time and space, and assigns elements where model parameters are believed to be constant. On the other hand, input for inversion contains options for parameter estimation, observations, and computational methods (Finsterle, 2007).

A number of commercial and academic pre-processors for building a complex 3D model mesh are available, e.g. pre-processors such as PETRASIM, GEOCAD, MULGRAPH, and WINGRIDDER. Advanced modellers create their own pre-processors in their preferred programming environment. Two new pre-processors are used in this study: a pre-processor using MATLAB developed by Ketilsson (Ketilsson, 2007); and a beta version of a pre-processor written in UNIX developed jointly by Björnsson and Arnaldsson through a cooperation project between Reykjavik Energy and Vatnaskil Consulting Engineers. The new pre-processor written in UNIX was used to set-up model mesh for studying BacMan geothermal reservoir.

6.2.1 MATLAB and UNIX pre-processors

Both MATLAB and UNIX pre-processors are capable of generating a mesh from a set of X and Y coordinates. Pre-processor by Ketilsson (2007) is used for mesh refinement because of its interactive graphical user-interface (GUI) which conveniently displays changes to mesh as elements are being added or deleted. Final coordinates after mesh refinement are used as an input (called by –c tag) for UNIX pre-processor to create mesh.

Succeeding discussion is written like a manual to give first-time users an overview of how to use pre-processor by Björnsson and Arnaldsson.

The following scripts from UNIX pre-processor are used to create an input deck for TOUGH2: ini_mesh, add_layers, set_incon, run_gravi_test, set_inactive, and set_rocks.

The main script for setting-up model mesh for TOUGH2 is BUILD_MODEL. BUILD_MODEL generates an initial mesh, adds layers, sets-up initial pressure and temperature conditions, performs a gravity test, and sets rock types to model. Scripts leave trail of the procedures used in setting-up model which is helpful in transferring knowledge and maintaining a model in the long run.

ini_mesh creates an initial input file for AMESH (Haukwa, 1998) using files containing mesh outer boundary (called by –b tag) and element centres (called by –c tag). AMESH is a program used for generating discrete grids for numerical modelling of flow and transport problems in which the formulation is based on the integral finite difference method (IFDM). The AMESH code can generate 1D, 2D, or 3D numerical grids for a given set of locations, like for example, the centres of each discrete sub-domain. AMESH creates a mesh of elements, within model domains, where the interfaces between neighbour elements are the perpendicular bisectors of the line connecting elements centres. From a list of element locations, like centre points, AMESH determines element volumes and connection information like areas, connection distances and angle. Output from AMESH can be used directly as a part of input file for TOUGH2 numerical simulator (Haukwa, 1998).

The input file "**in**" generated by ini_mesh for AMESH after grid refinement also serves as an input file for add_layers**.** add_layers adds identical layers by specifying centre and thickness of first layer and centre depth of additional layers.

Initial temperature and pressure conditions of the model is specified by a temperature gradient (°C/km) and initial pressure (in bars) using set_incon.

run_gravi_test runs a simple gravity test on the model to ensure connections between elements are correct and mass transport is negligible at steady-state conditions. Gravity test parameters are defined in a TOUGH2 input file called run_gravi_test.

A description of the scripts used in the UNIX pre-processor, including input and output files, are tabulated *(Table 6)*. A flowchart is shown in Figure 35 outlining the steps in setting-up a model mesh using UNIX and MATLAB pre-processors. BUILD_MODEL uses tags from scripts ini_mesh**,** add_layer**,** set_incon**,** set_inactive**,** and set_rocks. The tags identified in Table 6 are the tags used in this thesis. For a comprehensive listing of all script options, the reader is referred to accompanying help files for each pre-processor.

6.2.2 UNIX postprocessors

Simple UNIX shell scripts were written to extract and compare observations and simulated values: draw.contours to contour steady-state temperature and pressure; draw.wells to plot steady-state borehole temperature and pressure; and draw.histories to plot transient borehole temperatures and pressures.

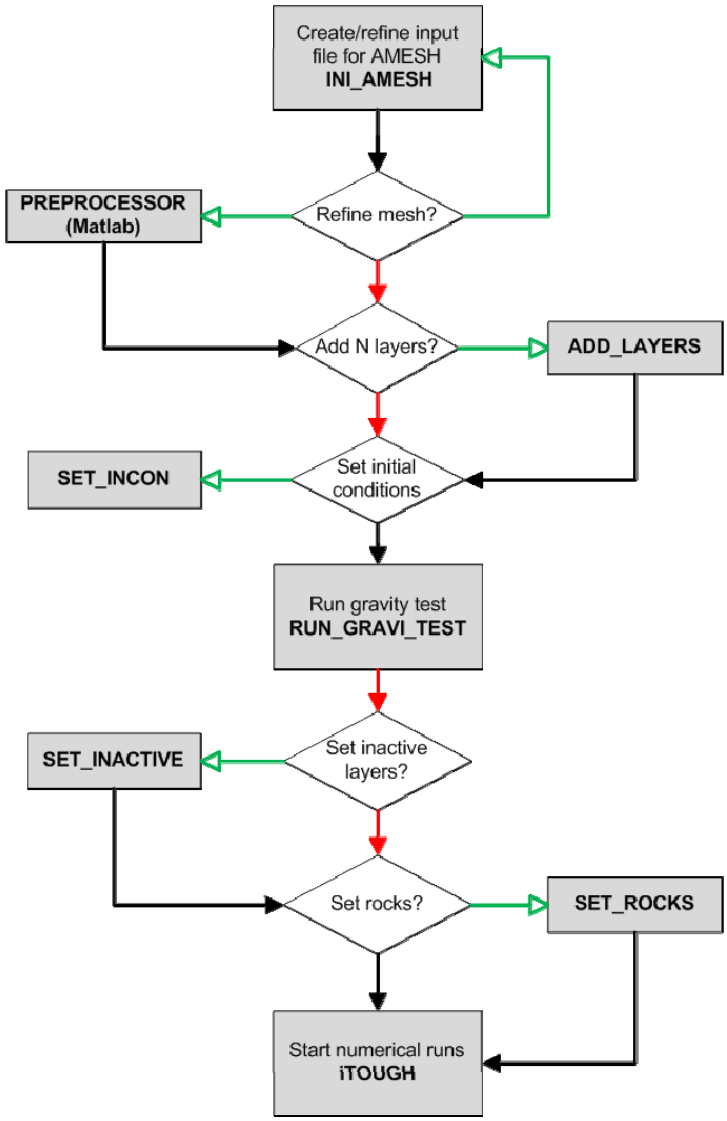

FIGURE 35: Flowchart for mesh creation using UNIX and MATLAB pre-processors

TABLE 6: Description of UNIX preprocessor developed upon request of Reykjavik Energy

Script name / purpose	Input/s	Output/s
INI_MESH /creates single layer input file for AMESH	- x and y coordinates of element centres (-c tag) - x and y coordinates of mesh outer boundaries (-b tag)	- ELEME and CONNE files - Postscript figure of mesh (mesh.ps)
ADD_LAYER /adds a new layer to an existing input file for AMESH	- old "in" file for AMESH	- Postscript figure of mesh grid, mesh.ps, new "in" file - New "in" file
SET_INCON /sets initial pressure and temperature conditions of elements through INCON block	- "in" file for AMESH - temperature gradient in °C/km (-g tag) - pressure in top layer in bars (-p tag) - pressure profile as a function of depth (-f tag)	- Postscript figure of layers showing centre of layers and initial conditions (P, T), (vert_incon.ps) - INCON block for TOUGH2 input files
SET_INACTIVE /sets inactive layers	- ELEME block file for TOUGH2/iTOUGH2 (-top, -bottom, -peri tag)	- ELEME and CONNE files with inactive layers set
SET_ROCKS /creates "colormap" of rock types; sets rock types for on a per-block mode, for a group of blocks inside given radius; within a polygon, and for inclusive layers	- ELEME block file for TOUGH2/iTOUGH2 (-c tag) - element name (-k tag) *For setting rocks types:* - radius of coverage (-r tag) - polygon area (-z tag) - elements above and below present layer (-l n1 n2 tag) - rock type (-t tag) - closed polygons for setting rock type (-poly flag) *For generating colour palette* - file specifying TOUGH2/iTOUGH2 ROCKS block (-pal tag)	- new "ELEME" block file for TOUGH2 /iTOUGH2 - Postscript figure of mesh grid showing rock types (layer_A.ps)
BUILD_MODEL /main script for generating mesh for running simulations using TOUGH2/iTOUGH2; adds new layers, sets initial conditions (P,T), runs a gravity test, set inactive layers, and sets rock types; uses tags from scripts: INI_MESH, ADD_LAYER, SET_INCON, SET_INACTIVE, and SET_ROCKS	- c and –b tags, INI_MESH) - elevation of first model layer (-z tag) - thickness of first model layer (-t tag) - elevation of additional layers (-de tag) - -th tag from ADD_LAYER - -g and –p tags from SET_INCON - option for running a gravimetric test using TOUGH2/iTOUGH2 (-gravi flag) - option for setting inactive layers, i.e. top, bottom, peri (-j tag)	- Postscript figure of mesh grid, mesh.ps - Postscript figure of layers showing centre of layers and initial conditions (P, T), vert_incon.ps

6.3 Numerical model

6.3.1 Computational mesh

An irregular 3-D cartesian mesh was developed using Voronoi tessalation method (Haukwa, 1998) in this study to model heat and mass transfer within BacMan geothermal system. BacMan's new computational mesh consists of 11 layers, each layer having 277 elements, and a total of 3047 elements. The top and bottom layer and perimeter blocks are set inactive. Model mesh covers an area of 49730 km^2 (223 km x 223 km) and is 2400 m in thickness. Vertical structure is arranged in alphabetical order starting from top (A) to bottom (K). Small grid blocks are used in mesh centre where most of wells are drilled to resolve detail with strong spatial variability while coarser block are used in perimeter where gradients are expected to be small. The model dimensions correspond to known volume of BacMan reservoir and include all of its main features (Figure 36)

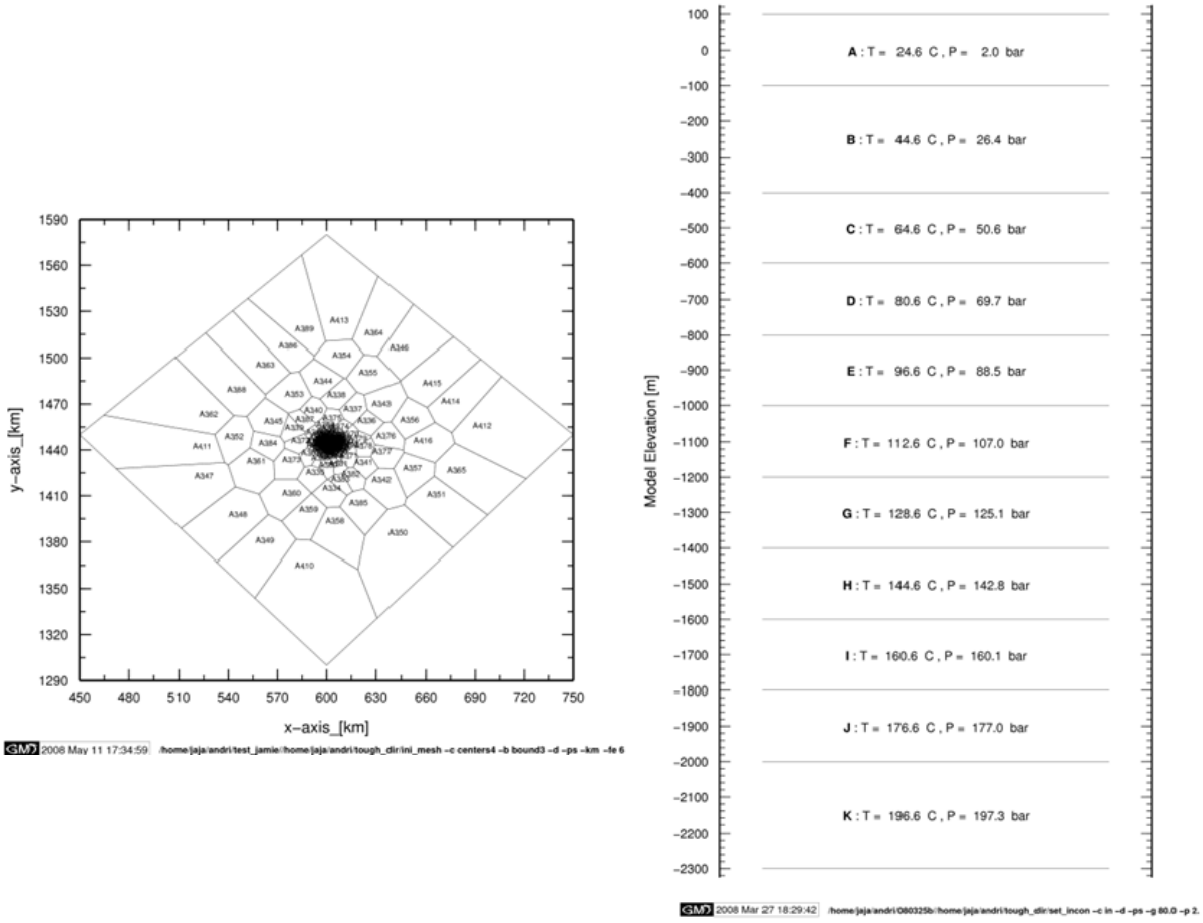

FIGURE 36: Column layout (l) and vertical structure (r) of BacMan

6.3.2 Mesh creation using MATLAB and UNIX pre-processor

Field map is taken with well locations, resistivity boundaries, elevation contours, and major geological structures and mesh is created in such a way that wells are separated into individual elements and mesh axes are oriented along structural grain of the field. Mesh is extended by adding peripheral elements 90 km from production area in order to avoid artificial boundary effects.

The UNIX script **ini_mesh** is used to create an initial input file for AMESH using mesh outer boundary and element centres provided in files "bound" and "centres"**.** On the other hand, the MATLAB pre-processor by Ketilsson is used for mesh refinement because it has an interactive graphical user-interface (GUI) which displays changes done to mesh, like when elements are added or deleted, immediately. Full mesh using pre-processor by Ketilsson is shown with all the element

centres in blue and the centres of wells of concern in green. Zoom view of wells of concern is provided (Figure 37).

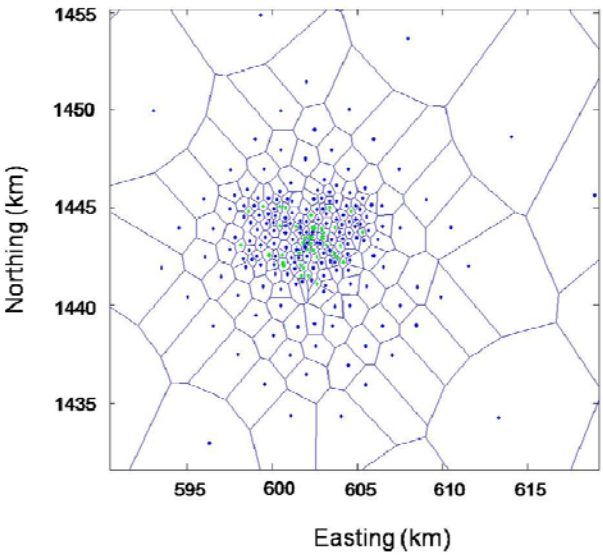

FIGURE 37: Element layout generated by Matlab

6.3.3 Vertical structure

Composite plots of stable formation temperature and pressure, distribution plots of permeable zones, and wellbore models are used to decide a 2300 m deep model with 11 layers (*Appendix 1*; Figure 38).

Model layers comprise of: (1) Surface (A), from 100 m to -100 mRSL and centred at 0 m; (2) Cap rock (B), -100 to -400 mRSL, corresponds to conductive gradient in most temperature profiles and also cased-off portion for most of the wells. Composite plots of stable temperature show that this is mainly a conductive region; (3-4) Shallow two-phase (C) from -400 to -600 mRSL, where PAL-11 is producing from, and (D) from -600 to -800 mRSL; (5-9) main production areas (E) from -800 to -1000 mRSL, (F) -1000 to -1200 mRSL, (G) -1200 to -1400 mRSL, (H) -1400 to -1600 mRSL and (I) -1600 to -1800 mRSL; (10) Fracture contact zone (J) from -1800 to -2000 mRSL; (11) Base layer (K) from -2000 to -2300 mRSL. The model produces from liquid reservoir at -900, -1100, -1300, -1500, -1700, and -1900 mRSL and two-phase reservoir at -700 mRSL.

6.3.4 Sinks and sources

Similarly, composite plots of stable formation temperature and pressure, distribution plots of permeable zones, and wellbore models are used to decide locations of sinks and source (*Appendix 1*; Figure 38). Well test results indicate presence of multiple feedzones encountered mostly between -600 and -1600 mRSL. These feed zones are associated predominantly with known faults majority of which are N-S and NW-SE trending structures.

The new "**in**" file for AMESH after doing refinements is used as input file for adding layers using **add_layers**. Centres of each layer set at 0, -250, -500, -700, -900, -1100, -1300, -1500, -1700, -1900, and -2150 mRSL *(Table 7)*.

TABLE 7: Layering of BacMan model

Layer name	Thickness (m)	Centre (mRSL)	Property
A	200	0	Inactive, impermeable
B	300	-250	Active, perimeter inactive
C	200	-500	Active, perimeter inactive
D	200	-700	Active, perimeter inactive
E	200	-900	Active, perimeter inactive
F	200	-1100	Active, perimeter inactive
G	200	-1300	Active, perimeter inactive
H	200	-1500	Active, perimeter inactive
I	200	-1700	Active, perimeter inactive
J	200	-1900	Active, perimeter inactive
K	300	-2150	Inactive, impermeable

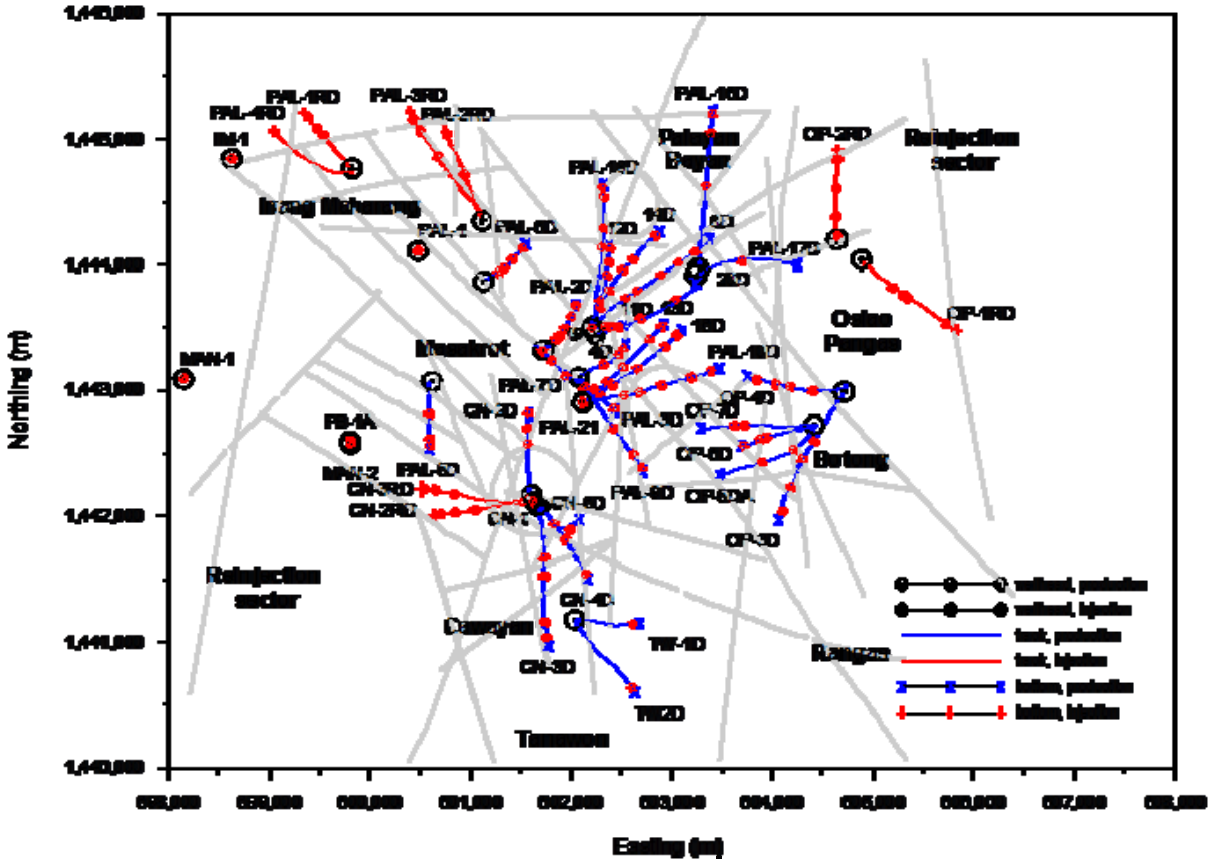

FIGURE 38: Location of feedzones of BacMan wells

6.3.5 Rock properties

Initial petrophysical parameters were assigned to model elements according to lithology of BacMan reservoir and permeability-thickness values from interpretation of cold-water injection fall-off data. Rock properties are assigned as follows: density is 2500 kg/m^3, specific heat is 1000 J/kg°C, fracture porosity is 8% and heat conductivity is 2.5 W/m°C. Petrophysical parameters for BacMan reservoir are summarized in *Table 8*.

In Figure 39, the permeability variation of elements in model mesh are inferred from temperature distribution by superimposing the computational mesh (black) together with fault structures (white), well tracks (gray dashed lines), well bottom (vector arrow), permeable zones (red dots), and wellhead locations (gray squares) on temperature contours. The initial permeability distribution assigns high permeability rocks to upflow zone and lower permeability rocks further out. An isotropic model but heterogeneous permeability structures has been considered for BacMan.

TABLE 8: Petrophysical parameters for BacMan reservoir

Petrophysical properties	Values
Rock density	2500 kg/m^3
Rock grain specific heat	1000 kJ/kg°C
Porosity	8%
Heat conductivity	2.5 W/m°C
Cap rock permeability	0.5 mD
Bed rock permeability	0.5 mD

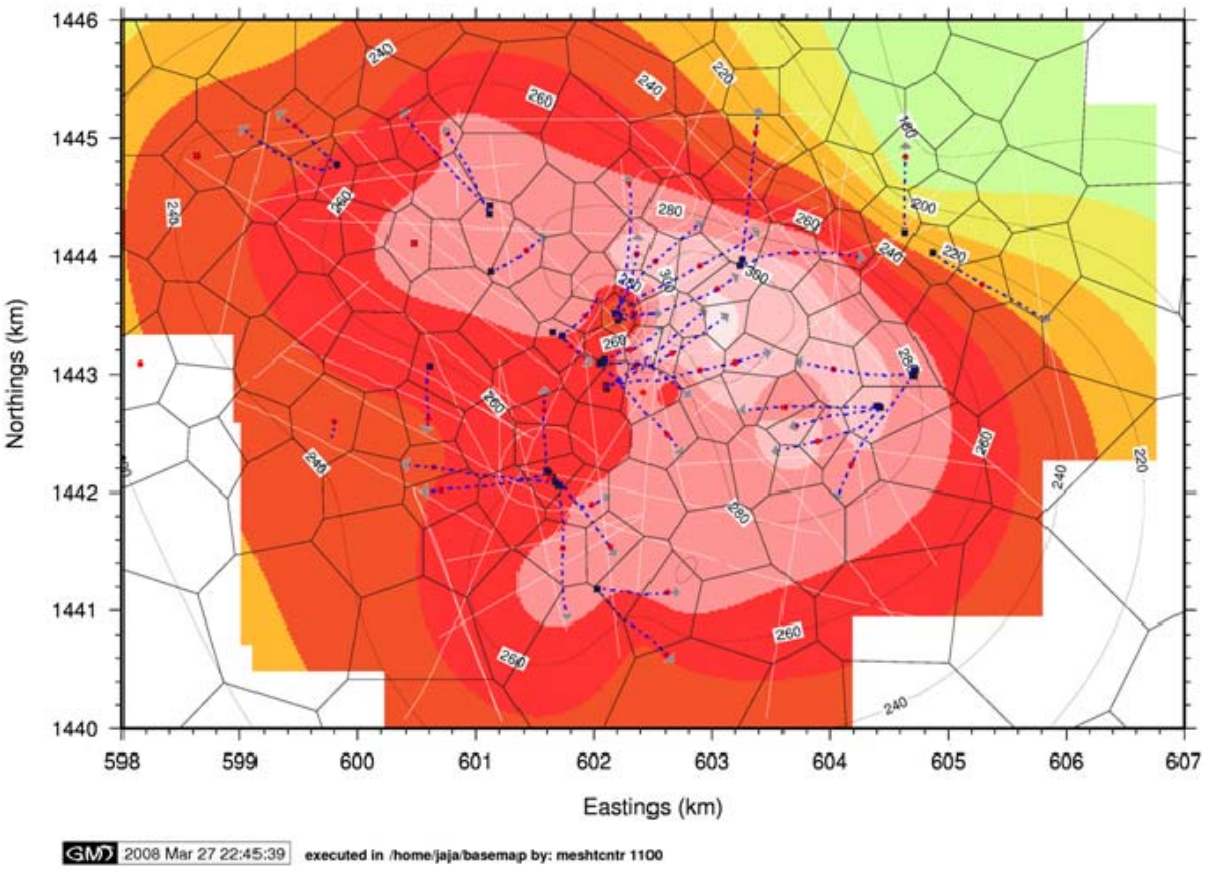

FIGURE 39: Mesh superimposed on temperature contour at -1100 mRSL

The distribution of rock types within model mesh was set using UNIX script **set_rocks.**which generates a map of all rocks in BacMan and assigns these rocks to each element. There are 12 material or rock types used. Distribution of materials in layer E using UNIX script **set_rocks** is shown in Figure 40. The complete permeability map showing different rock properties based on a best model is included in *Appendix 4*.

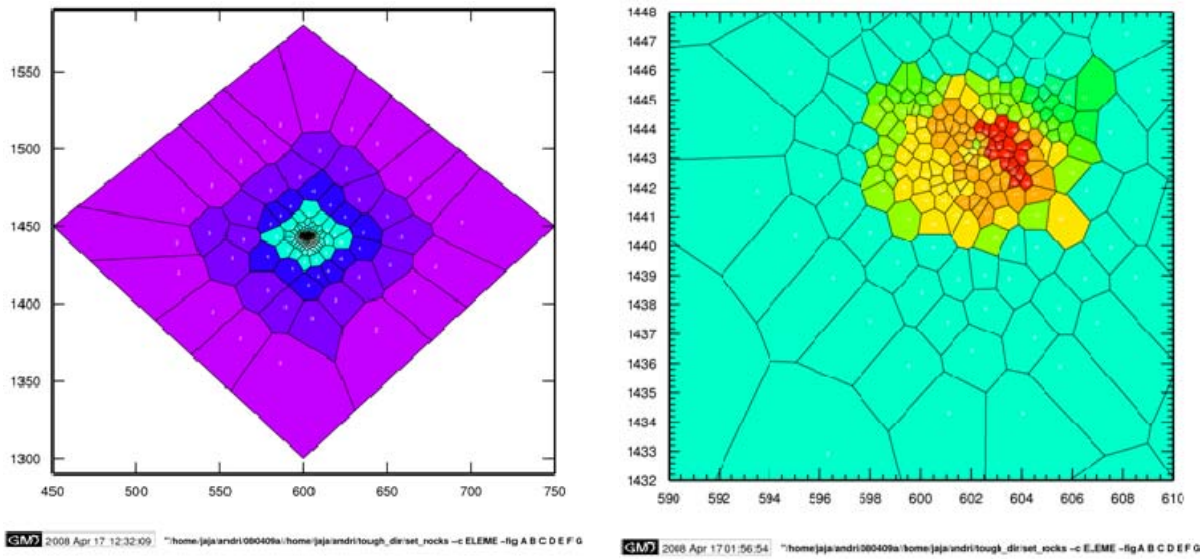

FIGURE 40: Permeability distribution of E-layer (enlarged view on the right)

6.3.6 Initial conditions

A temperature gradient of 83 °C/km and initial pressure of 2 bars at sea level are set as initial conditions using **set_incon**. The following prior information are provided to the model: hot recharge from below of 148.5 MW_t by hot fluid inflow (mf = 110 kg/s, h = 1350 kJ/kg) and 3.9 MW_t by heat conduction within a 4700 km^2 area (0.04% of total mesh area). Fumaroles are simulated by six (6) sinks on deliverability with a productivity index of $0.8x10^{-10}$. Top layer A and perimeter elements from B layer to K layer are set to a constant temperature and pressure allowing only heat transfer and no mass transport using UNIX script **set_inactive**. Inactive elements can also be set manually in TOUGH2 input deck. Please refer to Figure 41.

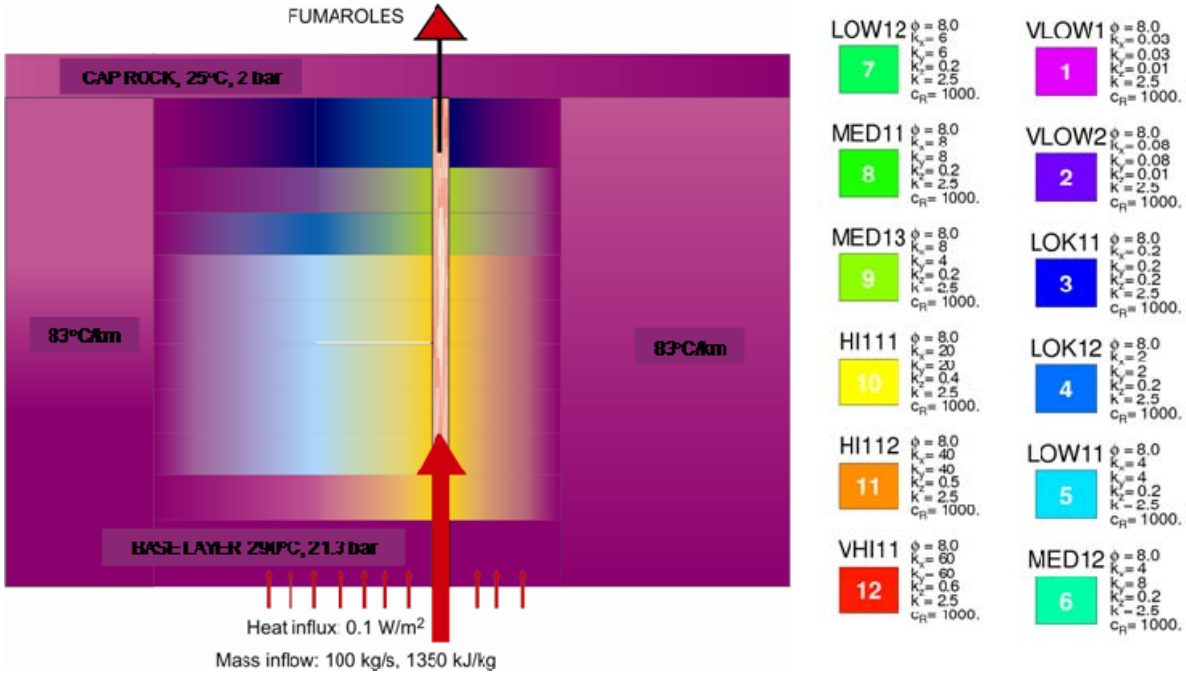

FIGURE 41: Permeability distribution, boundary and initial conditions

6.3.7 Key observations included in model calibration

The following data were included in the inverse model:

- Rock temperature and pressure profiles. These were assigned to the column containing the well and linearly interpolated to give values at layer centres;
- Pressure and temperature transients. These were assigned to the block containing the well feed zone; and
- Well flowing enthalpy transients. These were assigned to the block containing the well feed zone.

Interpreted initial temperatures-pressures (*Appendix 1*), temperature-pressure transients (Figure 42, 43) and enthalpy from flow tests of producing wells (Figure 44) are selected as

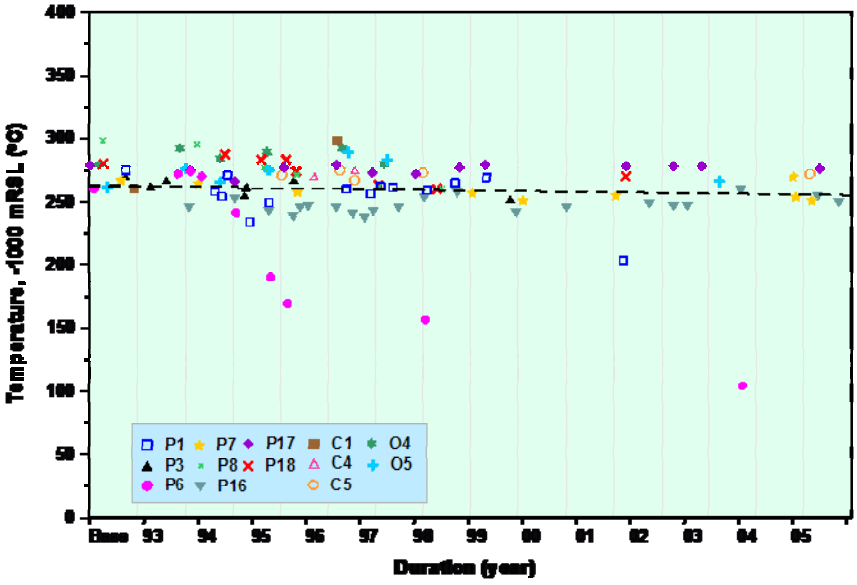

FIGURE 42: BacMan temperature transient measurements

key observations for well-by-well parameter estimation by iTOUGH2. Since temperature-pressure transients are compiled from downhole logs taken at irregular time intervals, data are linearly interpolated. Second level iTOUGH2 command **TIME** is used to select calibration points in time.

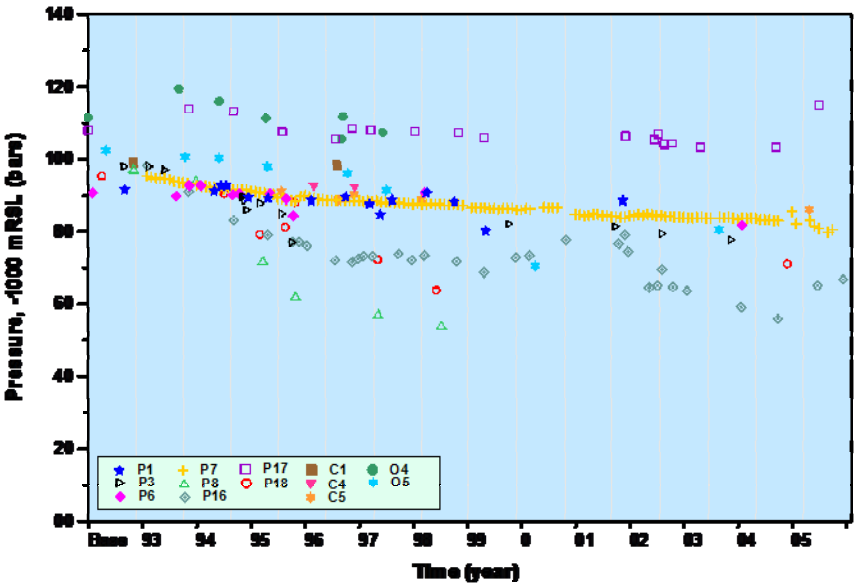

FIGURE 43: BacMan pressure transient measurements

Thermal decline in some wells is associated with pressure drawdown during initial phase of production. Some of the outliers seen in Figure 42, e.g. 150°C cooling in reinjection well PAL-6D, is an effect of brine injection. A high standard deviation σ_{zi} is assigned to temperature transient observations since most of these measurements are affected by production from nearby wells and also brine injection thus variability of final residuals is high.

In Figure 43, it is seen that the pressure response observed in well PAL-7D characterizes the mean pressure response to production. Pressure drawdown in BacMan field is dependent on mass extraction. Pressure recovers when mass extraction is low and declines when it is high. A standard deviation σ_{zi} of 1 bar is given to pressure transient observations.

In geothermal fields that are utilized moderately like BacMan, mass flow rates are controlled by the wellbore, thereby mass flow rates are fixed in this study according to a simplified production history of each production well (Figure 44). Production history data is simplified using a linear fit to interpolate massflow and enthalpy in equally-spaced yearly intervals. Blue labels on y-axis are baseline values prior to start of production.

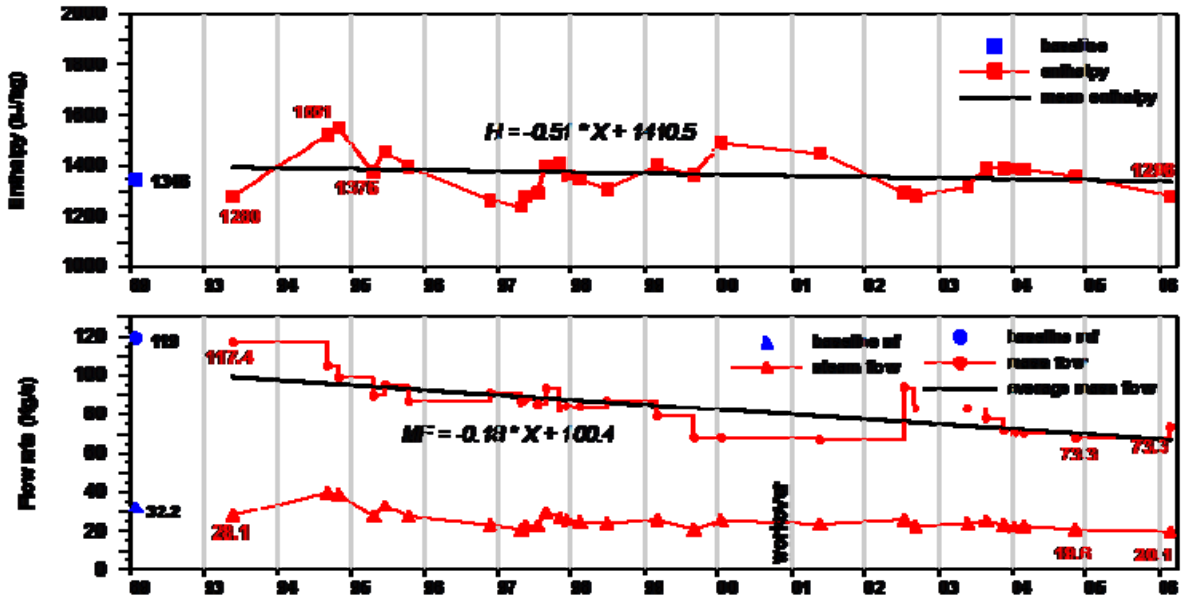

FIGURE 44: Simplified production history of PAL-14D

Once mass extraction becomes large enough to cause a large pressure drawdown, flow control shifts to the reservoir and wells start to produce on deliverability against a specific flowing bottomhole pressure, where $m_f = mobility \cdot PI \cdot (P_i - P_{bh})$, where PI is productivity index (m^3); P_i is reservoir pressure, and P_{bh} is bottomhole pressure.

6.3.8 Gravity test

Prior to actual simulation, a simple gravity test is performed on the model to ensure that connections between elements are correct and mass transport is negligible at steady-state conditions. Gravity test parameters are assigned in input file for TOUGH2. A uniform rock type is set for the entire model using test material ROCK1 having the following properties: grain density of 2650 kg/m^3; porosity of 10%; uniform absolute permeability of $20E^{-15}$ along the x, y, and z axes; formation heat conductivity of 2.5 W/(m°C); and rock specific heat of 1000 J/(kg°C). START is used so that INCON data can be in arbitrary order and need not be present for all grid elements. For record MULTI, the number of component and number of balance equations is set to 1 in which case only mass balances and no energy equations are solved. In case number of components is set to 2, results will simply show constant temperature in all layers. Equation of state 1 (EOS 1) for water and water with tracer is used to solve gravity test.

6.3.9 Trail of procedures

The use of scripts leaves a trail of procedures for tracing model development. The script used to generate the initial mesh, add layers, set initial conditions, and run the gravity test is executed using BUILD_MODEL and is given by:

./build_model -c centres -b bound -t 200 -z 0 -de -250 -500 -700 -900 -1100 -1300 -1500 -1700 -1900 -2150 -clear -g 80.0 -p 2. –gravi

The command means the first layer is at 0 m (-z tag), with a thickness of 200 m (-t tag) and succeeding layers midpoints are set at -250 m, -500 m, -700 m, -900 m, -1100 m, -1300 m, -1500 m, -1700 m, -1900 m and -2150 m (–de tag), temperature gradient is 80°C/km (-g tag), top model layer pressure is 2 bars (-p tag), and a gravity test is run (-gravi tag).

6.4 Results

6.4.1 Parameter optimization

A TOUGH2 simulation is performed with the current parameter vector $\boldsymbol{p}$ to obtain the elements of vector $\boldsymbol{z(p)}$. The simulation is repeated with updated parameters as proposed by Levenberg-Marquardt minimization algorithm.

The following observations contribute to changes in objective function $\boldsymbol{S_{obj}}$: steady state temperature with deviation of 10°C; steady-state pressure with deviation of 1 bar; pressure transients (drawdown) with deviation of 1 bar; and enthalpy of produced fluid with deviation ranging from 100 to 300 kJ/kg. Temperature transients are excluded from observations because they are affected by discharge of wells. After 10000 years, the steady-state save condition is achieved and the model proceeds from natural-state to production. The benefit of iTOUGH2 is that the model can go from natural-state to production, prediction, and recovery using the same input files and that all data sets contribute to the objective function which greatly reduces risk of making editing errors.

Parameter estimation $\Delta\vec{p}$ was performed on 15 parameters: mass source inflow, enthalpy of source inflow, heat flux, and 12 permeability values. A logarithmic distribution is used for k_x, k_y, and k_z. Results of parameter optimization is shown in *Table 9*: mass inflow decreased from 110 kg/s to 97.9 kg/s, enthalpy of source inflow increased from 1350 kJ/kg to 1830 kJ/kg, and permeability values decreased from initial guesses.

Sensitivity analysis showed that pressure drawdown is the most sensitive to the objectivity function (46%), followed by enthalpy (38%), temperature (14.3%), and pressure (1.4%).

TABLE 9: Estimated values of parameter after inversion

Parameters	Initial guess	Best estimate	Factor
Mass inflow (kg/s)	100	97.9	0.83
Enthalpy of inflow (kJ/kg)	1350	1830	1.36
Heat flux (MW_t)	3.9	7.9	2
Permeabilities (mD)			
vlow1_xy	0.78	0.49	0.62
vlow2_xy	0.64	0.63	0.98
lok11_xy	0.52	0.17	0.33
lok12_xy	1	1	-
low11_xy	0.58	0.32	0.55
low12_xy	6.11	6.02	0.99
med11_xy	0.53	0.41	0.77
med12_xy	5.39	5.01	0.93
hi111_xy	24.2	24	0.99
hi112_xy	100	100	-
vh111_xy	354	354	-

Note: mD = milliDarcy ≈ $1x10^{-15}$ m^2

6.4.2 Validation of model reliability

Results of isotropic and heterogeneous model show reasonable matches between simulated and observed values of steady-state temperatures and pressures (*Appendix 5*). Fine-tuning of vertical permeability is needed to get better match in temperature at I-layer of PAL-9D and PAL-10D, J-layer of PAL-18D, H-layer of PAL3RD, G to I layers of IM-1, I-layer of CN-1, and G-layer of CN-2RD and CN-3RD. In estimating permeability values, LOGARITHM gave better matches compared to log-normally distributed factor LOG(F). Inverting multiple data sets in a joint inversion resulted to lower objective function $\boldsymbol{S_{obj}}$.

Due to limitations regarding the number of datasets that the iTOUGH2 version used in this study can handle, total number of observations was limited to 377. Removed from observations are temperature transient measurements from wells drilled after the field started production in 1993. Temperature transients are affected by production from nearby wells and proved difficult to match in simulation. Removal of temperature transients reduced $\boldsymbol{S_{obj}}$. Steady-state temperature of PAL-19, PAL-20D, PAL-21, CN-1, CN-4, CN-5D, and OP-7D, included in early runs, are excluded in final run to improve $\boldsymbol{S_{obj}}$.

The contour planes provide a view of how the model captures plume propagation from bottom layer to top. Figure 45 to 52 show that the numerical model is able to reasonably follow the flow features of the conceptual model. Transient observations proved more difficult to match, hence, in order to improve model reliability, production history matching should be a continuing process. Model with parameters that are highly correlated will yield biased results and cannot readily be used for forecasting. In iTOUGH2, the correlation chart shown in Figure 53 is available for checking parameter correlation. All model parameters are connected to each other in this correlation chart. Vertical lines linking two parameters indicate the correlation coefficient, i.e. south_enth and sou_inflow are correlated by -0.8. The correlation chart displays a pyramid-like structure since the parameters are sorted according to their overall correlation. Long horizontal lines extend from the most strongly correlated parameter at the bottom to shorter lines connecting the most independent parameter at the top. In case of very strong correlations, where correlation = 1, parameters may be adjusted to lessen correlations.

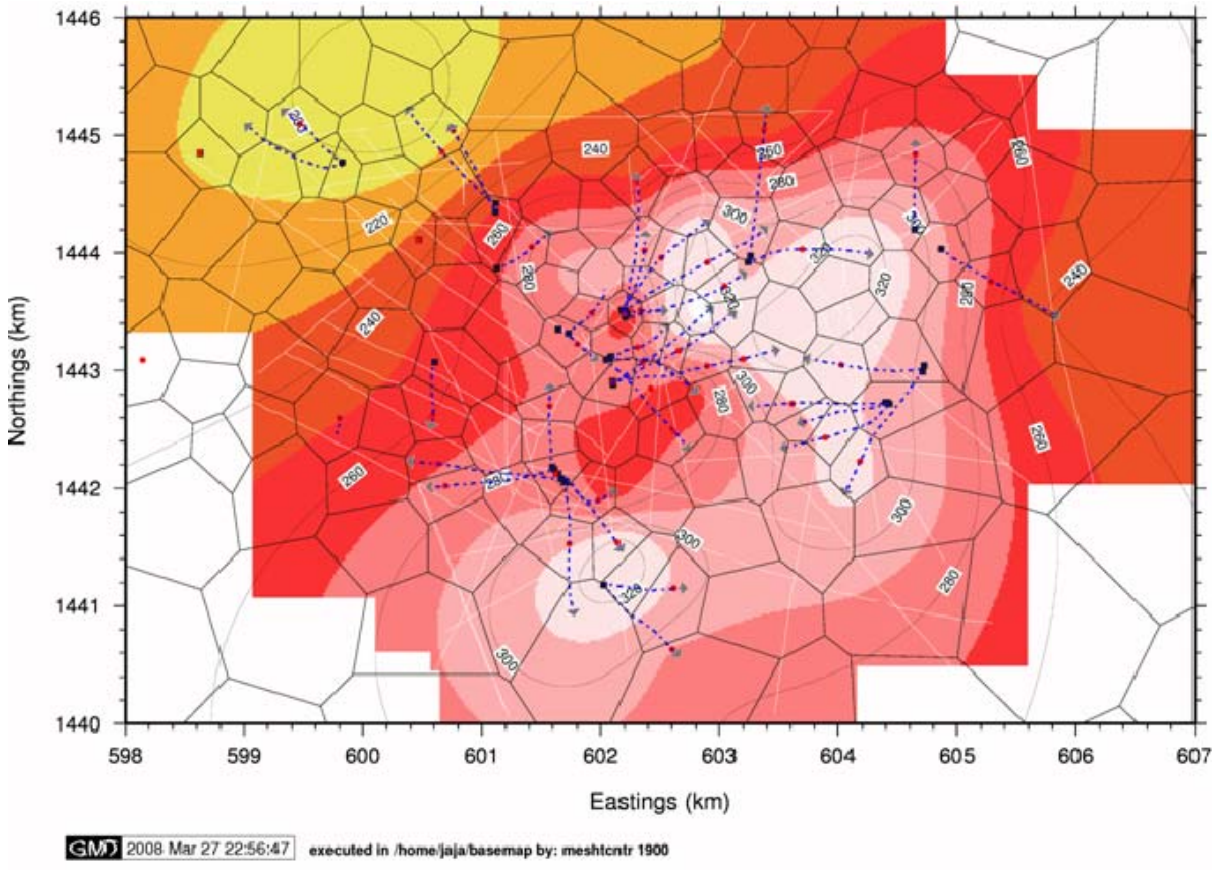

FIGURE 45: Temperature contours in J layer (-1900 mRSL), observed

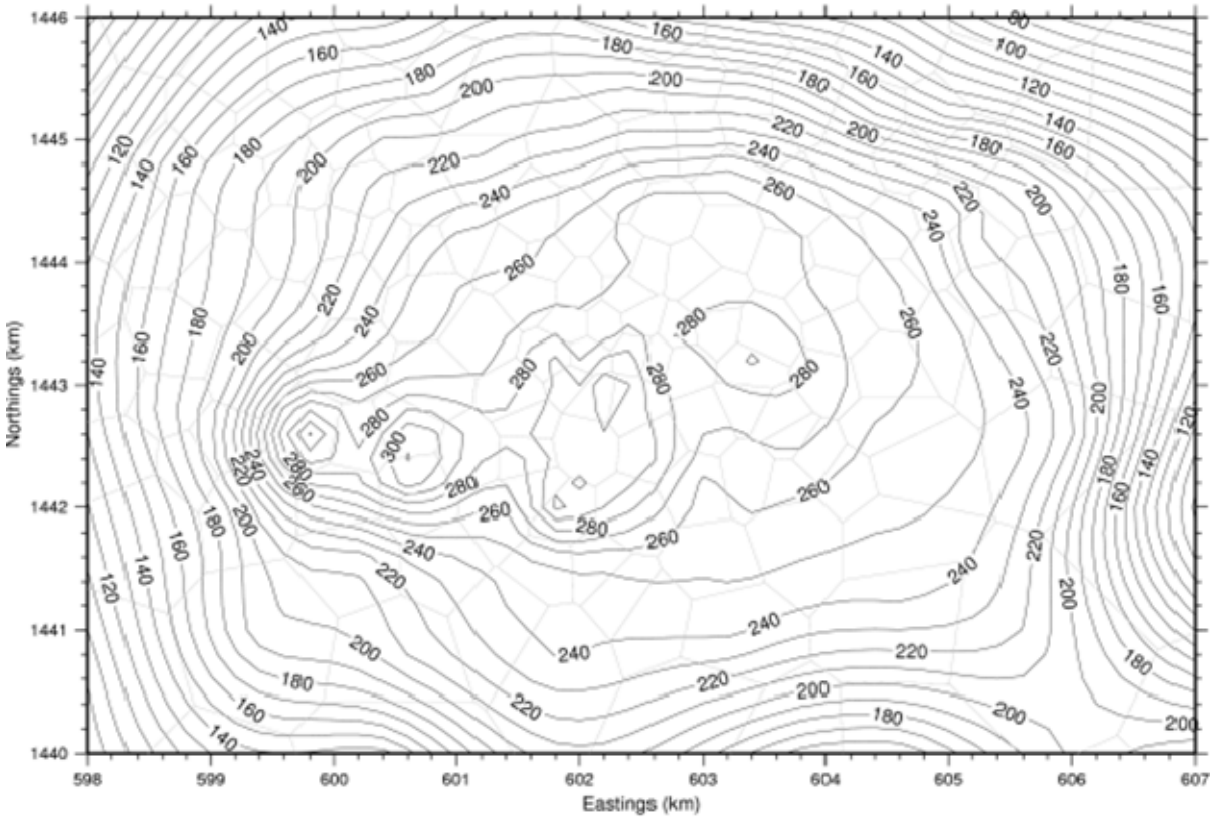

FIGURE 46: Temperature contours in J layer (-1900 mRSL), simulated

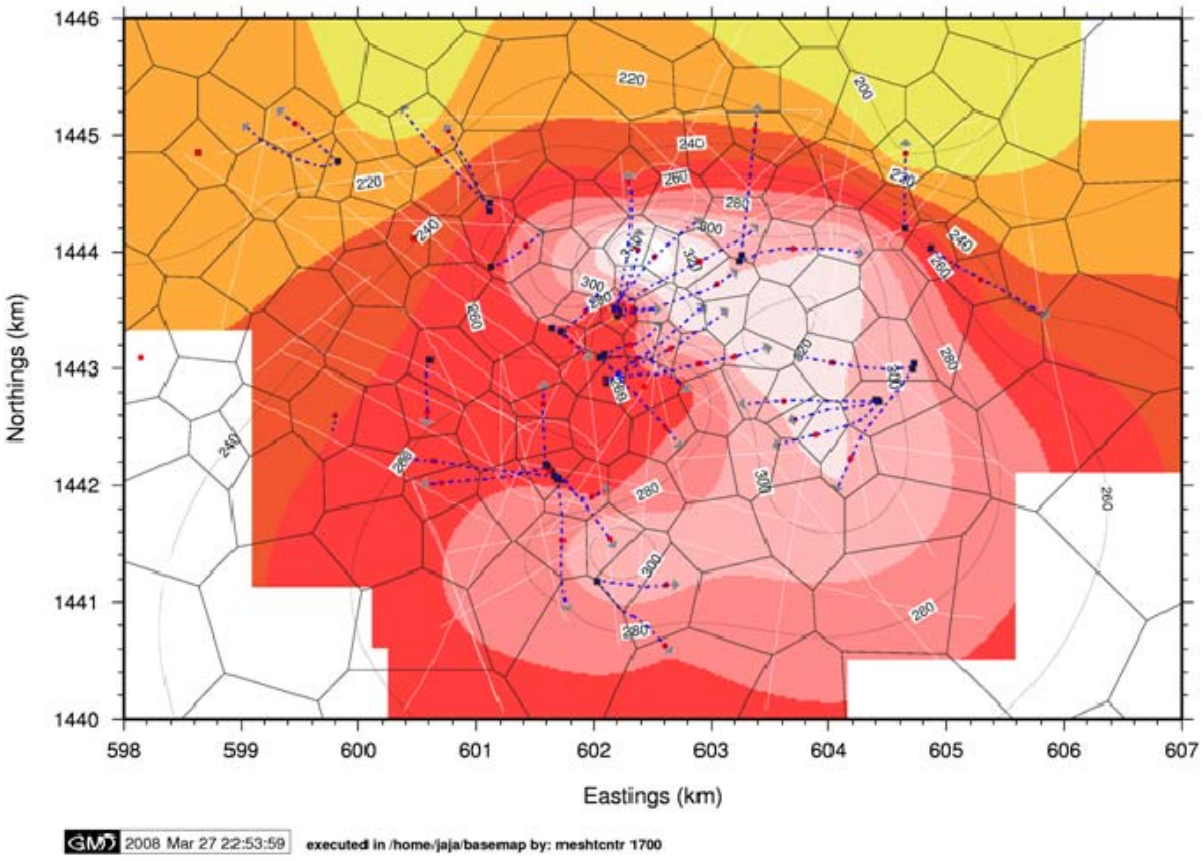

FIGURE 47: Temperature contours in I layer (-1700 mRSL), observed

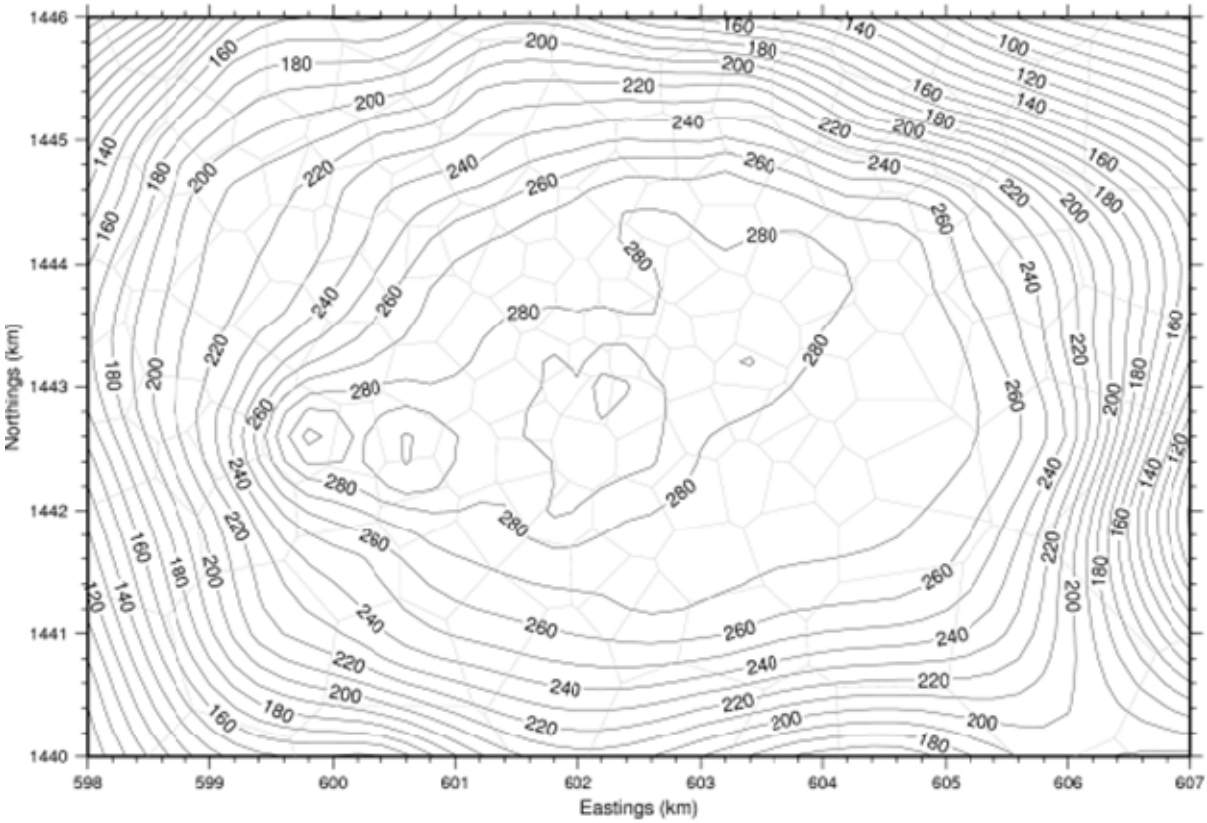

FIGURE 48: Temperature contours in I layer (-1700 mRSL), simulated

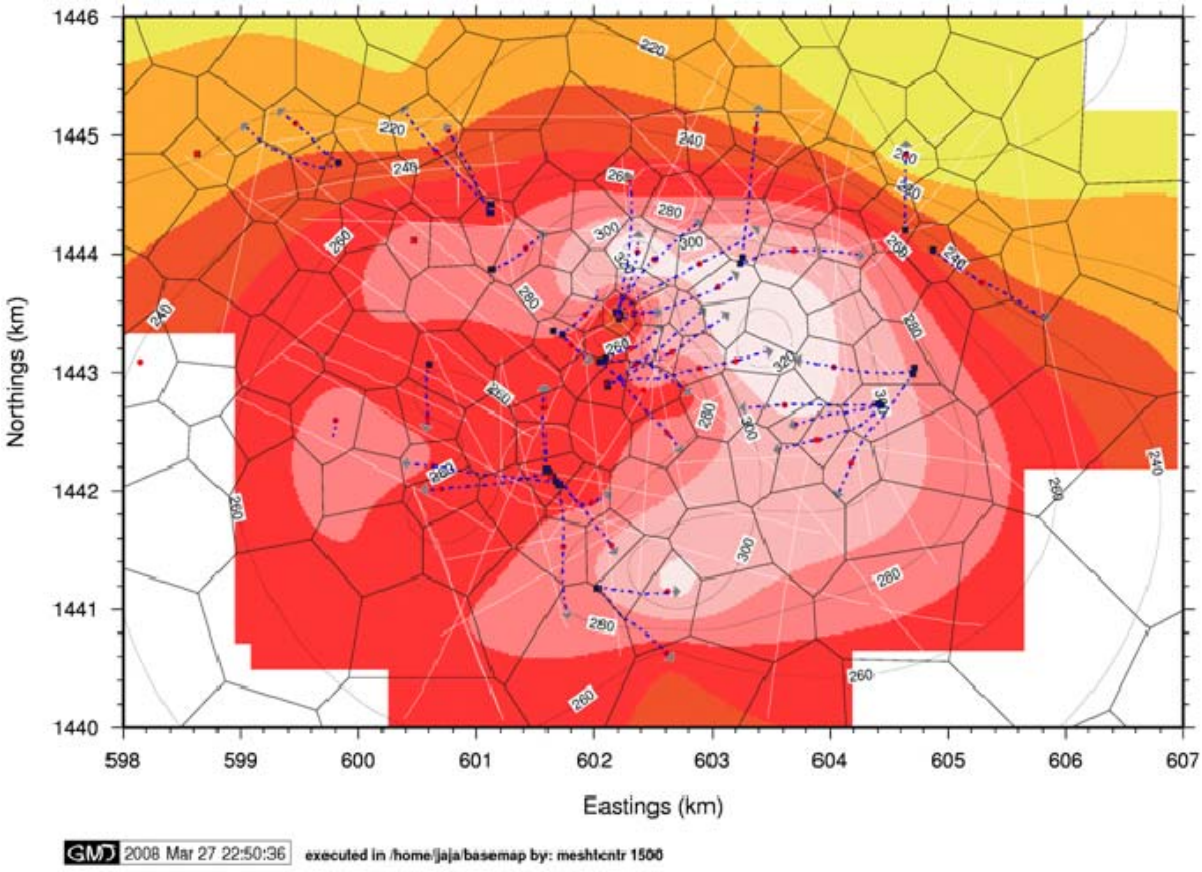

FIGURE 49: Temperature contours in H layer (-1500 mRSL), observed

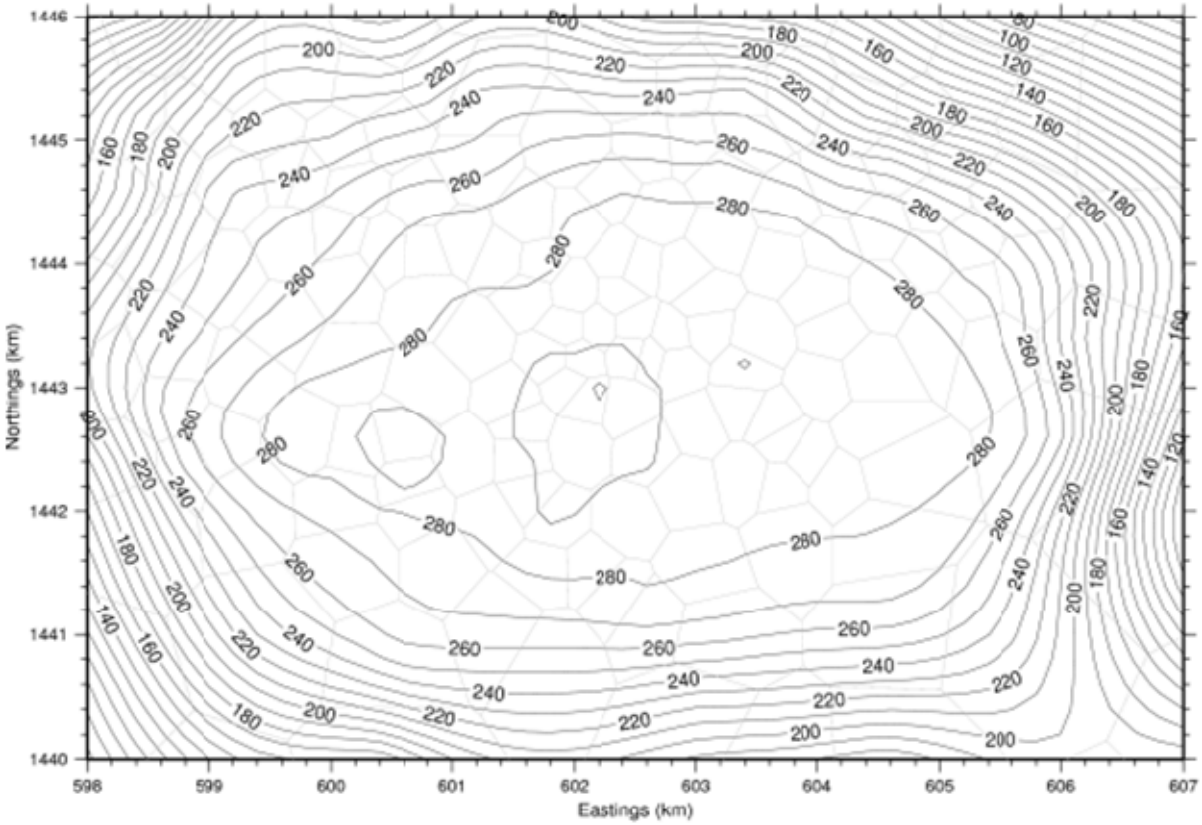

FIGURE 50: Temperature contours in H layer (-1500 mRSL), simulated

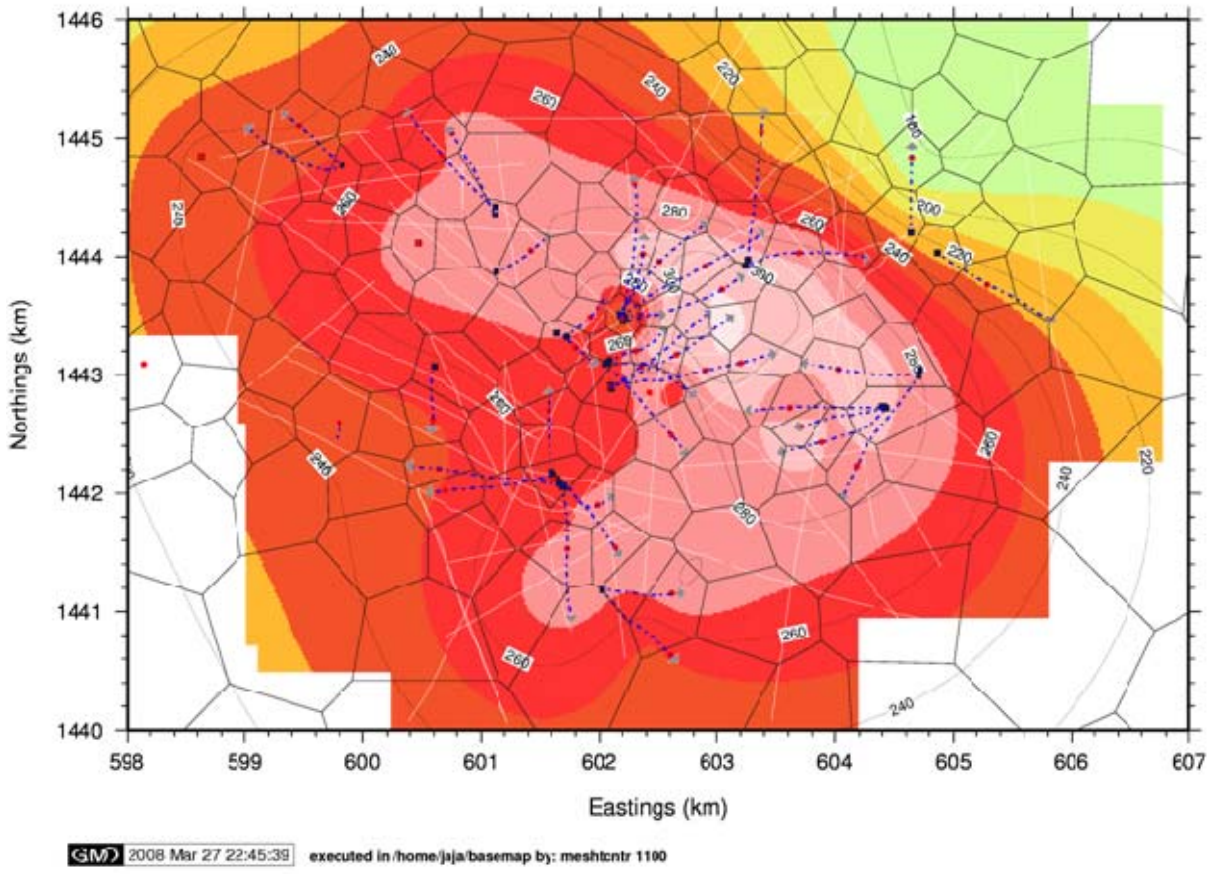

FIGURE 51: Temperature contours in F layer (-1100 mRSL), observed

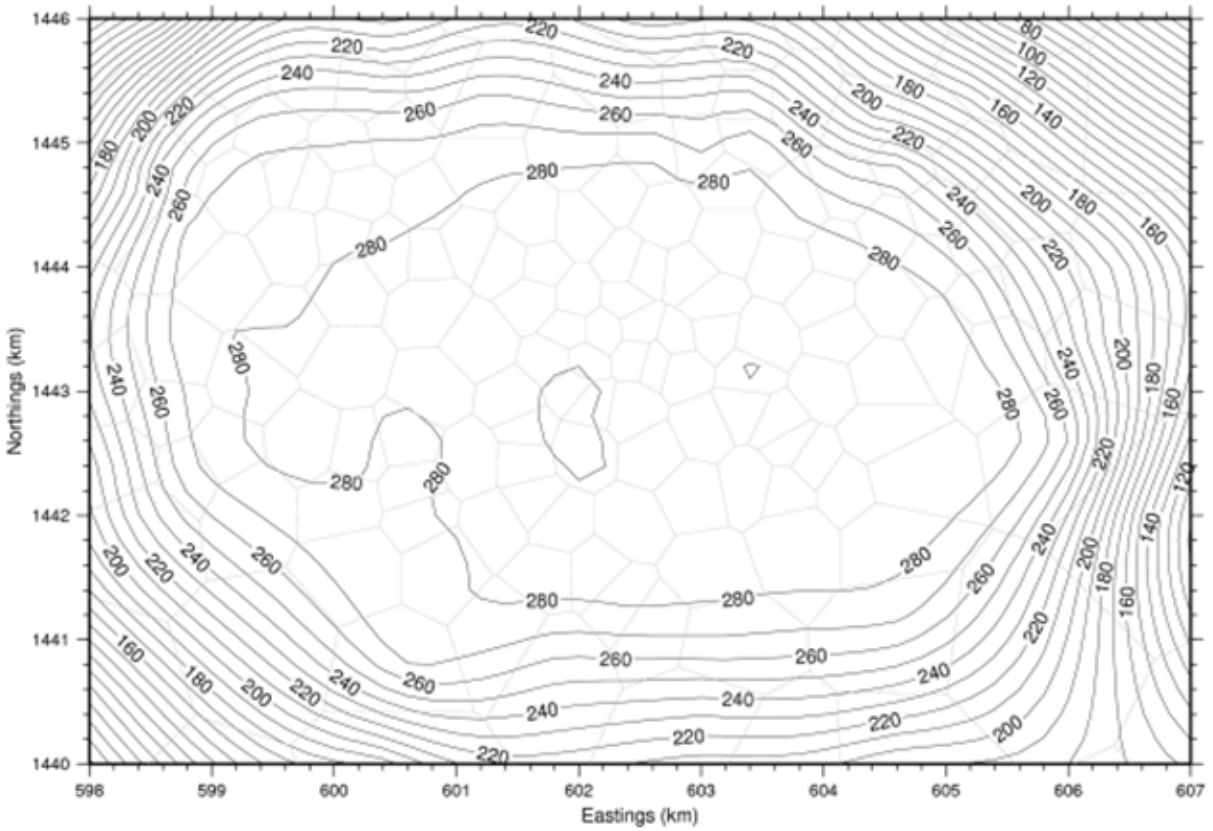

FIGURE 52: Temperature contours in F layer (-1100 mRSL), simulated

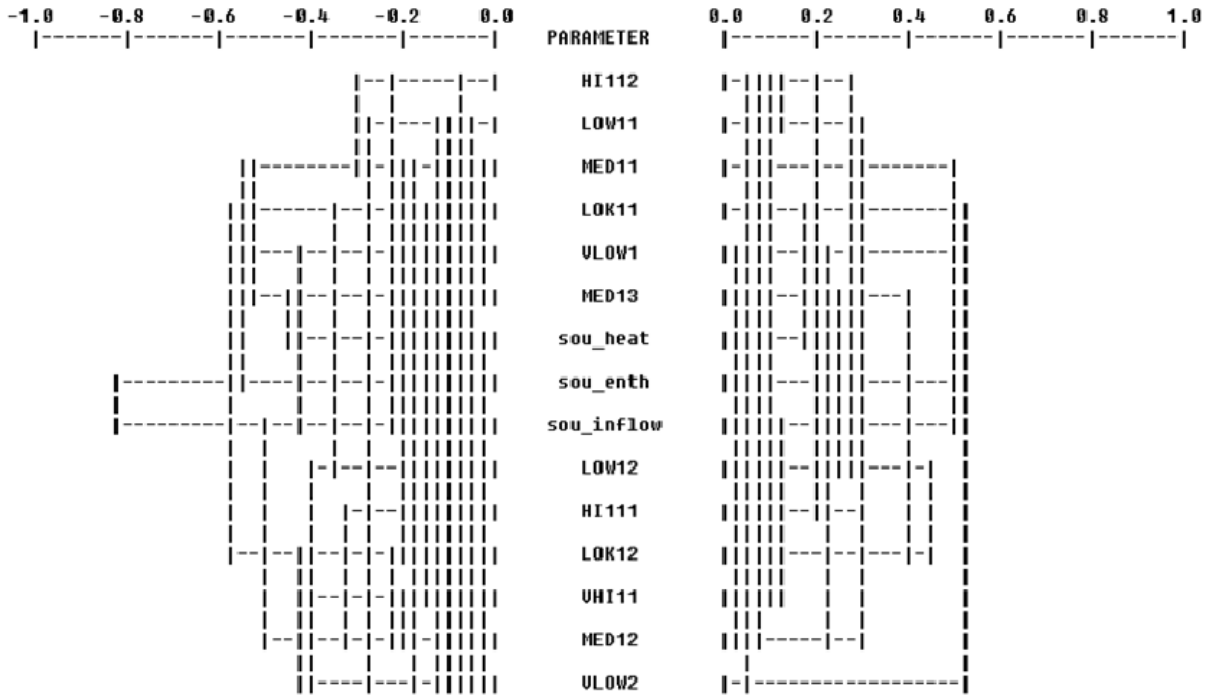

FIGURE 53: Correlation chart for detailed numerical model

Error analysis showed that enthalpy of inflow fluid is highly correlated to mass inflow. The 12 permeability parameters have direct correlation of no more than 0.6 hence the model may be tested for prediction purposes.

6.4.3 Sustainability assessment

In connection with the programmed privatization of NPC-owned power plants in BacMan and expected rehabilitation and operation at full-load condition until 2031, two production cases are studied (*Table 10*): (1) full-load operation with make-up wells producing from G, H, and I-layers (element IA395, GA164, GA169, HA174 and HA181); and (2) full-load operation with make-up wells producing from G-layer only (elements GA395, GA164, GA169, GA174, GA181).

TABLE 10: Production scenarios for BacMan model

Case	Generation (MWe)	Duration (years)	Make-up wells (layer)
1	150	2010-2031	G, H, I
2	150	2010-2031	G

Selection of location for make-up wells prioritized infill drilling with the exception of a step-out well in Tanawon (IA395, GA395). Numerical model predicted that at least five production wells need be drilled to sustain the full-load requirement up to 2031. Moreover, at least three reinjection wells need to be drilled to handle increased brine load from make-up wells assuming an average acceptance of 80 kg/s per well. All five make-up wells added in 2010 and are producing on deliverability began flowing in 2010. Productivity indices of make- wells are adjusted so that each well will yield at least 16 kg/s of high-pressure steam which is consistent with power density estimate ranging from 8 to 12 MWe/km^2 from volumetric model. It is assumed that 2.2 kg/s of high-pressure steam generate 1 MWe electric.

In Figure 54, it can be seen that both production cases gave similar trends for gross generation, amount of high-pressure steam, amount of separated brine, and mean enthalpy. Mean enthalpy is very stable showing no signs of cooling in the reservoir. Supply of high-pressure steam is also very stable.

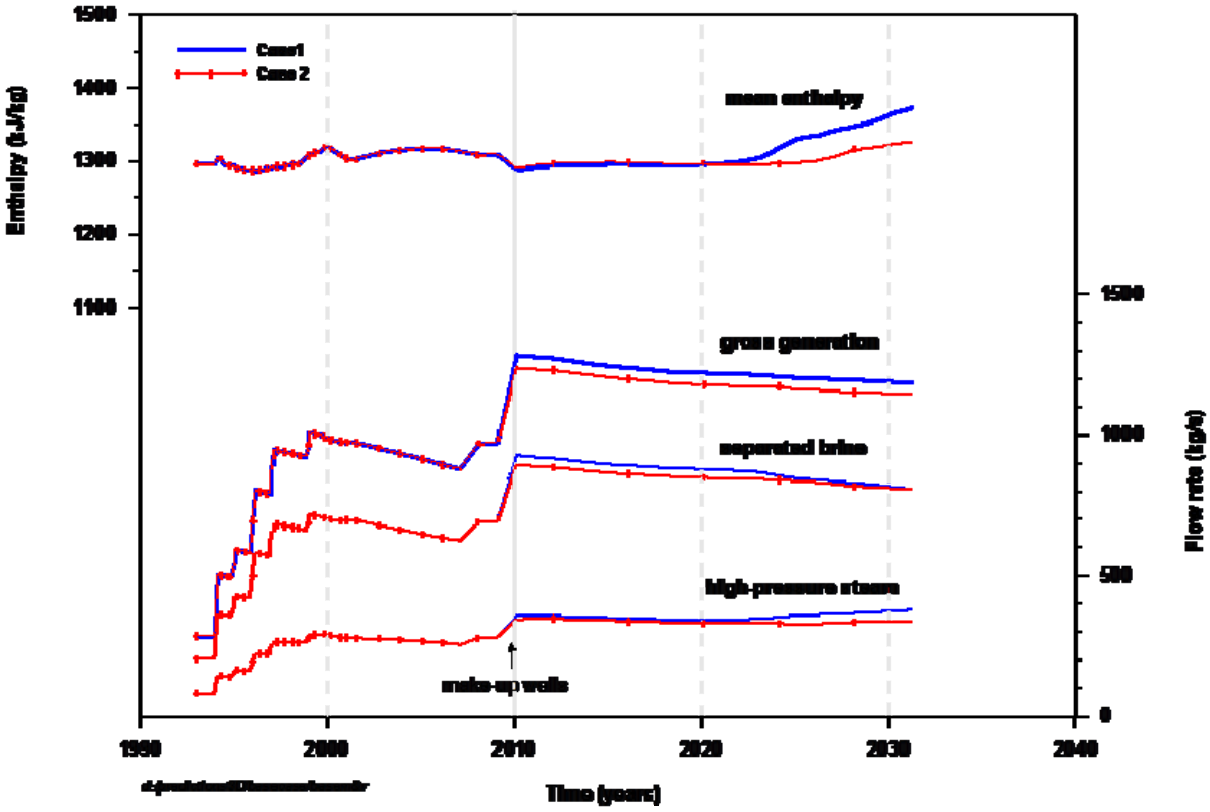

FIGURE 54: Predicted generation rates and mean enthalpy

Decline in separated brine and increase in steam flow and enthalpy in year 2025 indicates formation of two-phase zones. Predicted flow at different separation pressures (7, 8, and 9 bar) are shown in *Appendix 6*.

Using a couple of imaginary no-load production scenarios, no-load after year 2031 and year 2060, the model is tested for reversibility. A staged recovery of reservoir pressure is observed which may be explained by behaviour of steam saturation at different layers as shown in Figure 55 and 56. A steam-cap had to be collapsed first before pressure starts recovering. The behaviour may be model-related and should be investigated further. Very strong permeability contrast between layers can be looked into. In Figure

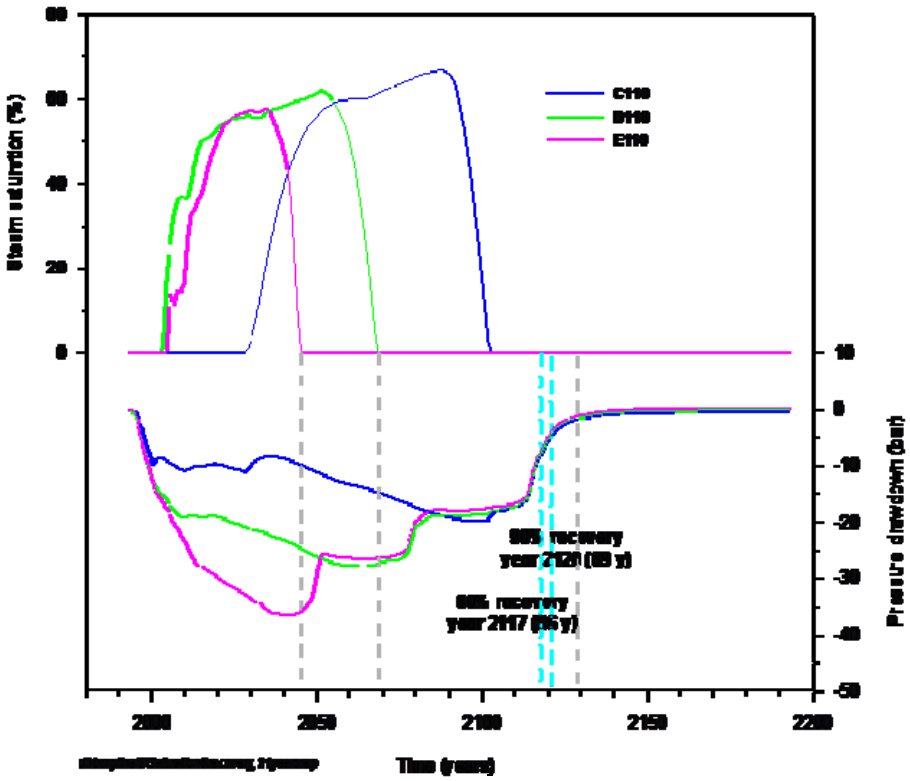

FIGURE 55: Steam saturation and pressure trend, 21 years of forecasted production

55 and 56, pressures in elements C, D, and E near the depth of observation well PAL-7D are investigated. It is seen that steam from deeper layer E-layer condenses first followed by succeeding layers above. 80% recovery takes place in the following time frame: a) after ~86 years after 21 years of production; and (b) after ~87 years after 50 years of production. The model predicts a total pressure drawdown to be 40 bar by year 2031.

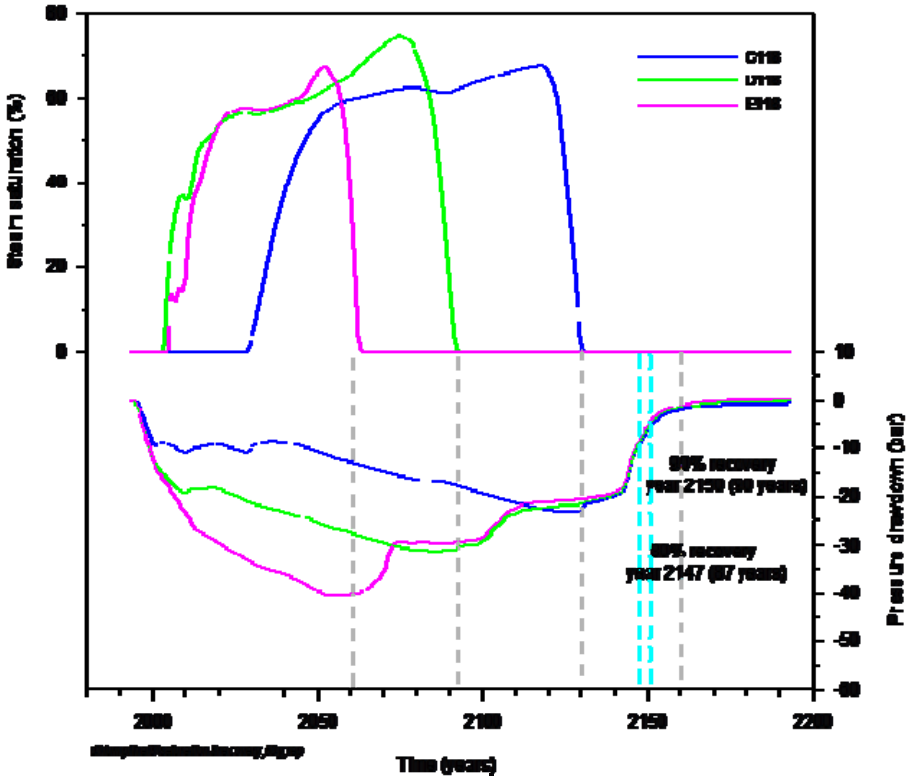

FIGURE 56: Steam saturation and pressure trend, 50 years of forecasted production

In Figure 57 and 58, full recoveries of pressure and temperature are compared after producing the field for 40 years. The model predicts pressure and temperature will take ~100 and ~800 years respectively to achieve full recovery.

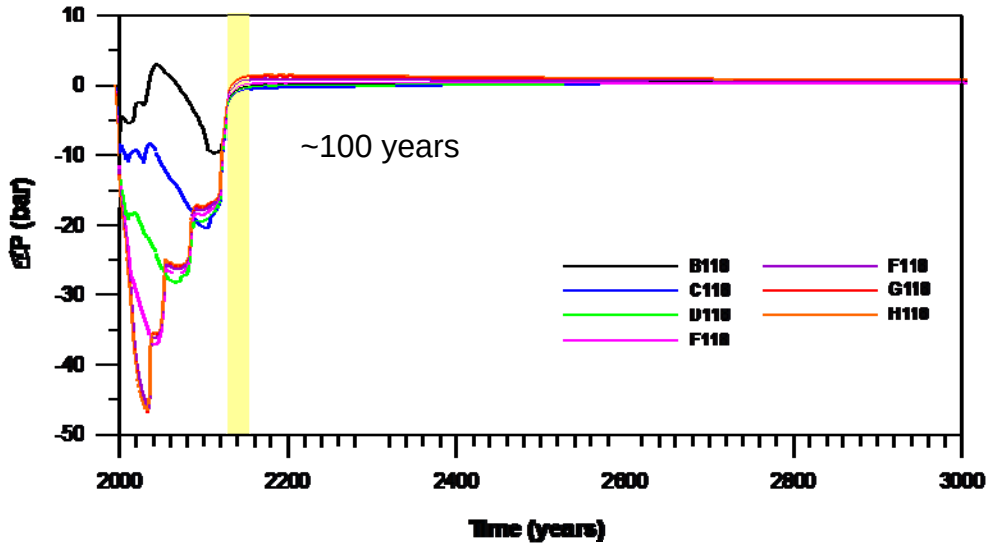

FIGURE 57: Pressure recovery after 40 years of production

6.4.4 Summary of sustainability assessment

Inverse modelling has been applied with modest success in model calibration. Presently, 15 parameters have been inverted on a single node of a Linux cluster. The model has been calibrated against 466 datasets. Sensitivity analysis showed that the pressure drawdown is most sensitive to objective function (46%) followed by flowing well enthalpy (38%). Deep recharge was calibrated at 98 kg/s of 1830 kJ/kg enthalpy. Recharge enthalpy of 1830 kJ/kg indicates that 365°C fluid can be extrapolated from bottom of BacMan wells using the 2300 m deep model. Permeability values should be in the range of 0.5 to 5 mD for far-field and 25 to 100 mD for productive wellfield. The 12

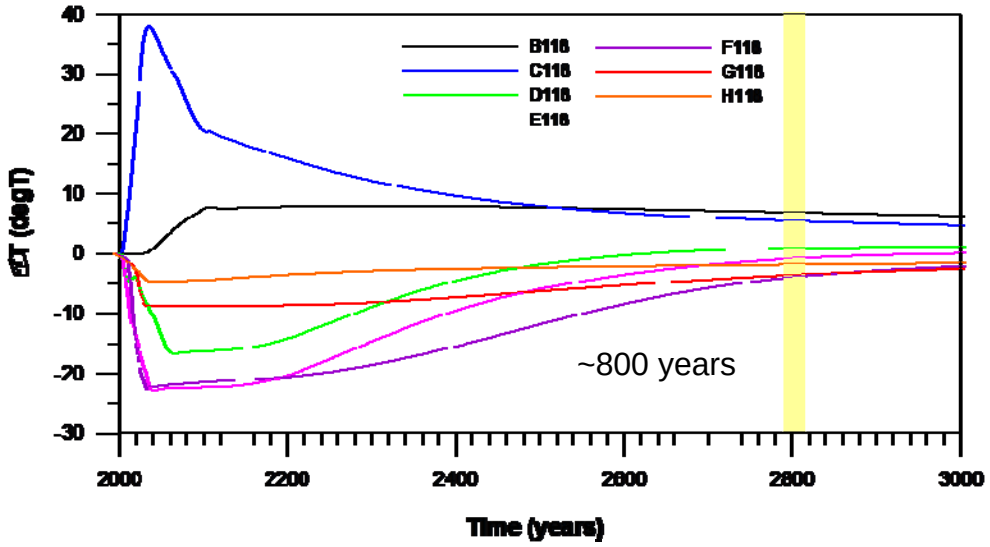

FIGURE 58: Temperature recovery after 40 years of production

permeability values have direct correlation of no more than 0.6. The steady-state distribution of temperatures, pressures, and reservoir flow patterns as seen in conceptual model sketches have been generally confirmed.

In order to meet and sustain high-pressure steam requirement (330 kg/s) for the full-load operation until 2031, at least five production and 3 reinjection wells need to be drilled. Mean enthalpy is very stable showing no signs of cooling in the reservoir. Supply of high-pressure steam is also very stable. Decline in separated brine and increase in steam flow and enthalpy in year 2035 indicates formation of two-phase zones.

Numerical model predicts total pressure drawdown to be 40 bar by 2031. The model is reversible and pressure will attain 80% recovery after 86 years. On the other hand, recovery after long-term production of 50 years will take 87 years.

Finally, full recoveries of temperature and pressure are compared after producing the field for 40 years. Pressure and temperature took ~100 and ~800 years to recover respectively.

7. COMPARISON OF DIFFERENT MODELS

The volumetric method is used to estimate generating capacity as a first stage assessment when data is scarce. When production data is available, lumped parameter modelling can estimate the production potential of a geothermal system and the effects of different production scenarios through pressure response predictions. When sufficient production data is available, well-by-well numerical models can be used to evaluate field response to different production scenarios. Detailed numerical models include boundary recharge; a reservoir property which allows successful utilization of a resource for generations.

Volumetric model does not consider the dynamic response of reservoir to exploitation, e.g. pressure response, hence the use of volumetric model solely to decide the generating capacity of a field is an aggressive approach. Negative effects of neglected pressure response may lead to undesirable reservoir effects such as fast drawdown rates and cooler fluid intrusion which are mitigated at later stages in utilization history by make-up drilling and changed reinjection strategies. This aggressive approach may lower initial costs but also increase cost of maintaining steam flow rates at later times (Sarmiento and Björnsson, 2007). Volumetric model also does not consider permeability and recharge. Reservoirs with same heat content may have different permeabilities and recharge and, hence, very different production potentials. Volumetric method does not consider dynamic response to exploitation; hence, it cannot validate the sustainability or reversibility of generating capacity it yields.

Although lumped parameter models have been developed for isothermal, single phase conditions, lumped parameter models are able to match measured responses under two-phase conditions in BacMan reservoir very accurately. Open and closed tank models can differentiate effects of recharge. Evaluation of lumped models using LUMPFIT, however, must be used with caution for boiling reservoirs as the governing equations of lumped models is based on mass conservation only excluding conservation of heat.

Detailed numerical models take more time to prepare but are extremely powerful tools for studying various field management options. Inverse modelling using iTOUGH2 can validate if model parameters are highly correlated and thus over-parameterized. Over-parameterized models can yield biased forecasts hence should be calibrated further before using for forecasting. The correlation chart available in iTOUGH2 can be used to estimate the correlation between parameters which will decide whether the model can be used for prediction.

The full-load capacity of 150 MWe for BacMan is within the estimated recoverable reserves by volumetric model. In Figure 59, the comparison of simulated pressure drawdown using lumped parameter and well-by-well numerical model is shown. Pressure drawdown as estimated by lumped and numerical models can be summarized as follows: 0.67 bar/year (lumped, optimistic case) and 1 bar/year (numerical, pessimistic case). Pressure recovery, at 80%, can be summarized as follows: 39 years (lumped, optimistic case) for a production: recovery ratio of 1:1, and 86 years (numerical, pessimistic case) for a production: recovery ratio of ~1:2.

The question as to which is a better model is difficult to answer as the accuracy of model predictions will depend on how successful the modeller is in preparing a model, may it be analytical, lumped, or distributed, that will accurately model available data considering the inherent limitations of each model. What is essential is to use the different reservoir models within the inherent limits for which they were designed.

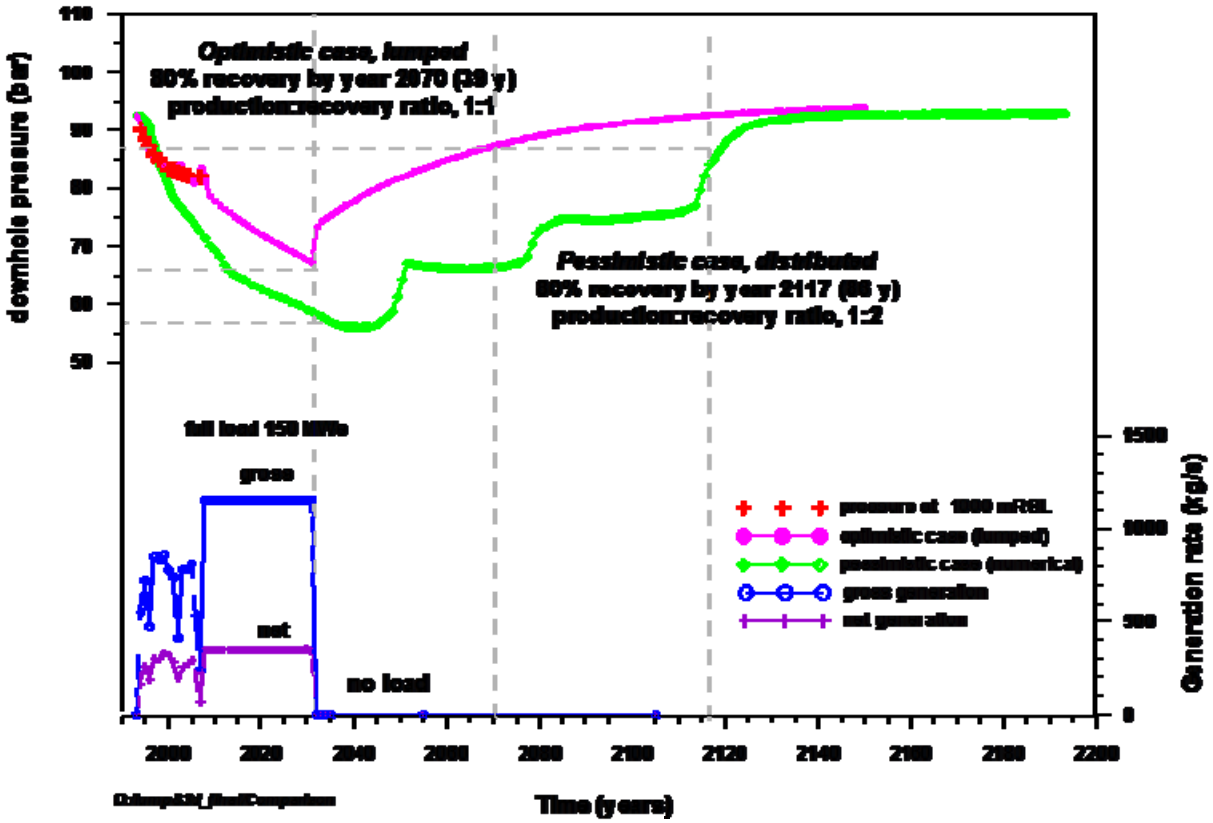

FIGURE 59: Comparison of drawdown and recovery from lumped and numerical models

8. CONCLUSIONS AND RECOMMENDATIONS

In this study, sustainability of Bacon-Manito geothermal resource operating at full-load capacity was assessed using a well-by-well numerical model. Results were compared with a lumped parameter model while a volumetric model provided a robust estimate of generating capacity.

The conceptual reservoir model has been revised. All downhole temperature and pressure data were analyzed applying methods like boiling-point with depth, pivot-point, and Horner method.

The conceptual model confirmed the heat source is at the bottom of wells PAL-10D and OP-4D which logged a maximum temperature of 326°C. The highest chloride concentration is observed in upflow zone. The conceptual model shows a mushroom-type reservoir explaining the inversion found in wells intersecting the reservoir boundaries. A low permeability caprock extends from surface to -500 mRSL as manifested by a linear temperature gradient along these depths. Fluid flows preferentially west-northwest towards Inang-Maharang where fluids emerge as hot springs in Inang-Maharang. Fluid also flows in south-easterly direction flow towards Rangas which is facilitated by structural permeabilities related to Makabug, Botong, and Dome faults. The flow directions are consistent with magnetotelluric and geochemical data which define major outflows to the northwest and southeast. Geochemical field trends are consistent with measured temperature trends.

The area and thicknesses defined in conceptual model and physical characteristics derived from related geoscientific researches are used for the volumetric model. The volumetric model using Monte Carlo method showed that there is 90% probability of obtaining a mean reserve of 94.1 MWe for BacMan 1 and 106.3 MWe for BacMan 2 for 25-year period (2006 to 2031). The use of volumetric model solely to decide the generating capacity of a field is an aggressive approach since volumetric model does not consider the dynamic response of reservoir to exploitation, hence, cannot validate the sustainability or reversibility of generating capacity it yields.

Fourteen years of production history was carefully analyzed to come-up with the net generation of the reservoir. Net mass withdrawal of 360 kg/s and pressure data from monitoring well PAL-7D were used to set-up a lumped model. Although lumped parameter models have been developed for isothermal, single phase conditions, lumped models are able to match measured responses under two-phase conditions in BacMan reservoir very accurately. The best lumped model predicted that BacMan reservoir can support full-load operation for at least 23 more years with minimal pressure drawdown of 0.67 bar/year. The lumped model provides an optimistic scenario where pressure recovery at 80% takes 39 years, for a recovery ratio of 1:1.

Availability of 14 years of production data justified a well-by-well numerical modelling approach. The detailed numerical model included boundary recharge, a reservoir property which allows successful utilization of a resource for generations, which makes it preferable when it comes to addressing environmental issues like sustainable development and renewable power generation. Detailed numerical model accounted for most of the field data requiring major effort. The model mesh covers an area ~49730 km^2, has 11 layers having 277 elements/layer for a total of 3047 elements. The top, bottom, and outermost elements in each layer are inactive. Initial temperature and pressure is set to be 83°C/km and 2 bar respectively. Model was calibrated against 466 datasets supporting the mesh at all times. Some data sets are faked to get a reading of mass generation from wells.

Inverse modelling resulted in the optimization of the following parameters: permeability of outermost elements characterizing outer wellfield ranging from 0.49 mD to 5 mD; permeability of innermost elements characterizing inner wellfield ranging from 24 mD to 100 mD; mass inflow to be 97.9 kg/s having an enthalpy of 1830 kJ/kg; and heat flux to be 7.0 MW_t. Mass venting from fumaroles, which are not part of inversion process and were put on deliverability, was estimated to be ~200 kg/s. The deep reservoir is a pressure low which siphons recharge, which is essential to get reversed temperatures in boundary wells. Sensitivity analysis showed that pressure drawdown is most dominant (46%), followed by enthalpy (38%), temperature (14.3%), and pressure (1.4%). Results of isotropic and heterogeneous model show reasonable matches between simulated and observed values of steady-

state temperatures and pressures. Contour planes are in reasonable agreement with flow features of conceptual model. Transient observations are more challenging to match. To improve reliability of predictions, numerical model must be continuously recalibrated against new production history.

Correlation chart shows model parameters are not strongly correlated hence the detailed numerical model may be used for prediction. Since this a study on sustainability, the wells were put on forced mass production except in predictions where make-up wells were put on deliverability. Detailed numerical model predicted that at least five production and three reinjection wells are needed to be drilled to complete high-pressure steam requirement (330 kg/s) for full-load operation while allowing pressure drawdown. Mean enthalpy appears to be very stable showing no signs of cooling in the reservoir. Supply of high-pressure steam is also very stable. An opportunity presenting itself in this study is the steady flow (~800 kg/s) of high-temperature (170°C) separated brine until 2031. Predicted separated brine flow may be used as a guide for future power plant optimization which may consider a second-flash bottoming plant if injection of lower temperature brine will not have a negative effect on reservoir temperature. Decline in separated brine and increase in steam flow and enthalpy in year 2035 indicates formation of two-phase zones. The numerical model provides pessimistic scenario where pressure recovery at 80% takes 86 years, for a production: recovery ratio of ~1:2. Detailed numerical showed that both mass and heat mining are reversible.

Lumped parameter and well-by-well numerical model showed that full-load utilization at 150 MWe is both sustainable and reversible making renewal of power plants feasible.

To improve data management for detailed numerical modelling, databases may be created to facilitate creation of input files of temperature and pressure transients and production histories for iTOUGH2. The model pre- and processors used and developed in this thesis may be enhanced by programming seamless integration with databases. To ensure sustainable utilization of geothermal resources, geothermal operators should establish a protocol for assessing sustainability of their geothermal resource. Ultimately, the modelling tools and techniques used and developed in this thesis should be used to sustainably manage and develop present and future geothermal resources in the Philippines.

NOMENCLATURE

°C	Degrees Celsius (°C)
$\vec{D}_{\beta}^{\kappa}$	Hydrodynamic dispersion tensor
E	Total energy (SI, energy)
E_o	Maximum energy production (SI, energy)
$\overrightarrow{F}$	Advective mass flux
$\vec{g}$	Acceleration due to gravity (m/s^2)
GWh	Gigawatt-hour (GWh)
H	Enthalpy (kJ/kg)
h_{β}	Specific enthalpy in phase ß
K	Thermal diffusivity (m^2/s)
K	Absolute permeability (m^2)
$k_{r\beta}$	Relative permeability
k_x	Permeability in x direction (mD)
k_y	Permeability in y direction (mD)
k_z	Permeability in z direction (mD)
mD	Millidarcy (mD)
mf	Mass flow (kg/s)
mMD	Metres measured depth (m)
mRSL	Metres reduced sea level (m)
MTOE	Million Ton-of-Oil-Equivalent (10^6 tons)
mVD	metres vertical depth (m)
MWe	Megawatt electric (10^6 watts)
MWt	Megawatt thermal (10^6 watts)
q	Conductive heat flux (W/m^2)
Ra_c	Critical Rayleigh number (dimensionless)
R^2	Coefficient of determination (dimensionless)
S	Storativity (kg/m^3Pa)
S_{β}	Saturation of phase ß
S_{obj}	Objective function (dimensionless)
T_{ref}	Temperature, reference/abandonment/rejection (°C)
T_{res}	Temperature, reservoir (°C)
$\vec{u}_{\beta}$	Darcy velocity, multiphase
V	Volume of reservoir (m^3)
Vn	Volume normalised extensive quantity

Acronyms, initialisms

BacMan	Bacon-Manito Geothermal Production Field
CN	Cawayan
DOE	Department of Energy
GENZL	Geothermal Energy New Zealand Ltd.
GMT	Generic Mapping Tool
IFDM	Integral Finite Differencing Method
IM	Inang-Maharang
MAN	Manito
MO	Malanto
MT	Magneto-telluric
NCG	Non-Condensible Gas
NPC	National Power Corporation
OP	Osiao-Pangas
PAL	Palayan-Bayan
PB	Puting-Bato
PNOC EDC	Philippine National Oil Company - Energy Development Corporation

TOUGH	Transport of Unsaturated Groundwater and Heat
TW	Tanawon
VES	Vertical Electrical Sounding
WellTaPPs	Wellbore Temperature and Pressure Plotting Software

Greek letters

α	Thermal expansion coefficient
β	Phase ß
ΔT	Temperature difference (°C)
$\Delta\vec{p}$	Parameter estimation
K	Heat capacity (J/kg°C)
κ	Mass capacitance, LUMPFIT (ms^2)
λ	Thermal conductivity (W/m°C)
λ_{Lev}	Levenberg parameter
μ_β	Internal energy in phase ß
μ_β	Viscosity, TOUGH2
ν	Kinematic viscosity (m^2/s)
ν_{Marq}	Marquardt parameter
ρ_β	Density of phase ß
ρ_R	Grain density
σ	Conductance, LUMPFIT (ms)
κ	Mass or heat component, TOUGH2
ϕ	Porosity (%)

REFERENCES

Arason, Th., Björnsson, G., Axelsson, G., Bjarnason, J.Ö., and Helgason, P., 2004: *ICEBOX – geothermal reservoir engineering software for Windows. A user's manual.* ISOR, Reykjavík, report 2004/014, 80 pp.

Axelsson, G., 1989: Simulation of pressure response data from geothermal reservoir by lumped parameter models. *Proceedings of the 14th Workshop on Geothermal Reservoir Engineering, Stanford University, California,* 257-263.

Axelsson, G., 2007: *Lecture notes on geothermal power development*. University of Iceland.

Axelsson, G., and Arason, P., 1992: *LUMPFIT: Automated simulation of pressure changes in hydrological reservoirs.* Version 3.1 user's guide, Orkustofnun, Reykjavík, 32 pp.

Axelsson, G., Björnsson, G., and Quijano, E.J., 2005: Reliability of lumped parameter modelling of pressure changes in geothermal reservoirs. *Proceedings of the World Geothermal Congress 2005, Antalya, Turkey, 24-29 April 2005,* 8 pp.

Axelsson, G., Gudmundsson, A., Steingrimsson, B., Palmason, G., Armannsson, H., Tulinius, H., Flovenz, O.G., Björnsson, S., and Stefansson, V., 2001: Sustainable production of geothermal energy: suggested definition. *IGA-News, 43, January-March 2001,* 1-2.

Axelsson, G., Stefansson, V., and Björnsson, G., 2004: Sustainable utilization of geothermal resources. *Proceedings of the 29th Workshop on Geothermal Reservoir Engineering, SGP-TR-175, Stanford, California.*

Björnsson, G., 2004: *Using temperature and pressure logs to determine reservoir condition and well status.* UNU-GTP, Iceland, unpublished lecture notes.

Björnsson, G., 2008: *Personal notes and lectures for MSc thesis.* Report, unpublished.

Bodvarsson, G.S. and Witherspoon, P.A., 1989: Geothermal reservoir engineering part 1. *Geotherm. Sci. & Tech., 2,* 68 pp.

Castillo, R. M., 1990: *A preliminary numerical simulation of the BacMan geothermal production field*, PNOC-UNDP joint project on geothermal reservoir management (PHI/86/006), 75 pp.

Department of Energy, 2008: website: http://www.doe.gov.ph/.

Esberto, M.B., Austria, J.J.C., and Sarmiento, Z.F., 2005: WellTaPPs: a web-based Oracle database wellbore temperature and pressure plotting Software. *Proceedings of the World Geothermal Congress 2005, Antalya, Turkey,* CD.

Fajardo, V.L.R., 2000: Lumped parameter model of the Bacon Manito geothermal production field, Albay, Philippines. *Proceedings of the World Geothermal Congress 2000, Kyushu-Tohuku, Japan, pp.* 2551-2554.

Fajardo, V.L.R., Malate, R.C.M., and Sarmiento, Z.F., 2004: *Update on the evaluation of the geothermal reserves for the Bacon-Manito geothermal production field*. PNOC-EDC, Reservoir and Drilling Division, internal report, 64 pp.

Finsterle, S., 2007: *iTOUGH2 Users guide.* Berkeley, University of California.

Finsterle, S., Björnsson, G., Pruess, K., and Battistelli, A., 1999: Evaluation of geothermal well behaviour using inverse modelling. *International Symposium on Dynamics of Fluids in Fractured Rocks Concepts and Recent Advances, Lawrence Berkeley National Laboratory,* 10-12.

Flovenz, O.G., 2007: *Lecture notes in geothermal power development*. University of Iceland.

Haukwa, C.B., 1998: *AMESH: a mesh creating program for the integral finite difference method. User's manual.* Earth Sciences Division, Ernest Lawrence National Laboratory, Berkeley, California, 52 pp.

Iceland Deep Drilling Project, 2008: website: http://www.iddp.is/.

Ketilsson, J., 2007: *Production capacity assessment of geothermal resources by numerical modelling*, University of Iceland, Department of Mechanical Engineering, MSc thesis.

Layugan, D.B., 2008: *Interpreted geophysical boundaries based on MT with major structures*. PNOC EDC, internal memo.

Menke, W., 1984: *Geophysical data analysis: Discrete inverse theory*. Academic Press, Orlando, 260 pp.

Mesquite group et al., 1990*: BacMan II resource assessment review report.* PNOC EDC, internal report, 172 pp.

Michaelides, E.E., 1981: Thermodynamic properties of geothermal fluids. *Geothermal Resources Council, Trans., 5,* 361-364.

Muffler, L. J. P., 1977: 1978 USGS Geothermal resource assessment. *Proceedings of the 3rd Workshop of Geothermal Reservoir Engineering, Stanford, SGP-TR-25-1.*

Ocampo, M.L.:2007: *Power supply and demand situationer and power sector reforms update.* The Energy Investment Forum 2007, Renaissance Hotel, Makati.

O'Sullivan, M.J., Pruess, K., and Lipmann, M.J., 2001: State of the art of geothermal reservoir simulation. *Geothermics 30,* 395-429.

PNOC EDC, 1989: *BacMan II resource assessment*. PNOC EDC, Philippines, 209 pp.

PNOC EDC Geoscientific Department, 1985: *A resource assessment for the proposed 110 MWe BacMan 1 Geothermal power plant*. PNOC EDC, Geoscientific Department, internal report, 115 pp.

Pruess et al., 1996: *TOUGH2 software qualification.* Lawrence Berkeley National Laboratory, 140 pp.

Pruess, K., Oldenburg, C., and Moridis, G., 1999: *TOUGH2, user's guide version 2.0.* Lawrence Berkeley National Laboratory, 197 pp.

Ramos, S.G., 2002: Potential constraints to the development of the Rangas sector based on petrologic evaluation of the BacMan geothermal field, Philippines. *Proceedings of the 27th Workshop on Geothermal Reservoir Engineering, SGP-TR-171, Stanford, California.*

Reyes, A.G., Zaide-Delfin, M.C., and Bueza, E.L., 1995: Petrological identification of multiple heat sources in Bacon-Manito geothermal system, the Philippines. *Proceedings of the World Geothermal Congress 1995, Florence, Italy, 2,* 713-717.

Sarmiento, Z.F. and Björnsson, G., 2007: Reliability of early modelling studies for high-temperature reservoirs in Iceland and the Philippines. *Proceedings of the 32nd Wworkshop on Geothermal Reservoir Engineering, SGP-TR-183, Stanford, California.*

See, F. S., 2001: Geochemical response to exploitation of the BacMan geothermal production field, Philippines. *Proceedings of the 21st Annual PNOC-EDC Geothermal Conference, Makati City, Philippines.*

See, F.S., 2004: Sustainability of the BacMan geothermal field. *Proceedings of the 25th Annual PNOC-EDC Geothermal Conference, Makati City, Philippines,* 16 pp.

Solis et al., 1994: *Bacon-Manito Geothermal production field exploitation baseline geochemistry data*. PNOC EDC, Geoscientific Department, 377 pp.

Stefansson, V., and Axelsson, G., 2005: Sustainable utilization of geothermal resources through stepwise development. *Proceedings of the World Geothermal Congress 2005, Antalya, Turkey, CD.*

Vasquez, N.C., Javellana, S.P., and Ferrer, H.P., 1999: Present and future geothermal development in the Philippines. *IGA News, 37.*

Wessel, P. and Smith, W.H.F., 2007: *The GMT webpage*: http://gmt.soest.hawaii.edu/.

World Commission on Environment and Development, 1987: *Our common future, report of the World Commission on Environment and Development*. Published as an annex to General Assembly document A/42/427, Development and International Co-operation: Environment.

APPENDIX 1: Rock temperature and pressure

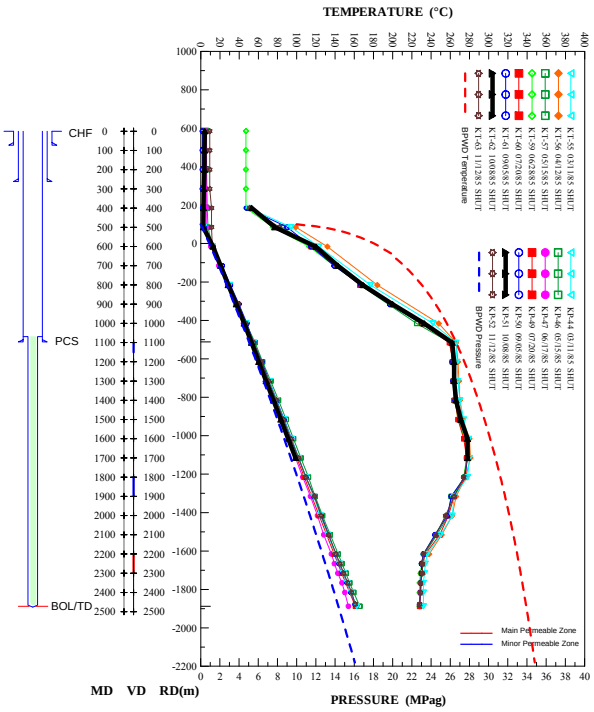

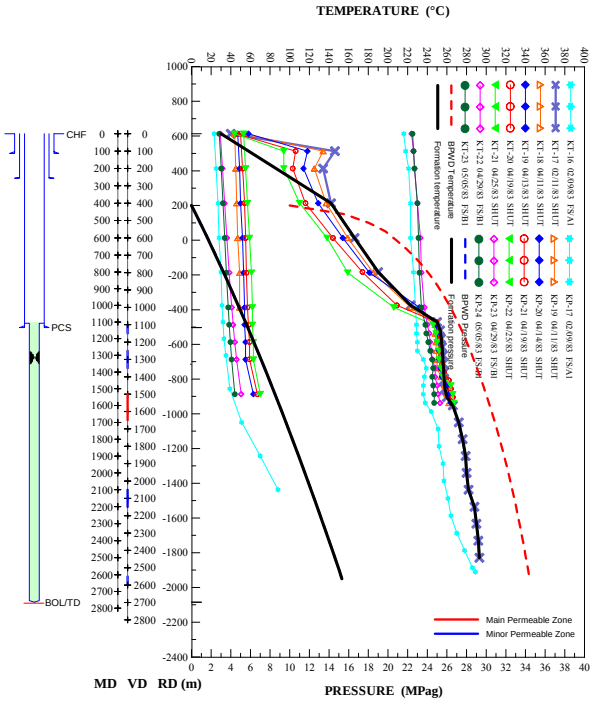

PAL-2D TEMPERATURE & PRESSURE GRAPH

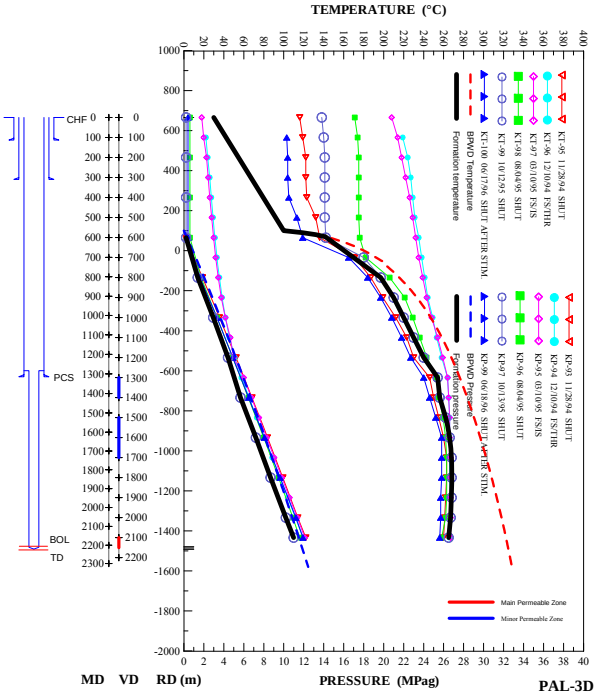

PAL-3D

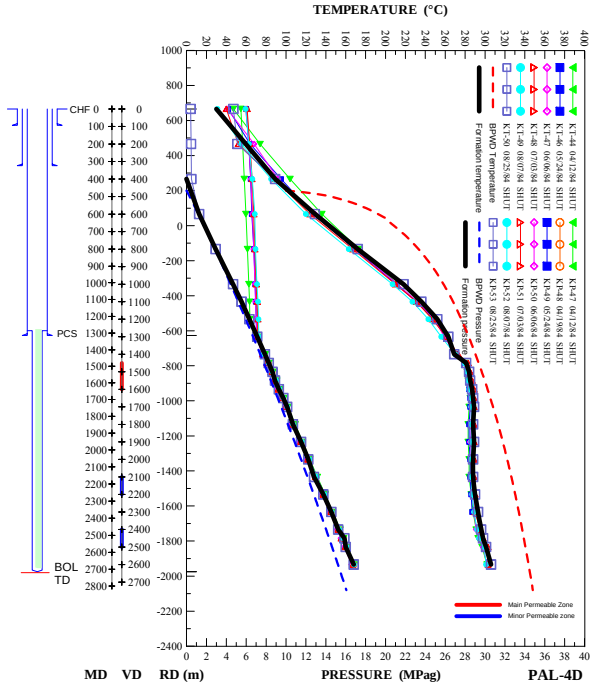

PAL-4D

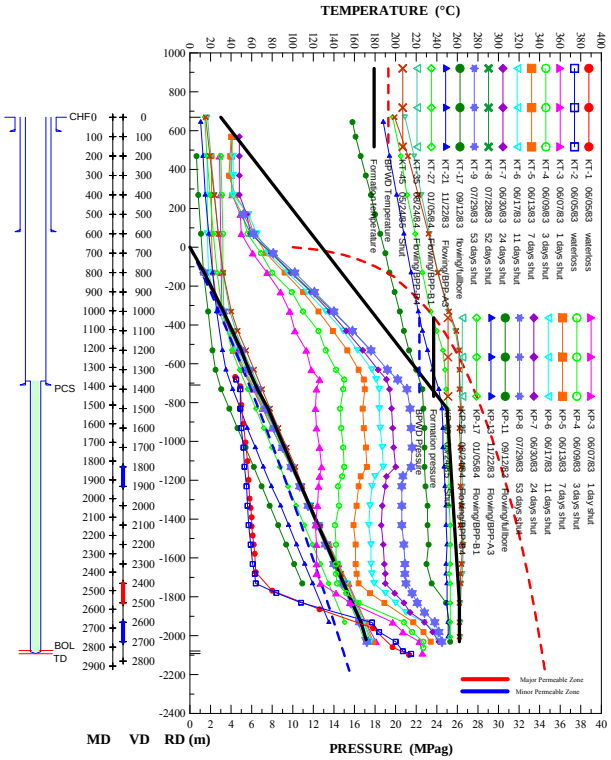

PAL-5D TEMPERATURE & PRESSURE GRAPH

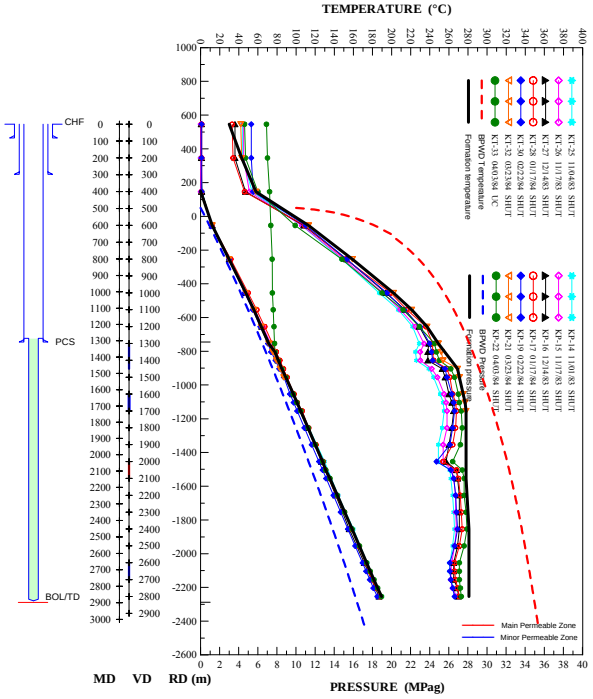

PAL-6D TEMPERATURE & PRESSURE GRAPH

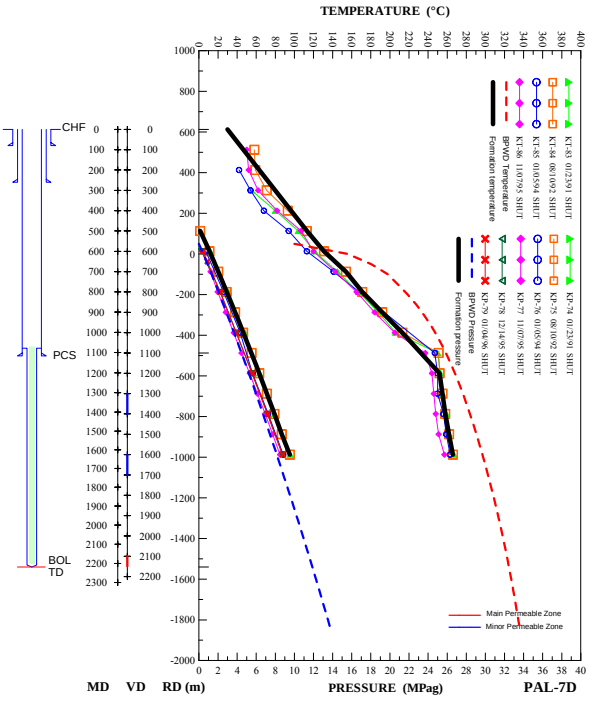

PAL-7D

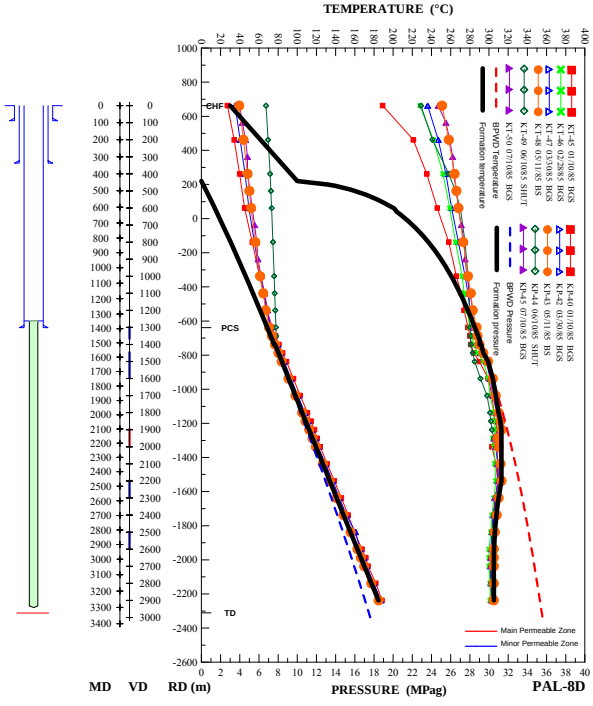

PAL-8D

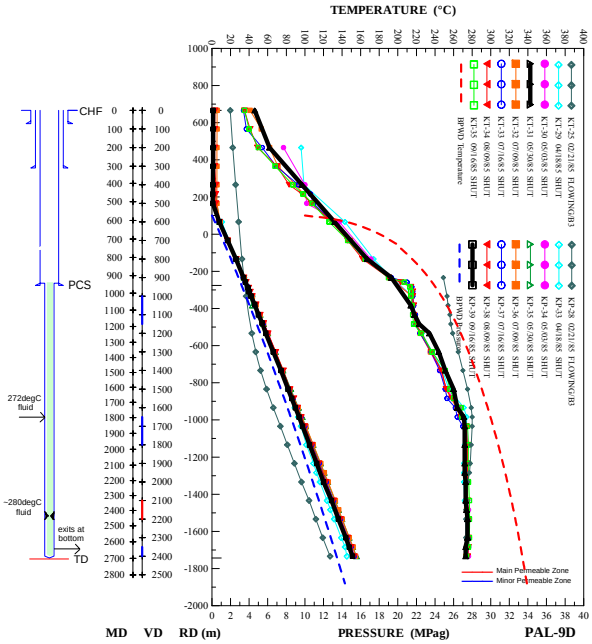
TEMPERATURE (°C)
CHF
PCS
272degC fluid
~280degC fluid
exits at bottom
TD
Main Permeable Zone
Minor Permeable Zone
MD VD RD (m)
PRESSURE (MPag)
PAL-9D

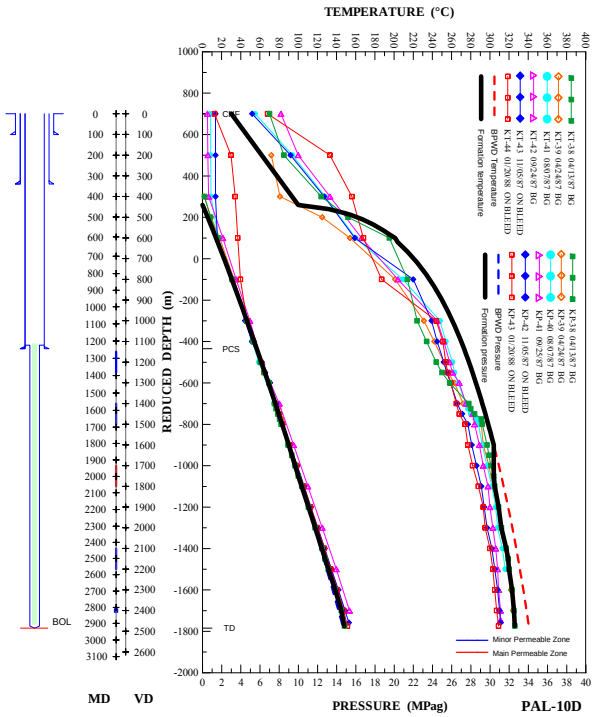
TEMPERATURE (°C)
REDUCED DEPTH (m)
CHF
PCS
BOL
TD
Formation temperature
BPWD Temperature
Formation pressure
BPWD Pressure
Minor Permeable Zone
Main Permeable Zone
MD VD
PRESSURE (MPag)
PAL-10D

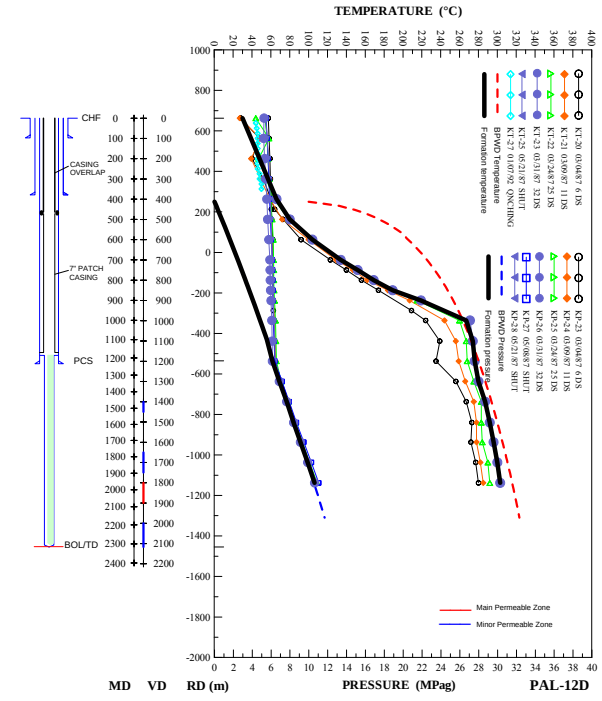
TEMPERATURE (°C)
CHF
CASING OVERLAP
7" PATCH CASING
PCS
BOL/TD
Formation temperature
BPWD Temperature
Formation pressure
BPWD Pressure
Main Permeable Zone
Minor Permeable Zone
MD VD RD (m)
PRESSURE (MPag)
PAL-12D

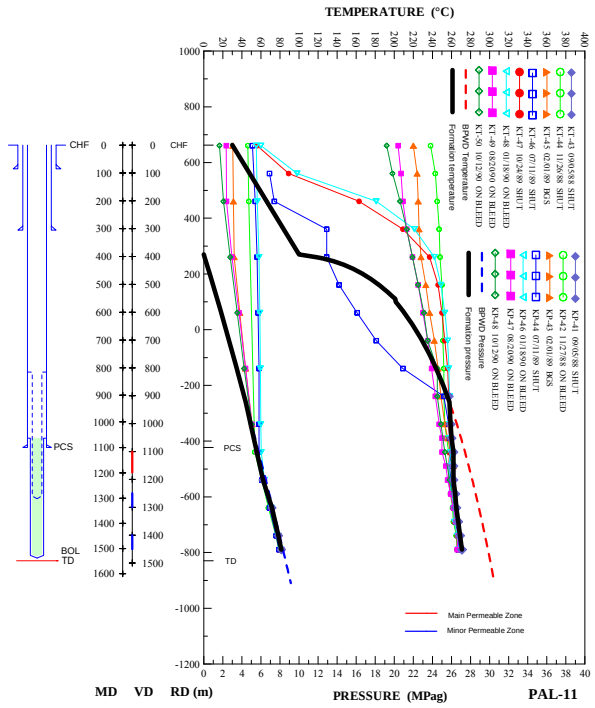
TEMPERATURE (°C)
CHF
PCS
BOL
TD
Formation temperature
BPWD Temperature
Formation pressure
BPWD Pressure
Main Permeable Zone
Minor Permeable Zone
MD VD RD (m)
PRESSURE (MPag)
PAL-11

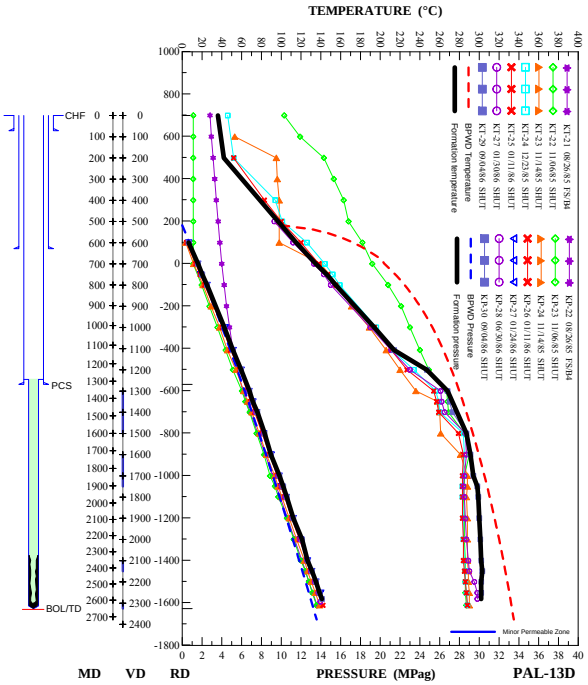

PAL-13D

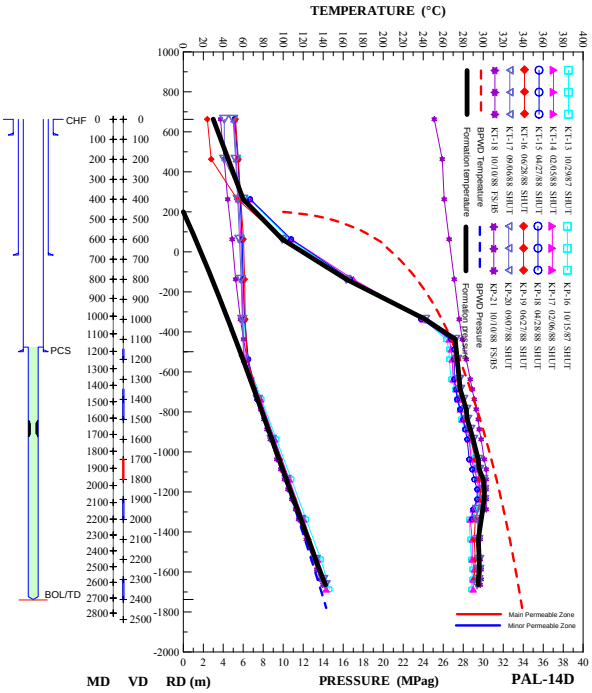

PAL-14D

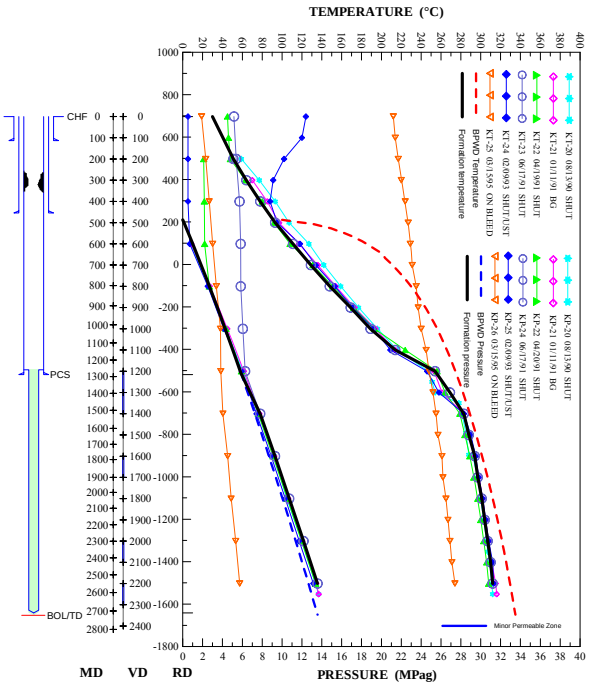

PAL-15D

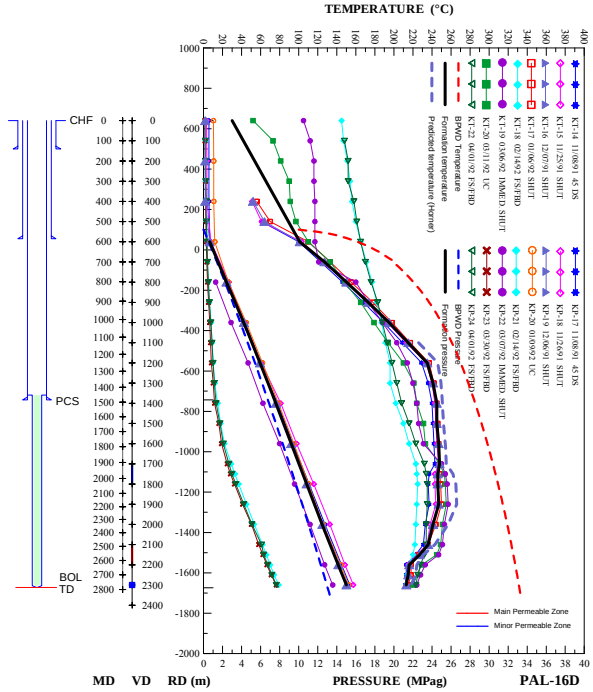

PAL-16D

PAL-15D TEMPERATURE & PRESSURE GRAPH

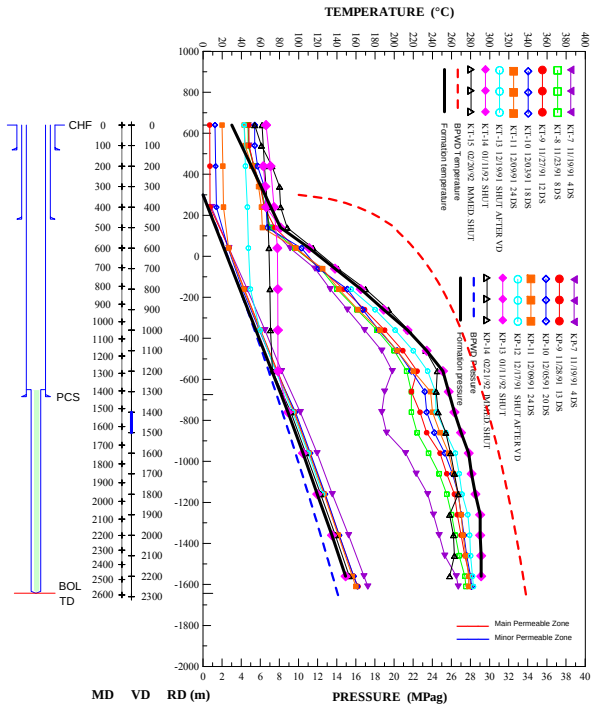

PAL-17D TEMPERATURE & PRESSURE GRAPH

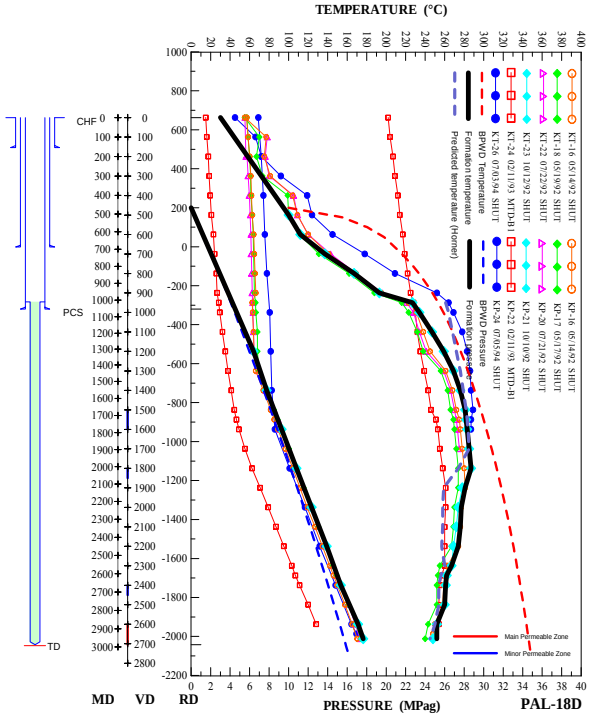

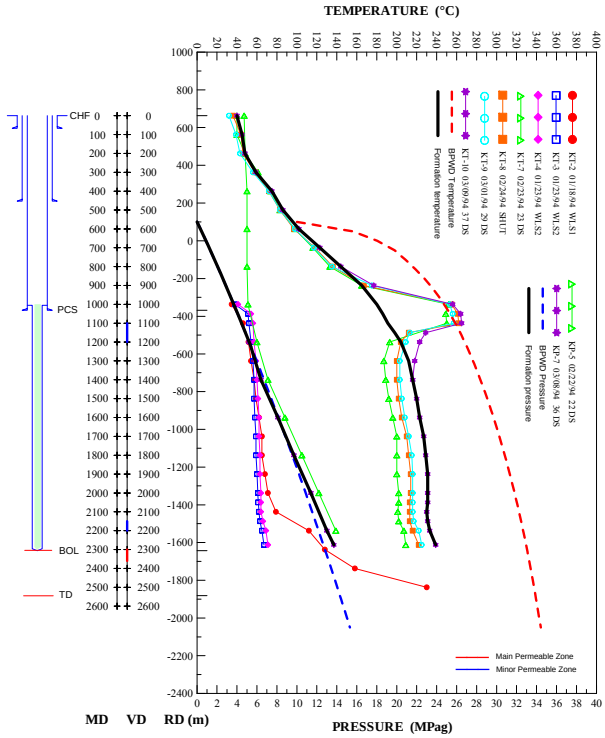

PAL-19 TEMPERATURE & PRESSURE GRAPH

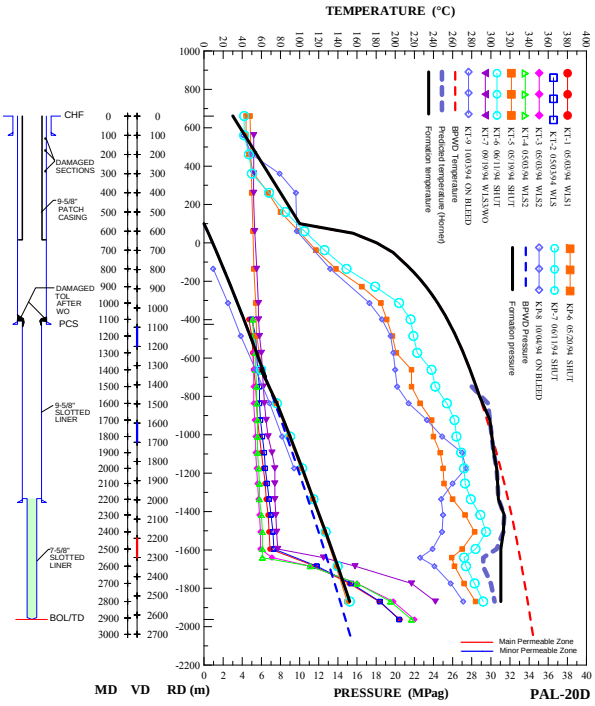

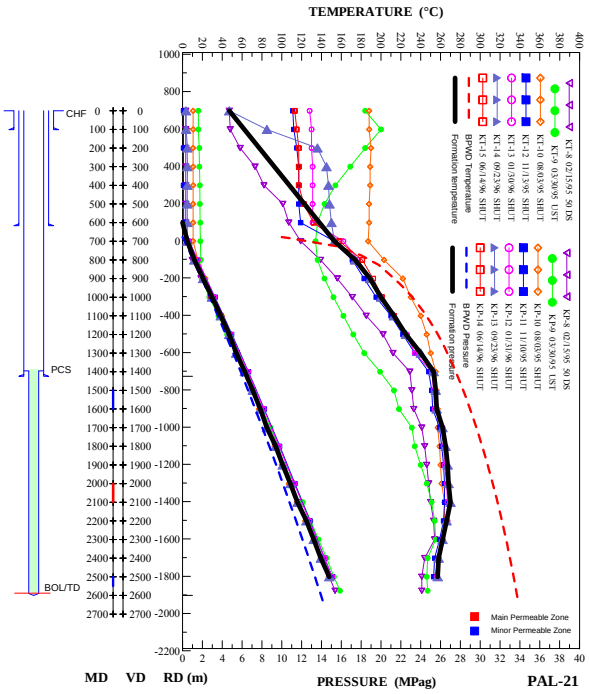

PAL-21

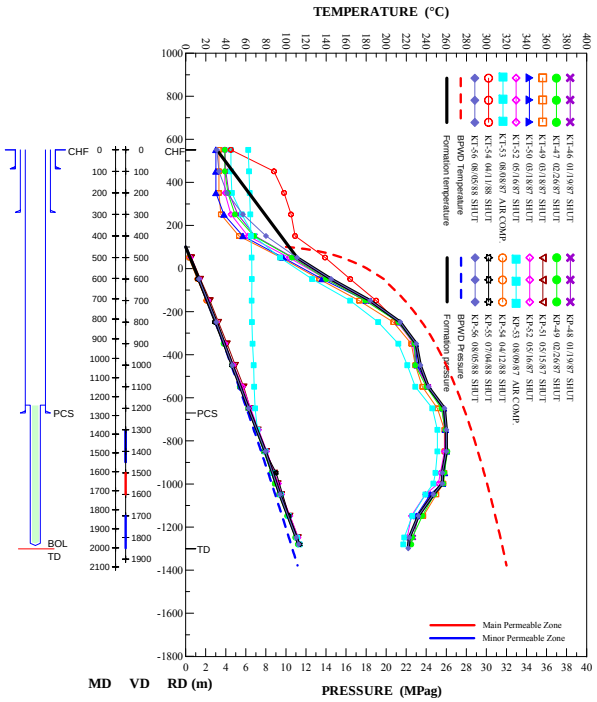

PAL-1RD TEMPERATURE & PRESSURE GRAPH

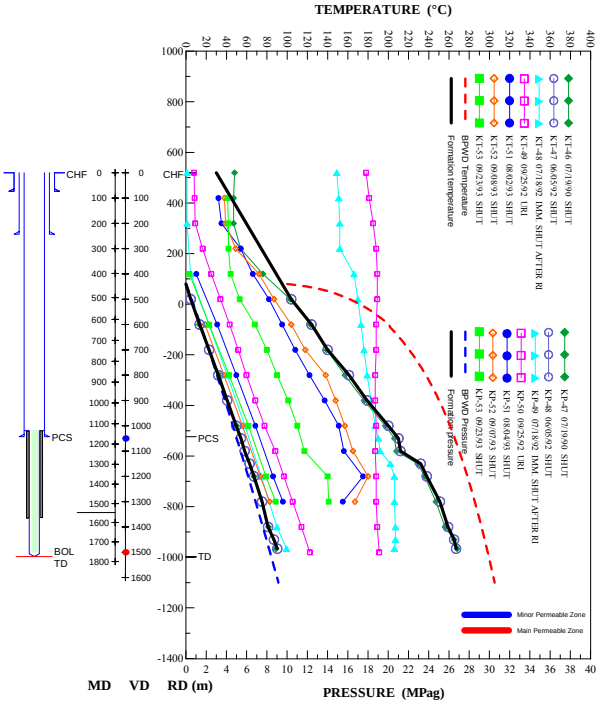

PAL-2RD TEMPERATURE & PRESSURE GRAPH

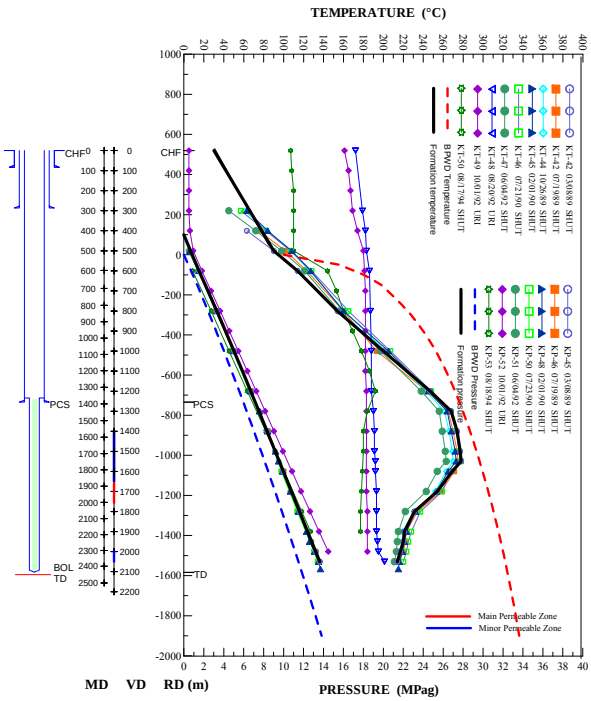

PAL-3RD TEMPERATURE & PRESSURE GRAPH

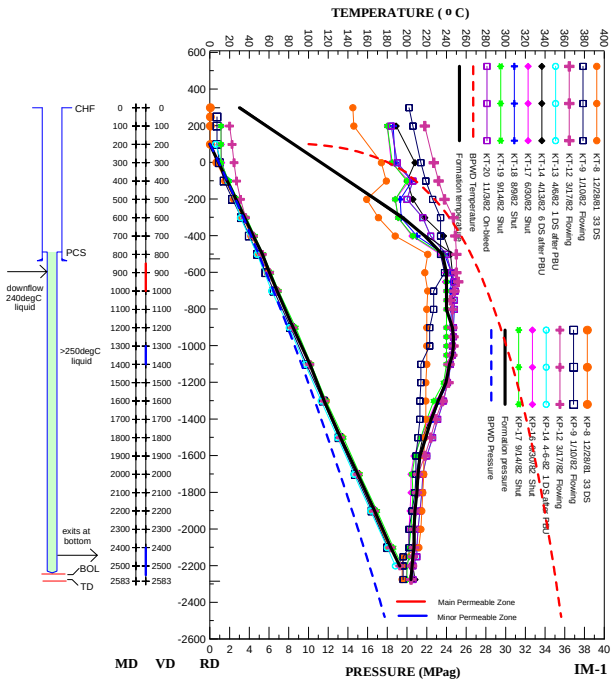

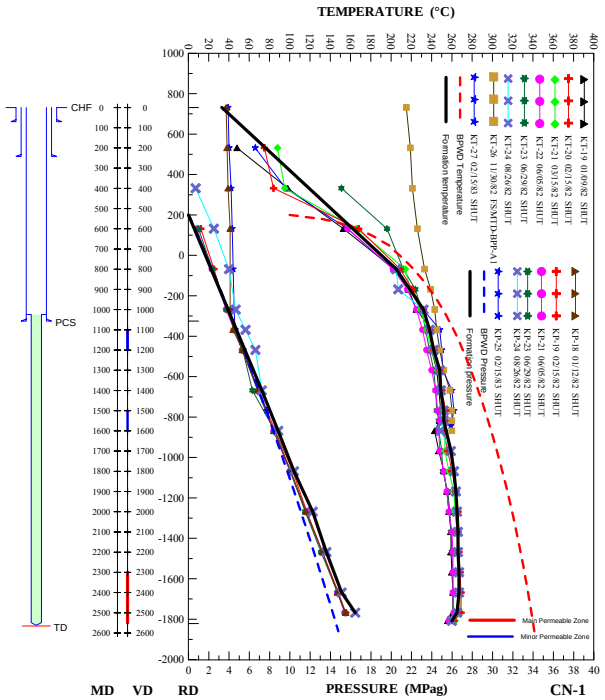

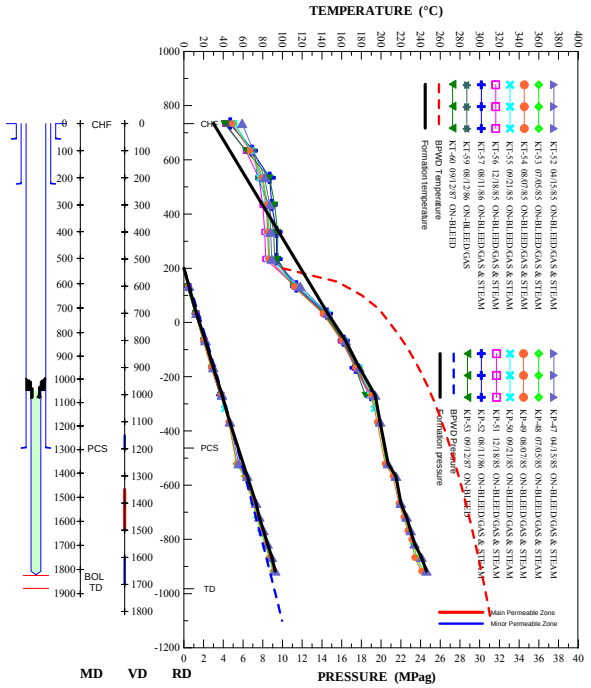

CN-2D TEMPERATURE & PRESSURE GRAPH

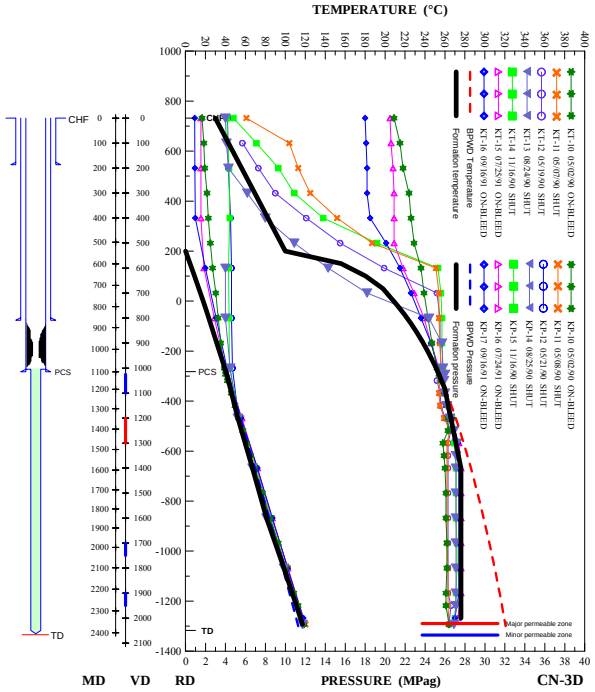

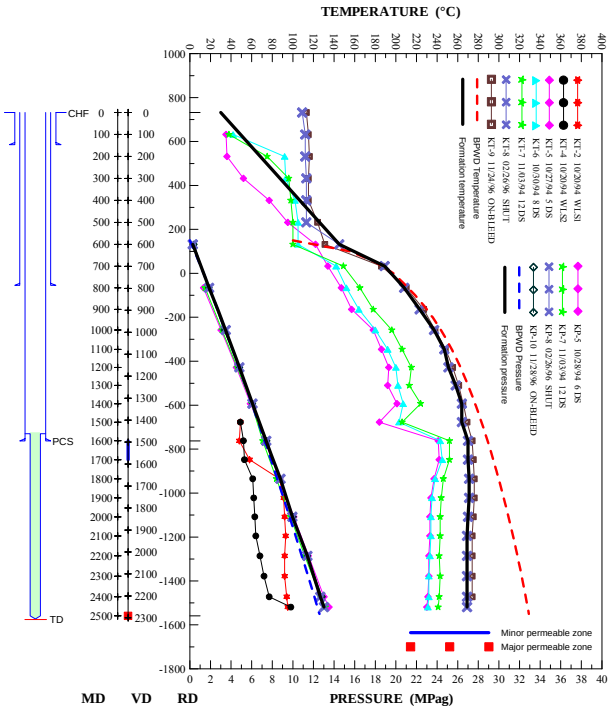

CN-4D TEMPERATURE & PRESSURE GRAPH

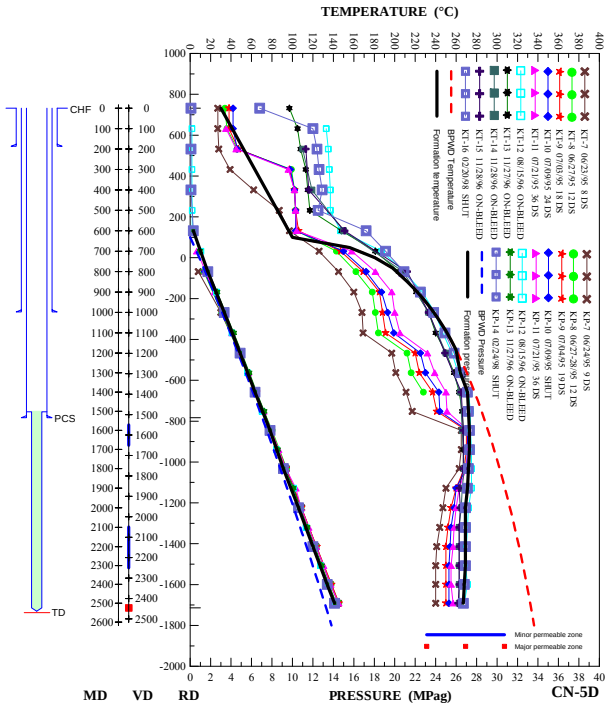

CN-5D

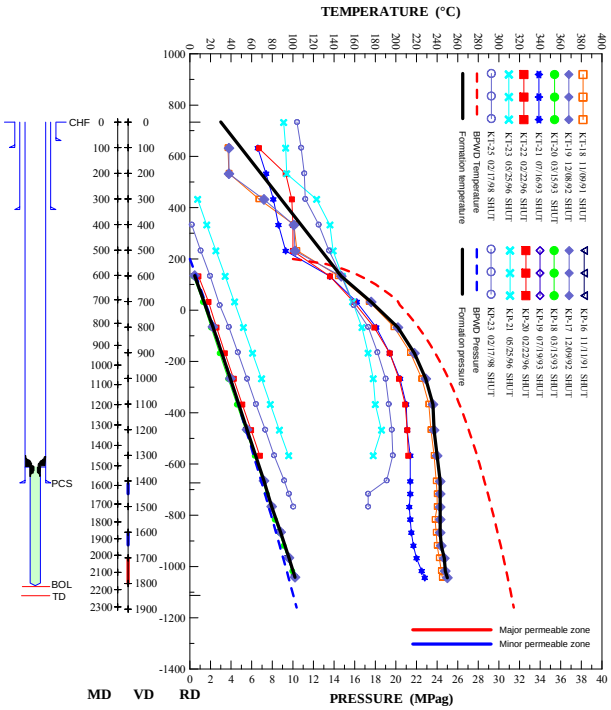

CN-2RD TEMPERATURE & PRESSURE GRAPH

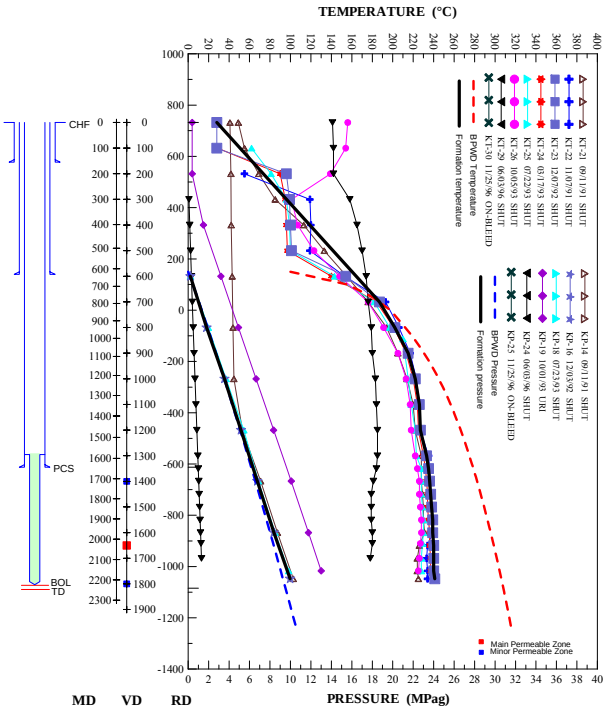

CN-3RD TEMPERATURE & PRESSURE GRAPH

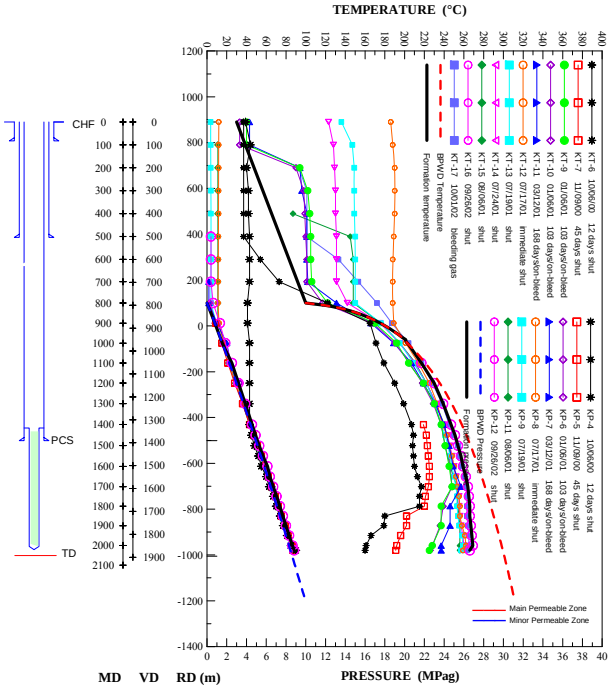

TW-1D TEMPERATURE & PRESSURE GRAPH

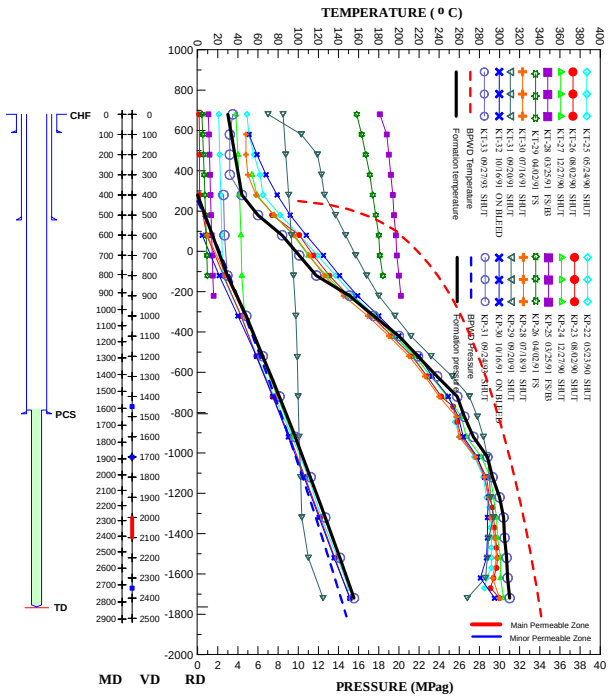

OP-3D TEMPERATURE & PRESSURE GRAPH

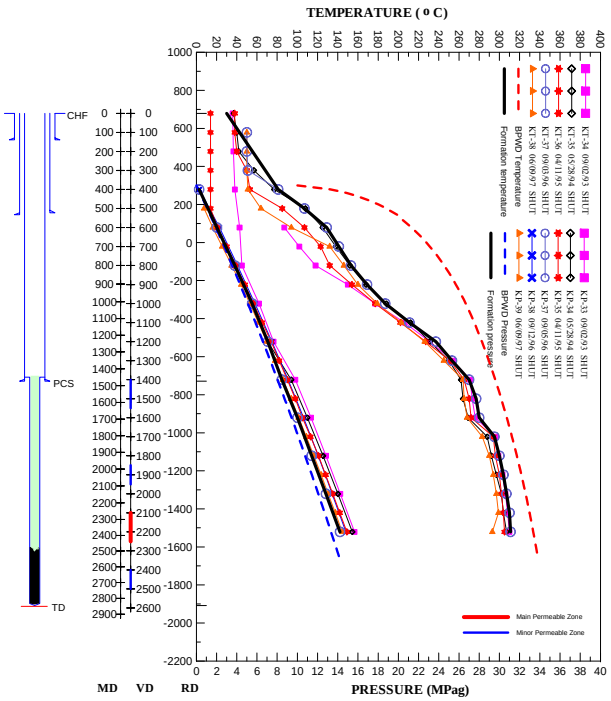

OP-4D TEMPERATURE & PRESSURE GRAPH

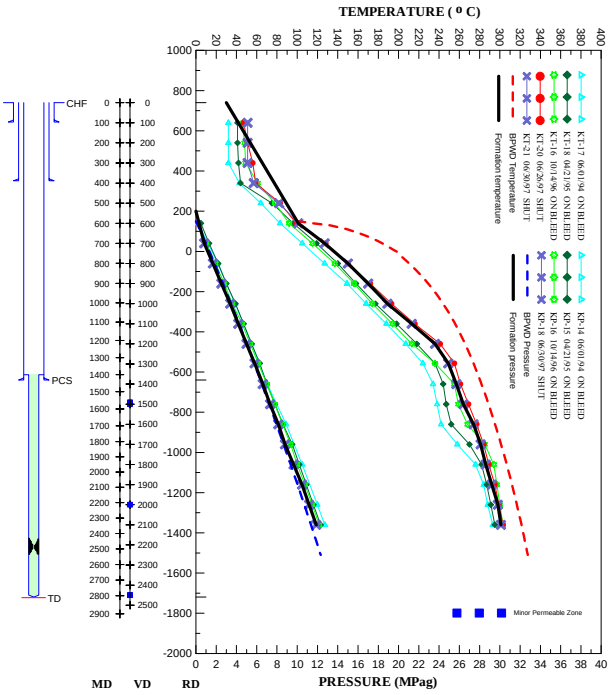

OP-5DA TEMPERATURE & PRESSURE GRAPH

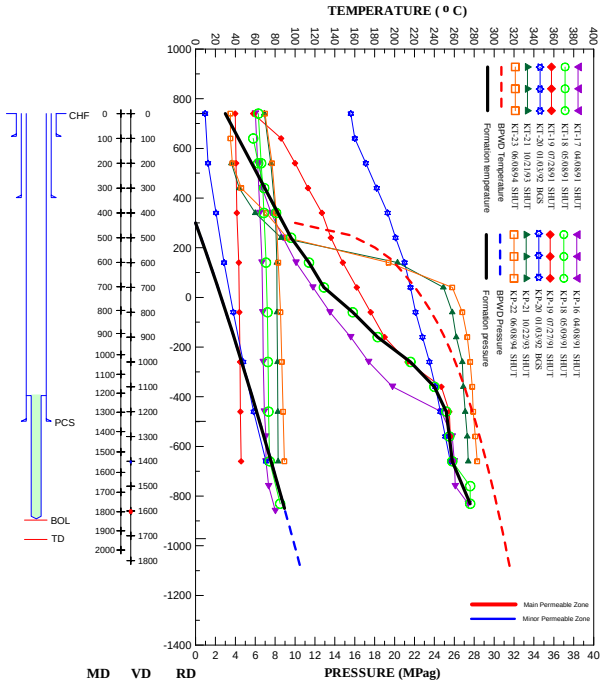

OP-6D TEMPERATURE & PRESSURE GRAPH

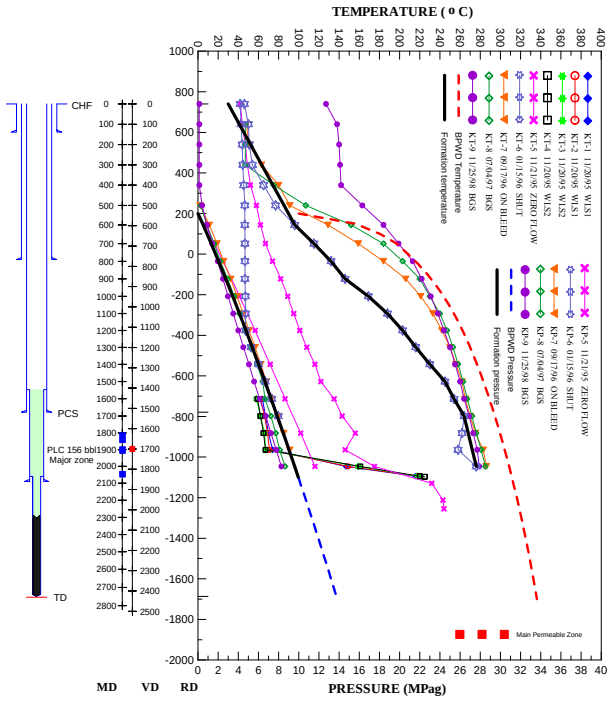

OP-7D TEMPERATURE & PRESSURE GRAPH

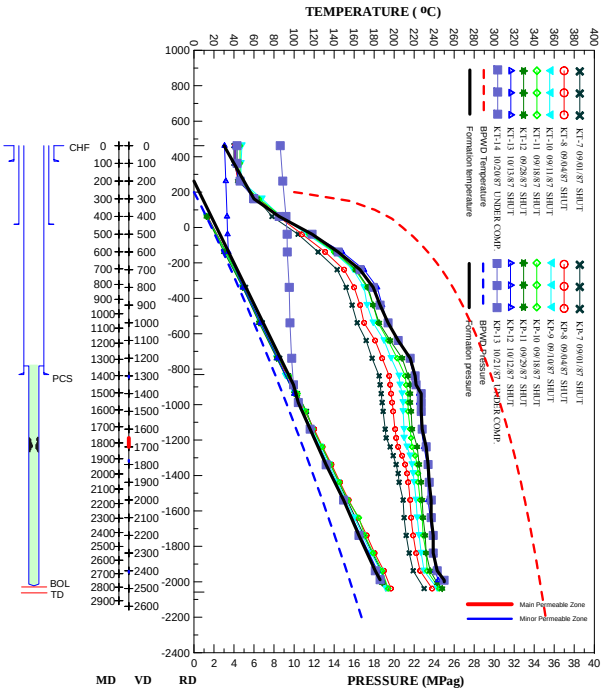

OP-1RD TEMPERATURE & PRESSURE GRAPH

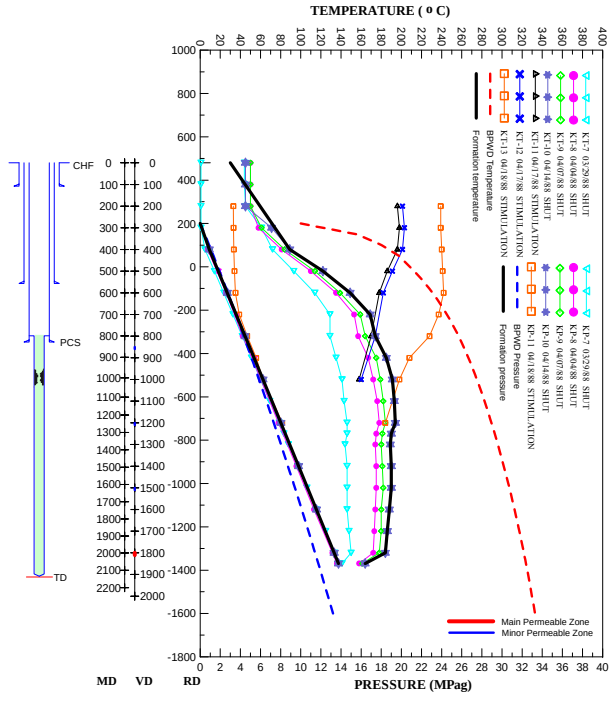

OP-2RD TEMPERATURE & PRESSURE GRAPH

APPENDIX 2: Basic well data

Well name	Year of drilling	Wellhead location		Elevation, (mRSL)	Depth, (mVD)	Well status (2007)
		Easting (m)	Northing (m)			
BacMan 1 Palayan-Bayan						
PAL-3D	1982	602073.4	1443319.5	613.3	2698.7	Production
PAL-4D	1983	602090.8	1443119.1	665.8	2641.1	Production
PAL-9D	1984	602049.2	1443088.0	666.0	2409.3	Production
PAL-10D	1984	602102.2	1442914.7	700.6	2485.1	Production
PAL-13D	1985	602107.2	1442893.4	697.6	2326.2	Production
PAL-15D	1989	602180.9	1443506.7	697.0	2338.2	Production
PAL-21	1994	602105.2	1442904.4	697.0	2600.0	Production
PAL-8D	1983	602201.2	1443350.1	662.4	2973.0	Production
PAL-11D	1984	602221.3	1443482.7	662.6	1491.8	Production
PAL-12D	1984	602190.4	1443501.1	662.6	2117.5	Production
PAL-14D	1986	602180.9	1443506.7	662.6	2400.0	Production
PAL-18D	1991	602213.8	1443490.4	662.6	2707.1	Production
PAL-19	1994	602202.3	1443493.9	663.0	2544.7	Production
PAL-20D	1994	602203.8	1443447.1	660.9	2623.2	Production
PAL-1RD	1983	599820.7	1444767.8	551.4	1852.0	Hot brine reinjection
PAL-3RD	1984	601121.7	1444422.0	519.6	2103.5	Hot brine reinjection
PAL-1	1982	600468.4	1444109.1	584.5	2472.0	Hot brine reinjection
PAL-6D	1983	601130.3	1443870.3	546.4	2833.9	Cold reinjection
IM-1	1981	598629.6	1444847.8	298.0	2583.0	CT blowdown
BacMan 2 Cawayan						
CN-1	1981	601629.2	1442115.9	731.6	2553.3	Production
CN-4D	1994	601645.0	1442116.0	732.0	2290.9	Production
CN-5D	1995	601706.6	1442060.6	732.0	2446.1	Production
CN-2RD	1990	601612.9	1442165.4	733.8	1846.8	Hot brine reinjection
CN-3RD	1991	601669.0	1442075.0	732.2	1816.7	Hot brine reinjection
PB-1A	1981	599799.0	1442603.7	456.3	2662.1	CT blowdown
BacMan 2 Botong						
OP-3D	1988	604707.3	1442989.8	680.0	2443.4	Production
OP-4D	1989	604719.4	1443037.1	679.0	2587.1	Production
OP-5DA	1992	604415.0	1442733.9	740.0	2459.7	Production
OP-6D	1990	604396.3	1442729.9	740.0	1711.5	Production
OP-7D	1995	604432.8	1442720.0	740.0	2426.8	Production
OP-1RD	1987	604869.0	1444031.9	462.0	2520.2	Brine reinjection
OP-2RD	1987	604639.1	1444202.5	480.0	1897.8	Cond. reinjection
BacMan 1 Palayan-Bayan						
PAL-7D	1983	601647.7	1443350.1	613.0	2153.2	Pressure monitoring
PAL-16D	1991	603259.2	1443965.6	639.9	2314.2	Pressure monitoring, shut; retested;
PAL-2D	1982	601727.3	1443319.5	613.3	2697.7	Possible make-up production well, shut, for poss. rehab.;
PAL-5D	1983	600606.2	1443072.2	669.3	2761.6	Possible make-up production well, shut, monitor well;
PAL-17D	1991	603238.0	1443922.4	639.9	2283.4	Future make-up production well shut;
PAL-2RD	1984	601118.4	1444346.9	519.6	1517.9	Damaged liner; for poss. rehabilitation for future make-up reinjection well

Basic well data (continuation)

Well name	Year of drilling	Wellhead location		Elevation, (mRSL)	Depth, (mVD)	Well status (2007)
		Easting (m)	Northing (m)			
BacMan 2 Cawayan wells						
CN-2D	1982	601595.3	1442180.0	733.8	1716.0	Cold reinjection; for rehab.; poss. M&R reinjection well;
CN-3D	1990	601691.2	1442050.7	732.0	2049.5	Shut; for work-over; standby well
TW-1D	2000	602027.2	1441178.7	890.0	1888.1	Shut; tested; prod. well for future expan.
TW-2D	2001	602027.2	1441178.7	890.0	2375.1	Shut; tested; prod. well f. future expan.
Other wells						
MAN-1	1979	598147.1	1443093.0	320.8	1367.8	Shut; temp.gradient
MAN-2	1979	599805.0	1442582.4	456.3	1636.7	Shut; temp. gradient
SIH-1	1996	604775.0	1443290.0	651.0	372.0	Shut; temp. gradient

APPENDIX 3: Theoretical recovery factor as a function of reservoir porosity (from Muffler, 1977)

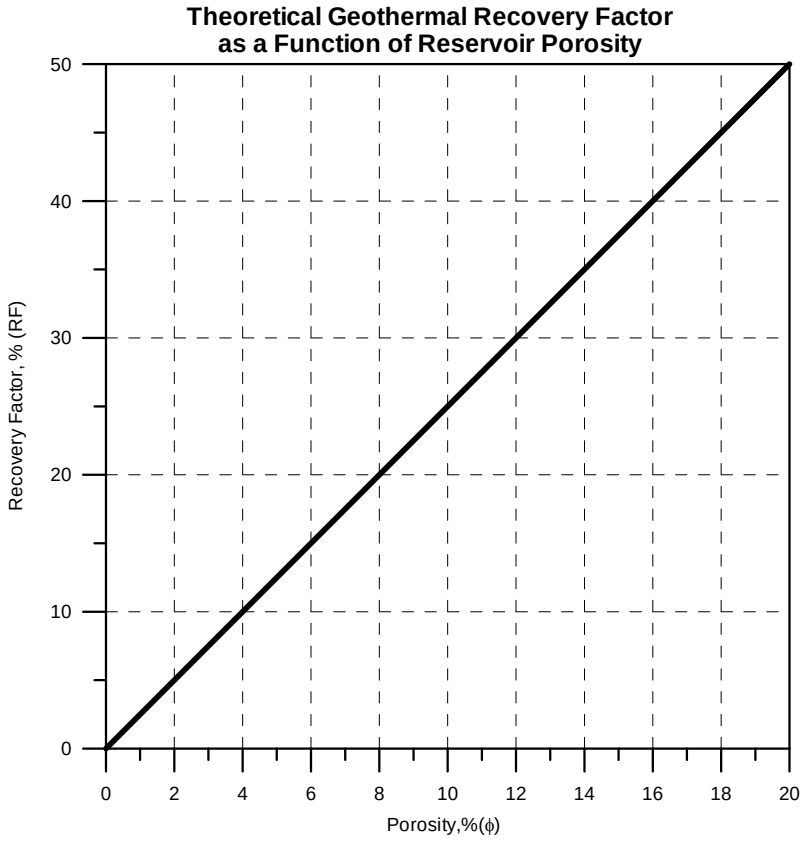

Graph showing possible variation of geothermal resource recovery factor as a function of effective porosity (ϕ) for reservoir produced by intergranular flow. Recovery factor (RF) is taken to be 50% for an ideally permeable reservoir in which total porosity = effective porosity = 20%. Adopted from Cataldi et al. (1978).

APPENDIX 4: Final rock permeability after parameter optimization

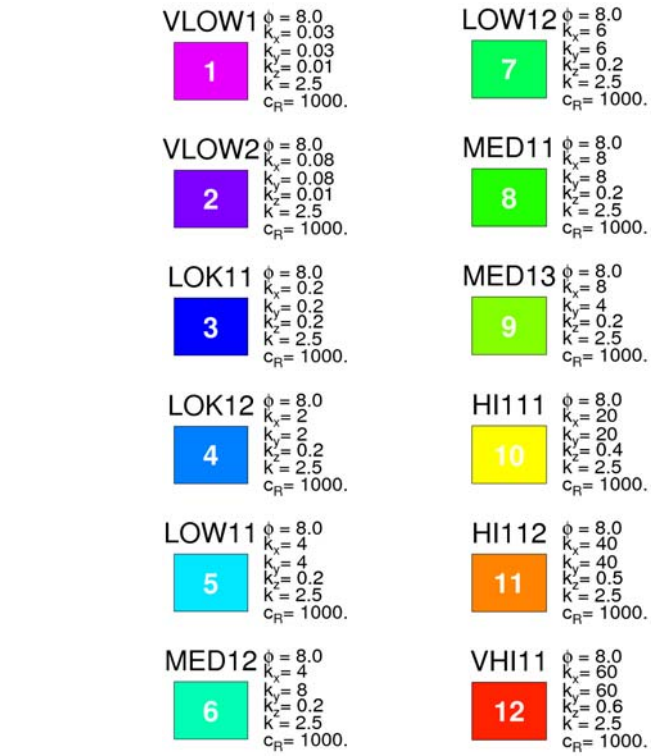

APPENDIX 5: Steady-state observations vs. simulations

Simulated ◊ **observed +**

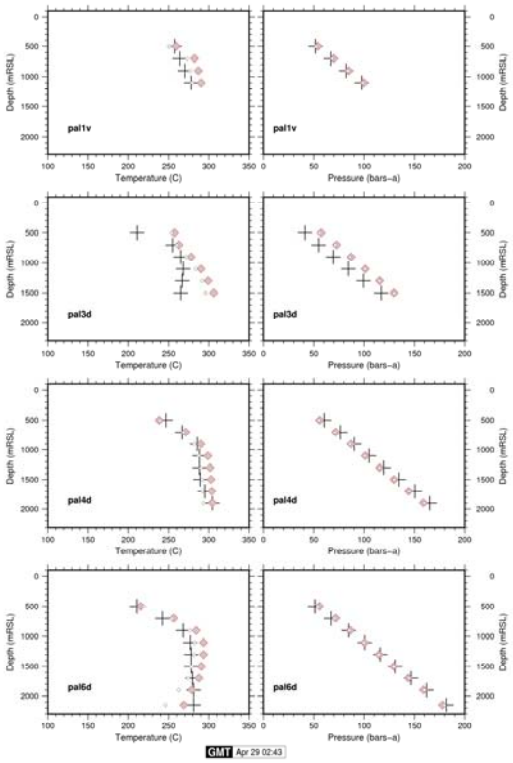

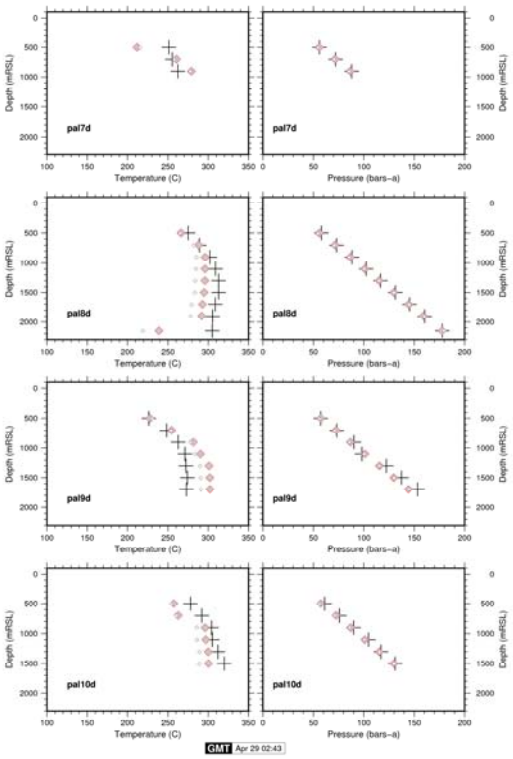

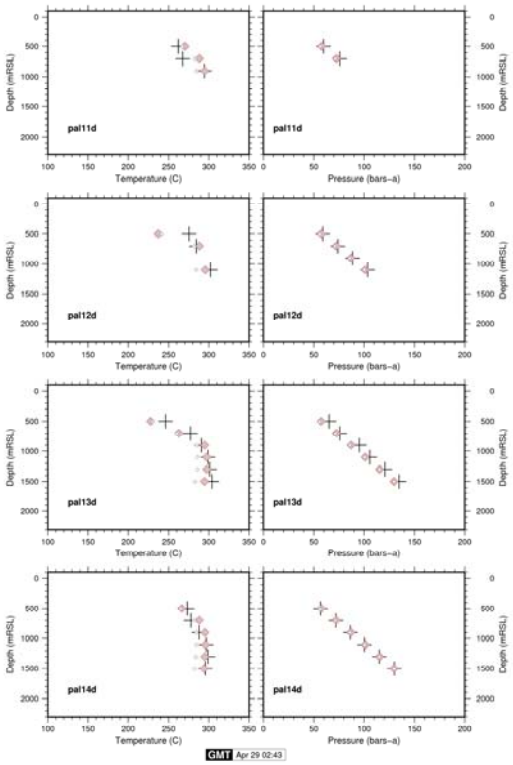

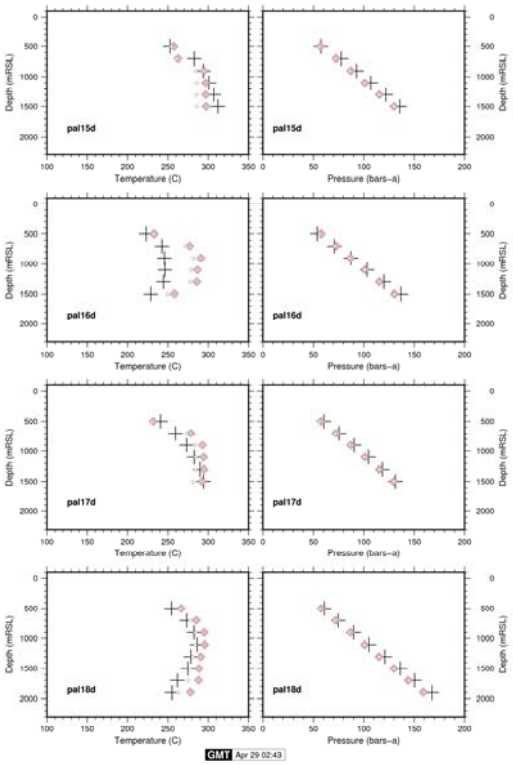

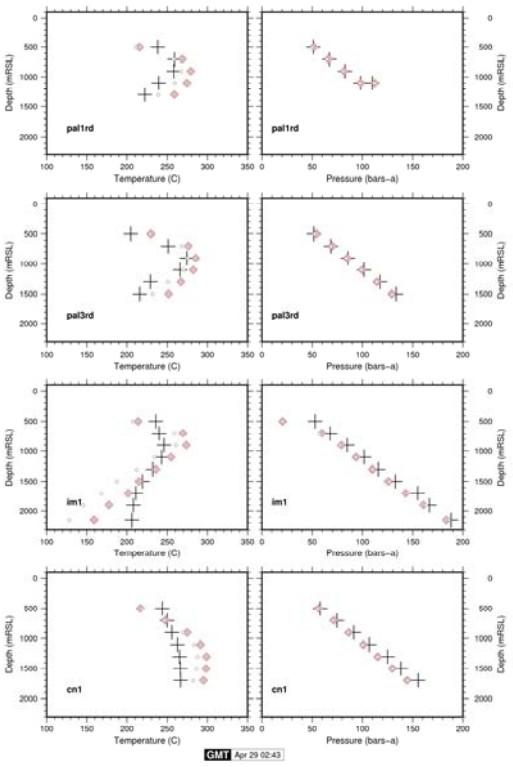
pal1rd
pal1rd
pal3rd
pal3rd
im1
im1
cn1
cn1
Depth (mRSL)
Temperature (C)
Pressure (bars-a)
GMT Apr 29 02:43

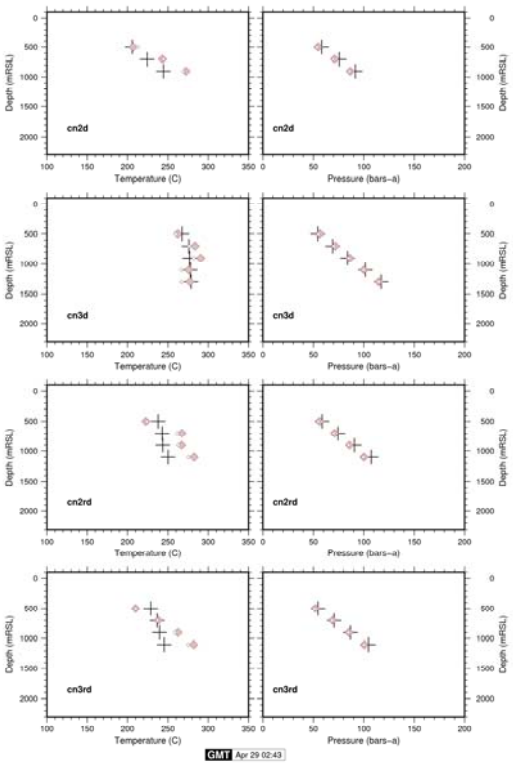
cn2d
cn2d
cn3d
cn3d
cn2rd
cn2rd
cn3rd
cn3rd
Depth (mRSL)
Temperature (C)
Pressure (bars-a)
GMT Apr 29 02:43

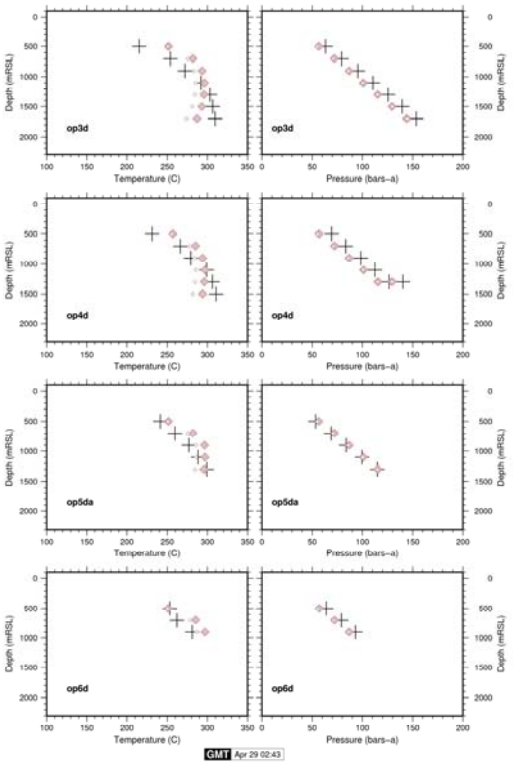
op3d
op3d
op4d
op4d
op5da
op5da
op6d
op6d
Depth (mRSL)
Temperature (C)
Pressure (bars-a)
GMT Apr 29 02:43

APPENDIX 6: Predicted generation at different separation pressures

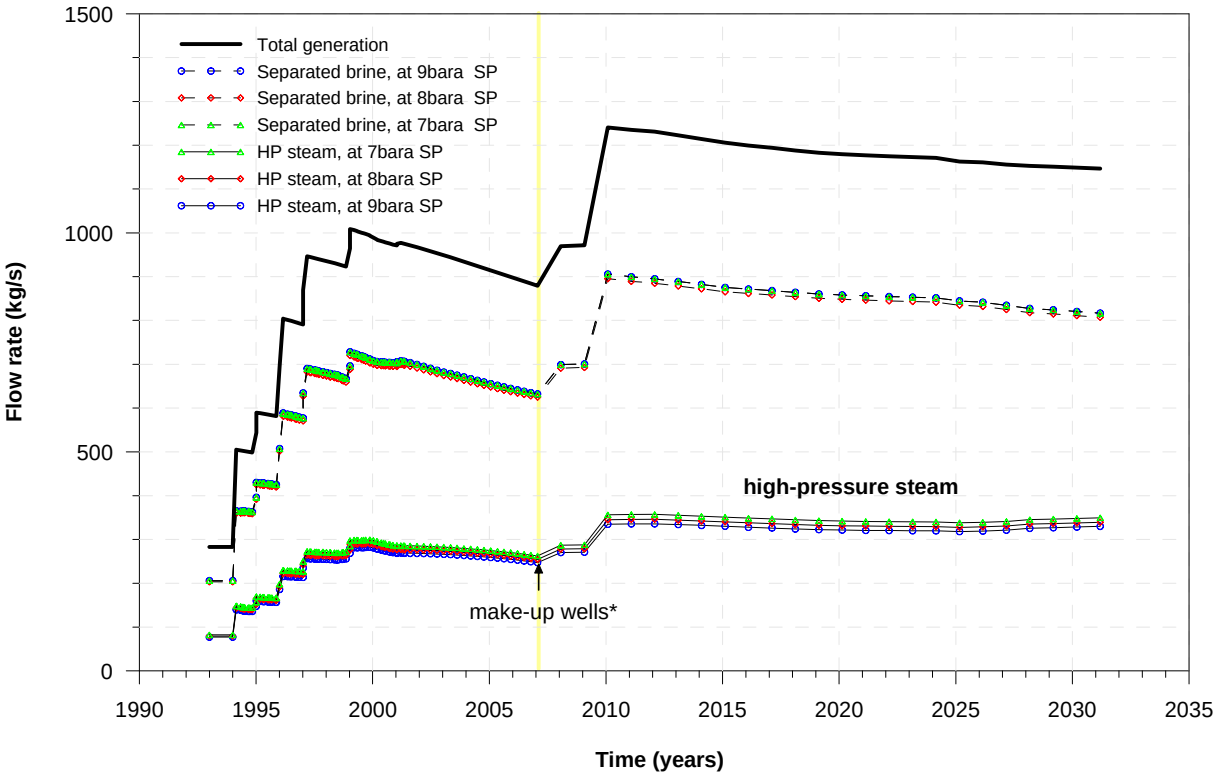

Predicted flows at different separation pressures for Case 1

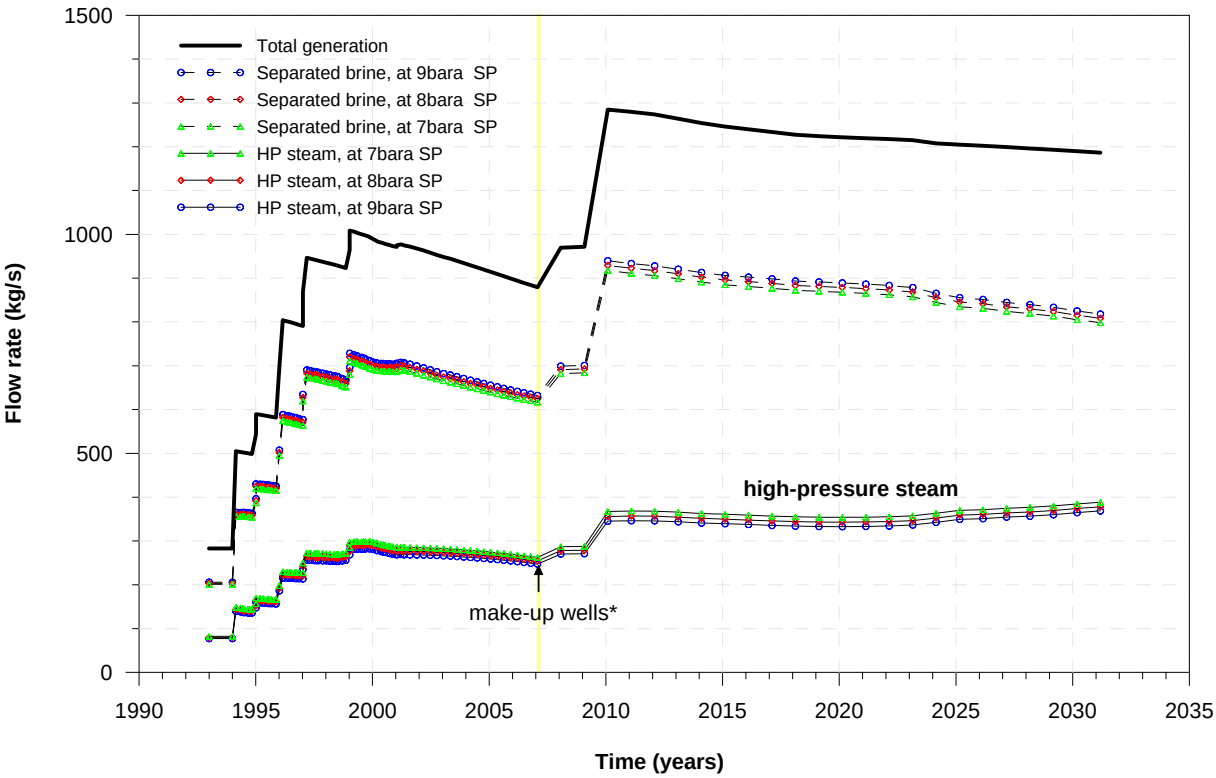

Predicted flows at different separation pressures for Case 2